A THEORETICAL AND EXPERIMENTAL INVESTIGATION OF THE DYNAMIC RESPONSE OF FLEXIBLE MECHANISM SYSTEMS FABRICATED FROM FIBROUS COMPOSITE MATERIALS

By

Cheng-Kuo Sung

A DISSERTATION

Submitted to

Michigan State University

in partial fulfillment of the requirements

for the degree of

DOCTOR OF PHILOSOPHY

Department of Mechanical Engineering

1986

ABSTRACT

A THEORETICAL AND EXPERIMENTAL INVESTIGATION OF THE DYNAMIC RESPONSE OF FLEXIBLE MECHANISM SYSTEMS FABRICATED FROM FIBROUS COMPOSITE MATERIALS

By

Cheng-Kuo Sung

The articulating members of linkage machinery must be designed with high stiffness-to-weight ratios in order that these machine systems operate successfully in a high-speed mode. One approach to satisfying this criterion is to exploit the high specific stiffnesses of polymeric fibrous composite laminates. This work is divided into two parts. First, the mechanism systems are operating under isothermal conditions. Candidate materials are subjected to mechanical testing and their constitutive behavior classified. A variational theorem is then derived to obtain the governing equation and the associated boundary conditions. A finite element formulation is also developed based on the variational equation of motion. The predictive capability of this analytical approach is evaluated by simulating the vibrational response of both experimental four-bar linkages and also slider-crank mechanisms prior to comparing the computer results with experimental data.

Secondly, the same mechanism systems are operating under adverse environmental conditions. The constitutive behavior of some of these

composite materials is, however, dependent upon the ambient environmental conditions, and hence models must be developed in order to predict the response of mechanism systems fabricated in this class of materials. A variational principle is presented that may be employed for systematically establishing the equations governing the dynamic response of planar flexible linkage mechanisms simultaneously subjected to both mechanical and hygrothermal loadings. As an illustrative example, the equations of energy balance and mass balance are validated by comparing the theoretical simulation with the experimental results performed by Browning and Whitney.

ACKNOWLEDGEMENTS

I wish to express my deepest gratitude to my advisor Dr. Brian S. Thompson for his guidance and assistance throughout this study and in preparation of this manuscript. His academic excellence and research philosophy have provided a constant source of encouragement.

I also wish to thank the members of my committee Drs. Rohan Abeyaratne, John J. McGrath and David Yen.

This research was financially supported through the effort of Dr. Brian S. Thompson by the National Science Foundation under grants CME-792124 and MEA-8216777, and by Division of Engineering Research at Michigan State University. This assistance is warmly acknowledged.

Finally, I would like to thank my parents for their tremendus support, my wife and two sons for their loving support and willingness to share their time with my work.

TABLE OF CONTENTS

LIST OF FIGURES

CHAPTER 1

INTRODUCTION

1.1 Current Trends in Industrial Machinery

The intense competition in the international marketplace for robots and machine systems which significantly enhance manufacturing productivity by operating at high speeds has resulted in the evolution of a new frontier in the machine design. Under these more stringent operating conditions, the traditional design methodologies are unable to adequately predict a machine's performance because elastodynamic phenomena are stimulated due to the inherent flexibility of the moving parts. The traditional design methodologies are based on dynamic analyses wherein all mechanism members are treated as rigid-bodies. A force and stress analysis of the members is undertaken subsequently.

When operating in a high-speed mode, vibrations and dynamic stresses in the members of a mechanism can drastically modify the performance characteristics, and the fatigue-life of parts becomes a significant design consideration. Furthermore, the radial clearances in sleeve bearings in mechanical and electro-mechanical systems, which are essential for the operation of these joints may result in excessive stresses and impactive loads, and these loads can generate more severe problems such as wear, loss of performance, reduced stability and more critical levels of noise and vibration.

Link flexibility has become an active field of research since the late 1960's and this work is documented in two comprehensive survey papers [52,95]. Upon reviewing these papers it is evident that for high-speed operation, mechanism links should be designed with high stiffness-to-weight ratios in order to reduce link deflections and power consumption. In all of the publications cited in references [52] and [95], the members were fabricated in the traditional steel and aluminum alloys, and the desired lightweight form-designs developed by using optimization software packages.

An alternative design methodology has recently been proposed by Thompson et al [158,160,173,178]. This methodology advocates that composite materials should be employed to reduce the elastodynamic phenomena, such as link deflections and dynamic stresses. As is well known, these materials have superior strength and stiffness-to-weight ratios than the commercial metals. Consequently, they offer the designer reduced inertial loading at specific speeds, or else higher speeds of operation because of smaller deflections and superior dynamic response characteristics.

1.2 Scope of This Investigation

In this section, a comparison between the theories developed in this thesis and other theories is undertaken in sub-section 1.2.1, such as the methodologies of developing the equations of motion which govern the dynamic behaviors of the mechanism systems, and the hygrothermal analysis of the linkage mechanisms fabricated from composite materials. An overview of this thesis is presented in sub-section 1.2.2 which outlines the content of each chapter.

1.2.1 Relationship between the Theories Developed Herein and Other Theories

The Lagrange's equation was employed by a few researchers in the field of machine dynamics in order to develop the equations of motion which govern the dynamic behaviors of the mechanisms. B.S. Thompson and A.D. Barr [172] proposed a mixed variational approach which incorporates auxiliary conditions such as the strain-displacement equation, constitutive equations and geometrical boundary conditions into the Hamilton's principle. So the functional depends upon displacements, stresses and strains. Moreover, the stationary conditions are the governing equations in primitive form: the kinematical, dynamical and constitutive relationship. More insights may be gained from this mixed variational principle via a finite element formulation which discretizes a continuous medium into several finite elements. As the basis of an elementary approximation, each field can be independently selected to achieve the discrete model, namely, the approximating function of stresses may be different from that of the strains. The discrete counterparts of the displacement, stresses and strains are governed by algebraic equations: kinematical, dynamical and constitutive. This approach offers an effective mean to achieve simple, efficient models that possess the desirable attributes of those derived by approximating the displacement in the potential.

The high-order theories modeling the elastic motion of links are developed in this investigation. These theories employ geometrically nonlinear analyses which retain the terms in the strain-displacement equations that couple the axial and flexural deformations [107,108,147,180,185]. These additional terms are readily handled by the numerical integration solution philosophy, but they present additional complications if the model superposition approach is employed.

A composite material is constructed by combining two or more materials on a macroscopic scale to form a useful material since the best qualities of the constituents are often significantly exposed in accordance to the intention of a designer. For example, if attention is focused on the first-ply failure of a composite material, then the first ply has to be designed strong enough by either selecting an appropriate fiber material or rearranging the stacking sequence in order to keep the first ply from being damaged.

Some, but not all, of the polymeric materials are very sensitive to both the environmental temperature and relative humidity fluctuations, the materials absorb moisture cause swelling and micro-crack formation under extreme conditions. These micro-cracks, in turn increase the diffusivity of the composite and this characteristic can be increased further by the dimensional changes associated with elevated temperatures. Consequently, the mechanical properties degrade and cause the structural components to fail.

The classical Fick's law is employed to model the diffusive process when the composite material is immersed in humid air or a liquid. The most important assumption invoked in the development of Fick's law is that the solid (in this case, the composite) is assumed to be rigid [145]. Several other assumptions have also been made on the nature of the kinematical quantities such as :

(1) The motion takes place under isothermal conditions.

(2) The velocity components are sufficiently small, therefore, the kinetic energy of the diffusing masses can be neglected.

(3) Body forces are absent.

Hence, it is not surprising that the Fickian model of diffusion proves to be inadequate for predicting the response of materials exposed to normal environmental conditions because of the complex interaction of a composite material and the diffusing moisture.

There are two theories developed in this thesis in order to closely describe the complex physical phenomena. One is based upon the first and second laws of thermodynamics, non-equilibrium thermodynamics and classical continuum mechanics. With the application of classical thermodynamics, the response of the materials which are exposed to the environmental conditions may be completely described by the following equations: the balance equations of mass, momentum and energy, constitutive equations and the equations of entropy inequality. The other is to derive the governing equations by developing a variational principle. Euler equations for the variational principle are the field equations of motion, heat conduction and mass diffusion, and the strain-displacement equations in terms of primary field variables. This principle also yields prescribed boundary conditions on heat flux, mass flux and surface traction vectors.

In most theoretical research publications on modeling the hygrothermal response of composites, the heat conduction and mass diffusion equations are generally decoupled in order to establish a mathematically tractable problem, but this approach is not always appropriate. For example, if a material is simultaneously subjected to both hygrothermal and mechanical loadings, and the rate of change of the material structure is of the same order of magnitude as the rate of change of temperature and moisture concentration, then the general equations governing the cross-effects, i.e. the coupling terms between the stress and temperature, or between the temperature and moisture concentration, are necessary for analyzing this physical problem. For example, a polymeric material which demostrates a strong viscoelastic characteristic is subjected to a prescribed strain, the relaxation of the stress inside the material will persist for a long time. In this case the rate of change of the stress relaxation of the material structure is of the same order of magnitude as the rate of change of temperature and moisture concentration, therefore, the cross-effects are significant and should be taken into account.

1.2.2 Review of This Thesis

The analysis of high-speed linkage mechanisms fabricated from composite materials is a very difficult task because of the complex constitutive behaviors. A fundamental investigation into the dynamic response of four-bar linkages and a slider-crank mechanisms made from a well-known elastic material is undertaken both theoretically and experimentally and is documented in chapter 2 in order to ensure that one has the ability to analyse the more complex mechanism systems. The links of both mechanisms are made from elastic metals. A variational theorem is developed based on extended Hamilton's Principle to establish the equations governing the geometrically nonlinear deformation of an elastic continuous medium subjected to the dynamical loading conditions. The geometrical nonlinearity is defined under the assumption that the deformation is small and so the strain is also small. However, the rotational terms in the strain-displacement equation have the same order of magnitude as the linear terms in the expression. A displacement finite element formulation for a single degree of freedom beam element is presented and all of the analyses performed in this thesis assume that joints are without clearance, thereby greatly simplifying the complexity of modeling the impactive bearing forces. The computer simulation results are compared with experimental results and some design guidelines are drawn from this study.

In chapter 3, an experimental study to demonstrate the superior dynamic response characteristics of mechanisms constructed with composite material is described. This work was performed following a sequence of theoretical research presented in references [158,173,176,178,179]. Mechanical material tests were performed to determine the constitutive behavior of unidirectional and $[\pm45]_s$ angle-ply composite laminates. The dimensions of each link are determined by synthesizing links with a constant flexural rigidity in order to compare the dynamic response of each link when it is incorporated on the mechanism. The damping coefficient of each link is measured by the method of logarithmic decrement. The experimental results clearly demonstrate the superiorities of constructing flexible mechanisms from these two composite materials because of lower stress levels and small deflections.

In chapter 4, the work of chapter 3 is extended in order to study flexible mechanism systems fabricated from composite laminates. The material characteristics from the experimental program were carefully examined and the unidirectional laminate was modelled as elastic material, because of the time-independent behavior, and the $[\pm45]_s$ composite laminate is modelled as viscoelastic material since the material behavior is time-dependent. A mixed variational principle which incorporated auxilary conditions such as the constitutive equation, strain-displacement equation and geometrical boundary conditions into Hamilton's Principle is presented using the Stieltjes convolution integral notation. This variational principle also provides a basis for the finite element formulation which is employed in order to obtain the numerical results. The discrepancy between the experimental results and computer simulations is 10% which may suggest the need for an improved modelling of the constitutive equation.

Composite materials are often sensitive to the environmental conditions such as the changes of temperature and moisture, and the degradation of the material properties are presented in a variety of references including [215,216,217]. A fundamental phenomenological study of the dynamic response of composite materials to a wide range of both mechanical and hygrothermal loadings is proposed and is presented in chapter 5. This study is based upon the first and second laws of thermodynamics, non-equilibrium thermodynamics and the classical continuum mechanics. The application of classical thermodynamics, permits the moving continuous media modeling a complex physical phenomenon, such as changing temperature and moist environment, to be completely described by the following basic equations: the balance of mass, the balance of momentum, the balance of energy and the entropy inequality.

In chapter 6, a variational principle is developed to obtain the linear coupled hygrothermoelastic response of flexible mechanism systems. The primary field variables are taken to be the displacement of a material point and two vector field variables called the entropy displacement and the flow potential displacement which is analogous to entropy displacement. Euler equations for the variational principle are the field equations of motion, heat conduction and mass diffusion, and the strain-displacement equations in terms of primary field variables. This principle also yields prescribed boundary conditions on heat flux vector, mass flux vector and surface traction vector, temperature, material displacement and moisture concentration. A finite element formulation is also performed in order to obtain a numerical mean to render a tractable solution to these complicate equations. An observation may be drawn from the final equations that the cross-effects may occur in the equations of motion, energy balance and mass balance, since a sudden change of temperature, moisture or finite strain may significantly result in the changes of stresses, heat and mass fluxes.

An example in which moisture diffuses into neat epoxy resin and graphite/epoxy composites was investigated by J. M. Whitney and C. E. Browning [217], is examined analytically and the non-Fickian diffusion in bidirectional composite laminates is also studied. The experimental data presented in Figure 3 of reference [217] showed a significant descrepancy from classical Fick's law i.e. the test data approach equilibrium at a slower rate than that predicted by Fick's law. Whitney and Browning postulated that the large in-plane tensile residual stresses which resulted from environmental change increase the initial through-the-thickness diffusivity; then as swelling relieves the residual stresses, the diffusivity decreases. The diffusion coefficient approaches the diffusivity of a unidirectional composite as the residual stresses are completely relieved. Direct proof of a stress-dependent diffusion process, however, requires a measurement of the diffusion coefficient under various constant-stress conditions. As an alternative solution philosophy, a modified Fick's law is proposed herein by incorporating a stress-dependent term in the diffusion equation; the results are compared with experimental data and after a parametrical study is completed, the computer results and the model are discussed. Finally, the extension of current work is proposed at chapter 7.

1.3 Literature Survey for Isothermal Elastodynamic Analyses

The mathematical model of a flexible linkage mechanism must generally capture the mass, stiffness and damping characteristics of the links, the external loading, the equation of closure for kinematic chain, the principal characteristics of the joints of the mechanism, the behavior of the drive shaft and the kinematics of the machine foundation. Finite elements from the structural mechanics literature have generally been employed to model the material properties of the links, and most analyses, with the exception of [29] and [148], assume that the absolute motion of each link may be decomposed into a rigid-body displacement upon which is superimposed a deformation displacement measured relative to a moving coordinate system fixed in the link in an undeformed reference state. Local element matrices [M], [C] and [K] are generally established to model the mass, damping and stiffness characteristics of each link before pre- and post-multiplying by transformation matrices relating the local and global (inertially fixed) reference frames. The trigonometrical functions contained in these transformation matrices are calculated from kinematic analyses of the rigid-linked system in a large number of different configurations.

This manipulation enables the global characteristics of the mechanism to be established by formulating the global matrices prior to incorporating the relevant boundary conditions.

Typically the global equations of motion [174] for a high-speed linkage are written

$$[M_G]\{\ddot{U}\} + [C_G]\{\dot{U}\} + [K_G]\{U\} = -[M_G]\{\ddot{R}\} + \{X\} + \{T\} \quad (1.1)$$

where $\{U\}$ is the column vector of deformation displacements, $(^{\bullet})$ is the absolute time derivative, $[M_G]$, $[C_G]$ and $[K_G]$ are the global mass, damping and stiffness matrices respectively, $\{X\}$ are body forces and $\{T\}$ are surface tractions. The nodal absolute acceleration terms, derived from a rigid-body kinematic analysis of the mechanism, are contained in the vector $\{\ddot{R}\}$, and when multiplied by the mass matrix yields the nodal inertial loading. The equations are then solved for the global degrees of freedom from which link deflections, vibrational response and dynamic stresses may be obtained.

In order that the finite element method be applied to a linkage mechanism, the articulating system is generally modeled as a series of instantaneous structures. Thus the continuous motion of the system is replaced by a sequence of structures at discrete crank angle configurations upon which is imposed the relevant inertial loading. In order that these structures may be solved by the finite element method, the rigid-body degrees of freedom of the linkage must be removed from the model in order to avoid singular matrices. The method of removing the rigid-body degrees of freedom is to assume that the crank may be modelled as a cantilevel beam at each time instant, therefore, the deformation at the build-in end is zero.

Winfrey [196] accomplished this by directly applying the principle of conservation of momentum to the complete mechanism. Imam, Sandor and Kramer [79] considered the crank as a cantilever beam to avoid this complication, and this approach was also employed by Midha et al [103], and Gandhi and Thompson [58]. Nath and Ghosh [107,108] removed the rigid-body degrees of freedom from the global matrices using a matrix decomposition approach.

Having previously reviewed the basic assumptions and nomenclature of finite element methods, attention is now focused on formulating these equations of motion. Winfrey [196,197] employed the displacement finite element method (the stiffness technique of structural analysis) to study the elastic motion of planar mechanisms in some pioneering publications. This popular finite element approach solves for the nodal displacements and requires displacement compatibility on inter-element boundaries. Erdman et al [53] employed the equilibrium finite element method (flexibility method of structural analysis) to study flexible mechanisms. With this approach, adjacent elements have equilibrating stress distributions on inter-element boundaries and the global degrees of freedom are the stress components. This approach is not as popular as the displacement formulation in most fields of finite element work since the additional compatibility equations have to be added in the equilibrium formulation, and mechanism design is no exception.

Midha et al [102-106] were responsible for developing linear and geometrically nonlinear finite element formulations for linkage mechanisms based on Lagrange's equation. The results of this latter work, with Turcic, were validated experimentally [184,185].

Bagci et al [13,14,154] have written a suite of publications on the dynamic response of flexible mechanisms using the linear theory of elasticity. These formulations are based on the stiffness technique of structural analysis.

Thompson et al [57,58,157-161,171-181] developed variational principles as the foundations for studying the linear and geometrically nonlinear elastodynamic responses of linkages. Unlike other methodologies, this class of formulation explicitly presents the boundary conditions and also the governing equations of motion in a single mathematical expression. The analyst then has the freedom to established displacement, equilibrium, mixed or hybrid finite element models from these general variational statements. Variational methods have also been employed to investigate linkages fabricated from light-weight viscoelastic composite materials [178,179,181] and also the acoustic radiation from linkage machinery [175]. This latter work involved modeling the operation of mechanisms submerged in a perfect fluid as a fluid-structural interaction problem based on interacting continua.

Having established the governing equations of motion, boundary conditions and the initial conditions for a particular design task, the engineer must then select the appropriate finite elements for modeling the physical phenomena to be investigated, and a number of questions need to be answered carefully. For example, in a study of the vibrational behavior of a linkage, the designer must decide whether the in-plane and also out-of-plane responses are relevant. Will information on the axial and flexural deformations suffice, or is the torsional deformation field also important? Should a linear or a geometrically nonlinear model be developed? And so on. Generally, these decisions will be guided by engineering intuition or experimental evidence.

A large number of papers [8-10,13-15,20,44-46,53,57,58,79-82,88, 102-108,153,161,177,181] have been devoted to studies of the planar elastodynamic response of flexible linkages by modeling the links using finite elements with only one spatial variable. The axial response is generally modeled by a linear interpolation function and the flexural response by a cubic interpolating polynomial using elements originally derived for structural applications. Bahgat and Willmert [15], in one of the pioneering works in this field, considered both the axial and flexural responses of a wide variety of flexible linkages using a finite element formulation employing higher-order hermite polynomial approximations for the deformation fields. The same quintic element was also employed by Cleghorn et al [44-46]. In [46], a comparison was undertaken between finite elements utilizing quintic polynomial approximations and those based on cubic polynomials. These results not only suggested that axial deformations may be neglected in the analysis of some flexible mechanisms, but also that fewer of the higher-order elements are required to generate a specified solution accuracy when compared with the results from a model incorporating a larger number of lower-order cubic elements. The finite-line-element nomenclature employed by Bagci et al [13,14,154] is an alternative terminology for the standard rod and beam elements of structural mechanics.

The two common formulations for mass matrices, namely the consistent mass matrix [45,53,57,58,102,108,157,158,173,178,179] and the lumped mass matrix [13,14,154] have both appeared in the mechanism design literature. Tong, Pian and Bucciarelli [182] demonstrated that while the lumped mass approach will not suffer any loss in the rate of convergence when utilizing simple rod elements, a consistent mass formulation is to be preferred when using higher-order elements such as beam elements.

Having discussed the mass and stiffness matrices employed to model mechanisms, attention is now focussed on damping matrices. Damping in materials is a complex phenomenon [23] which probably requires the development of thermo-mechanical models in order that it be fully understood.

The assumptions employed to develop damping matrices are partially governed by the solution technique to be adopted for solving the finite element equations. Generally in the mode superposition approach, the damping is assumed to be uncoupled and is given in each mode as a percentage of the critical damping. However, when adopting the step-by-step approach of numerical integration the complete damping properties of the mechanism must be established and this may be a difficult task.

In the appendix of reference [104], Midha, Erdman and Frohrib discussed the different damping matrices in the context of modal superposition solutions. Winfrey [196] assumed a damping matrix proportional to a linear combination of the mass and stiffness matrices (Rayleigh damping). In contrast to this, Alexander and Lawrence [8] assumed the damping coefficient, C_{ii}, for each orthogonal coordinate to be defined by $C_{ii} = 2\xi_i(K_{ii}/M_{ii})^{1/2}$, where ξ_i is the damping ratio, K_{ii} is the stiffness matrix and M_{ii} is the mass matrix. Furthermore, $(K_{ii}/M_{ii})^{1/2}$ are the natural frequencies of the mechanism system.

The energy-dissipation characteristics of a mechanism are dependent upon both the constitutive equations of the link material and also the characteristics of the joints of the mechanism. In recent combined experimental and finite-element-based investigations [159,166,176,177,180,185], logarithmic decrement transient response studies have been undertaken for a number of mechanism configurations and the experimental data employed to establish semi-empirical damping matrices for the damping in the mechanism. Bagci and Stamps [154] have undertaken preliminary work on coulomb damping in joints, which they then combine with the model for material damping employed in [8], thereby employing individual mathematical models for both mechanism joins and also the link materials.

Two computational methods are generally employed to solve the equations of motion for both linear and geometrically nonlinear vibrational analyses. These are the modal superposition approach [81,105,185,196] and the use of direct integration methods [8,29,58,107], such as Runge-Kutta algorithms or the Newmark method.

The former approach is based on the assumption that the displacement vector may be expressed as a linear combination of the vibrational mode shapes. This solution strategy is most efficient if the essential dynamic response of the mechanism is contained in the first few modal combinations. Hence it is most useful for studying the steady-state response of systems operating at constant crank frequencies. However, additional complexities arise when developing geometrically nonlinear elastodynamic responses [185]. The approach is not to be recommended for linkages fabricated with journal bearings because the inherent clearance needed for the operation of these joints creates impact loading which is often characterized by high frequency components necessitating a solution based on many modes in order to predict the response of the mechanism.

Numerical integration algorithms employ step-by-step procedures. Instead of attempting to solve the equations of motion at any time t, they only solve the equations at discrete time intervals Δt apart. Although, of course, this time interval may be made extremely small to closely approximate a continuous function. Furthermore, these algorithms assume a definite variation of the displacement, velocity and accelerations within each time interval, and this has a major effect on the stability, accuracy and cost of the solution. These approaches can be readily applied to determine both linear and geometrically nonlinear elastodynamic responses, and furthermore, they may be applied to accurately model systems subjected to complex loading, or loads containing significant high frequency components.

Imam, Sandor and Kramer [79] applied the rate of change of eigenvalue-vector method to mechanisms, in order to undertake deflection and stress analyses. This approach eliminated the need for an eigenvalue solution at all the mechanism configurations subjected to analysis.

Midha, Erdman and Frohrib [105] develped a technique for directly determining the steady-state solution of differential equations with time-periodic coefficients, which govern the elastodynamic motion of high-speed linkages. The same authors were also responsible for developing an alternative solution strategy to the same class of problem [103], and in addition, a numerical algorithm for performing transient analyses of linkages [106].

While the above procedures are dedicated to determine the elastodynamic response of linkages, some authors have advocated that a quasi-static analysis of a linkage mechanism is quite adequate for most design purposes in an industrial environment [84]. Since most of the complications associated with an elastodynamic analysis are avoided by adopting this philosophy, the results are less costly, but they are also less accurate. This approach requires the solution of a set of nonhomogeneous algebraic equations to be obtained, and this is readily accomplished using one of the Gaussian elimination family of algorithms.

All of the mathematical models for flexible linkages involve a large number of degrees of freedom and hence a large number of equations of motion must be solved. This is computationally inefficient and hence expensive. However, this may be overcome by using static condensation techniques and an approach was developed by Khan and Willmert [84]. This philosophy involves condensing all internal degrees of freedom of each link to create a super element with only the principal degrees of freedom retained, and has been used extensively in commercial codes for structural dynamics problems. The authors reduced the number of system equations by 50 percent, so that the computational effort, which is proportional to the cube of the number of equations, was considerably reduced. As they rightly indicated in [84], this approach is especially useful when the designer is searching for an optimal solution which generally involves many iterative analyses.

The vast majority of the papers on flexible mechanisms present vibrational analyses of slider-crank or four-bar linkages comprising one or more elastic members and sited on a stationary rigid foundation. Deformations are generally restricted to axial and flexural modes in the plane of the mechanism and column vectors [X] and {T} in equation (1.1) are often neglected. This approach yields, for example, a transverse flexural vibration comprising a periodic response upon which is superimposed a high frequency waveform near the fundamental natural frequency in flexure of the link being studied. Steady state responses

[15,45,103,108] and also transient responses [106] have been obtained. Since these classes of solution can be computationally time consuming, some authors [84,125] have advocated that a quasi-static analysis is adequate for the analysis of most industrial machinery. This approach neglects the terms $[M_G][\ddot{U}]$ and $[C_G][\dot{U}]$ in equations (1.1), thereby considering the mechanism to be a statically loaded structure. This assumption greatly simplifies the computational aspects of the finite element analysis and the response comprises only the periodic waveform component of the vibrational response cited earlier.

Inertial terms coupling the rigid-body kinematics and the elastodynamic response have been featured in some analyses [45,104,107,180,185]. However, while these analyses present a more accurate mathematical model of the mechanism, these terms have, so far, been found to have a negligible effect on the elastodynamic response of the experimental mechanisms investigated in the laboratory [159,184,185].

The higher-order theories modeling the elastic motion of links employ geometrically nonlinear analyses which retain the terms in the strain-displacement equations that couple the axial and flexural deformations [107,108,147,180,185]. These additional terms are readily handled by the numerical integration solution philosophy, but they present additional complications if the modal superposition approach is employed.

The early work on finite element analyses employed only one element to model each flexible link [8] and [196]. This naturally produced inaccurate results, since one of the fundamentals of finite element techniques is the assurance of solution convergence as the number of elements in a model is increased. This was originally highlighted by Alexander and Lawrence [7-9] in pioneering work on combined experimental and computational investigations of flexible four-bar linkages. Midha, Badlani and Erdman [102] reinforced these conclusions by demonstrating the effects of multi-element idealizations on the response of a structure. They showed that a 15 percent error existed in the second mode frequency and a 400 percent error in the third mode when a single element was employed. Similar errors were demonstrated by Gamache and Thompson [57] as part of a comparative study on modeling the flexural response of four-bar linkages using Timoshenko and Euler-Bernoulli beam elements.

Most of the work to date on planar flexible mechanisms has concentrated on the planar response, thereby neglecting the co-planar motion of industrially realistic systems in which torsional effects, due to the offset of the joint members, may be significant. Preliminary work on this subject has been undertaken by Stamps and Bagci [154].

Although the natural frequencies of a mechanism are continually changing during the operating cycle, as the stiffness and mass characteristics relative to a fixed reference frame change, nevertheless, critical speed ranges must be identified and avoided in practice. This class of problem has been investigated by Bagci et al [13,14] using finite line elements and lumped mass matrices to study slider-crank mechanisms, four-bar linkages and also six-bar mechanisms. Solutions were generated by an eigenvalue algorithm and compared with experimental data.

The synthesis of rigid-linked mechanisms may be accomplished by either precision-point procedures or else optimization techniques which impose constraints on the minimization of an objective-function [170]. In order that these latter modern techniques be applied to synthesize flexible mechanisms, where deflections and dynamic stress levels are also introduced as constraints, the synthesis package must iteratively interact with software for analyzing flexible mechanisms. This is because the analysis and synthesis procedures cannot be conveniently decoupled, as occurs in the design of rigid-linked mechanisms. While a considerable number of papers have been published on the analysis of flexible mechanisms, only a very small number have been written on the synthesis of these systems [44,80,81,84,125,202,203] and they are all based on finite element methods.

Before discussing the different solution strategies, it is appropriate to again review equation (1.1), which provides the key to understanding the proposed methodologies. Generally, when a mechanism is operating in a high-speed mode the body force and surface tractions may be neglected in comparison with the inertial loading, hence [X] and {T} disappear. Premultiplying all the terms by the inverse of the mass matrix $[M_G]^{-1}$ yields

$$[I][\ddot{U}] + [M_G]^{-1}[C_G][\dot{U}] + [M_G]^{-1}[K_G][U] = -[I][\ddot{R}] \quad (1.2)$$

Thus it is evident that for a given mechanism operating at a given speed, the elastodynamic response is governed by the energy dissipation per unit mass and also the stiffness-to-mass ratio of the mechanism links. In other words, a high stiffness-to-weight ratio will result in small deflections and stresses. This observation has spawned two design philosophies. The first [44,80,81,84,202,203] involves designing links in the commercial metals while optimizing the cross-sectional geometry of the members. The second [125] advocates that modern fiberous composite laminates should be employed because of their inherent superior damping, and higher stiffness-to-weight ratios.

Erdman, Sandor et al [52,53,79-81] developed a general method of kineto-elastodynamic analysis and synthesis in aluminum alloys using optimization techniques, which incorporated stress and deflection constraints, to develop special cross-sectional shapes and tapered members.

Willmert et al [84] developed the optimality criterion optimization technique for mechanism design. This is based on the Kuhn-Tucker conditions of optimality for the minimum-weight design of mechanisms subjected to stress limits with the variables being the cross-sectional geometry of the links.

Cleghorn, Fenton and Tabarrok [44] employ the same algorithm as in [84] with the modification that each interation incorporates the effect of the inertial loading of one link upon the stress levels as all the other links. This modification substantially reduced the number of interations needed to achieve the optimum solution when employing the finite element formulation presented in [45].

Zhang and Grandin [202,203] developed a novel approach which combines the previous optimality criterion technique with a kinematic refinement technique to achieve an optimal solution. This marriage involves a finite element analysis, a modern optimization algorithm and also a rigid-linked mechanism synthesis procedure for adjusting link lengths, location of fixed pivots, etc., in a unified approach. The authors achieve considerable success with this method, recording a design weighing only 27 percent of that obtained in [44] when addressing the same synthesis problem.

In contrast to the prevous approaches which are all concerned with homogeneous isotropic materials, Thompson et al [158,160,173,178] have proposed that material selection should enter the design process. No longer should the search for appropriate materials be restricted to the metals but it should also include composite materials which offer much more desirable properties [173,176-179,181]. Finite element models have been developed by extending the standard rod and beam elements to model the effect of ply angles upon link stiffnesses and to also represent viscoelastic materials. The models have been verified in combined experimental and computational studies [58-60,63,66,68] and the superior response demonstrated in experimental comparative studies [160].

A third approach for synthesizing flexible linkages [125] proposes that a microprocessor-controlled actuator should be introduced into the original mechanism in order to modify the inertial loading and hence stress levels in the system. The analysis phase of the synthesis algorithm is undertaken using standard finite element theory.

A systematic study is undertaken in the subsequent chapters for obtaining the dynamic response of high-speed linkage mechanisms fabricated from composite materials operating under both isothermal and extreme environmental conditions. A theoretical and experimental investigation of the dynamic response of flexible linkage mechanisms constructed from a well-known elastic material operating under isothermal conditions is presented in chapter 2 in order to ensure that one has the capability to analyse the more complex mechanism systems.

CHAPTER 2

A THEORETICAL AND EXPERIMENTAL INVESTIGATION INTO THE DYNAMIC RESPONSE OF FLEXIBLE MECHANISMS MADE FROM ELASTIC MATERIALS AND OPERATING UNDER ISOTHERMAL CONDITIONS

The analysis of high-speed linkages mechanism fabricated from composite materials is a very difficult problem because of the complex constitutive behaviors. The ability to predict the dynamic response of systems constructed from a well-known elastic materials is an essential step in order to ensure that one has the capability to analyse the more complex mechanism systems. This is what is undertaken herein.

2.1 A Variational Formulation for The Geometrically Nonlinear Finite Element Analysis of Flexible Linkages Made from Elastic Materials Operating under Isothermal Condition

The Lagrange's equation was employed by a few researchers in the field of machine dynamics in order to develop the equations of motion which govern the dynamic behaviors of the mechanisms. B.S. Thompson and A.D.S. Barr [172] proposed a mixed variational approach which incorporates auxiliary conditions such as the strain-displacement equation, constitutive equations and geometrical boundary conditions into the Hamilton's principle. So the functional depends upon displacement, stresses and strains. Moreover, the stationary conditions are the governing equations in primitive form: the kinematical, dynamical and constitutive relationship. More insights may be drawn from this mixed variational principle via a finite element formulation which discretizes a continuous medium into several finite elements. As the basis of an elementary approximation, each field can be independently selected to achieve the discrete model. Namely, the approximating function of stresses may be different from that of the strains. The discrete counterparts of the displacement, stresses and strains are governed by algebraic equations: kinematical, dynamical and constitutive. This approach offers an effective mean to achieve simple, efficient models that possess the desirable attributes of those derived by approximating the displacement in the potential.

The variational theorem forming the kernel of this theoretical study was originally developed in the doctoral thesis of B.S. Thompson [220]. It incorporates the geometrically nonlinear form of the field equations so that it may provide a basis for analyzing linkages susceptible to dynamic instabilities, and also mechanism systems that must be analyzed using higher-order theories. The deformation displacements are assumed to be small, and the strains are also assumed to be small, however, the rotational terms in the strain-displacement equations are assumed to be of the same order of magnitude as the linear terms in these expressions [116].

The variational equation of motion governing the motion of a continuum of volume V and surface area S representing a portion of a link incorporating a revolute joint and also a sliding joint may be written using a general tensor notation [220] as

$$\delta J = 0 = \int_{t0}^{t1} \Big[\int_V \delta\gamma_{ij}\big[\sigma_{ij} - \partial W/\partial\gamma_{ij}\big]\, dV$$

$$+ \int_V \delta u_i\big[\, X_i + \sigma_{ij,j} + u_{i,kj}\sigma_{jk} + u_{i,k}\sigma_{jk,j} - \rho\dot{p}_i \,\big]\, dV$$

$$+ \delta r_{oi} \Big[\int_V X_i\, dV + \int_{S_1} \bar{g}_i dS_1 - \int_V \rho\dot{p}_i\, dV\Big]$$

$$+ \delta\phi_j \Big[\int_V e_{ijk} X_i (\, r_{ok} + r_{Rk} + u_k \,)\, dV$$

$$+ \int_{S_2} e_{ijk}\bar{g}_i (r_{ok} + r_{Rk} + u_k)\, dS_2$$

$$+ \int_V e_{ijk}\rho\dot{p}_i (r_{ok} + r_{Rk} + u_k)\, dV \,\Big]$$

$$+ \int_V \delta\sigma_{ij} \big[\, \gamma_{ij} - 1/2(\, u_{i,j} + u_{j,i} + u_{k,i}u_{k,j} \,) \,\big] dV$$

$$- \int_V \rho\delta p_i\big[p_i - [\tilde{r}_{oi} + \tilde{u}_i + e_{ijk}\dot{\phi}_j (r_{ok} + r_{Rk} + u_k)]\,\big]\, dV$$

$$+ \int_{S_1} \delta u_i (\bar{g}_i - g_i - g_k u_{i,k}) dS_1$$

$$+ \int_{S_2} (\delta g_i + \delta g_k u_{i,k} + g_k \delta u_{i,k})(\bar{u}_i - u_i)\, dS_2$$

$$+ \int_{S_3} (\, \delta g_z + \delta g_k u_{z,k} + g_k \delta u_{z,k} \,)/\cos\phi$$

$$(u_x \sin\phi + u_z \cos\phi) dS_3 \,\Big]\, dt \qquad (2.1.1)$$

In Figure (2.1), the link has a Lagrangian axis frame oxyz fixed in the member in a reference state with zero stresses and strains, and the system parameters are defined relative to these coordinates. An arbitrary point P in the link is defined by the position vector $r_i = r_{oi} + r_{Ri} + u_i$, where r_{oi} are the components of the position vector of the origin of the body axes oxyz relative to the origin of an inertial reference frame OXYZ, r_{Ri} represents the position vector of point P in the undeformed reference state relative to the body axes, and u_i is the displacement vector.

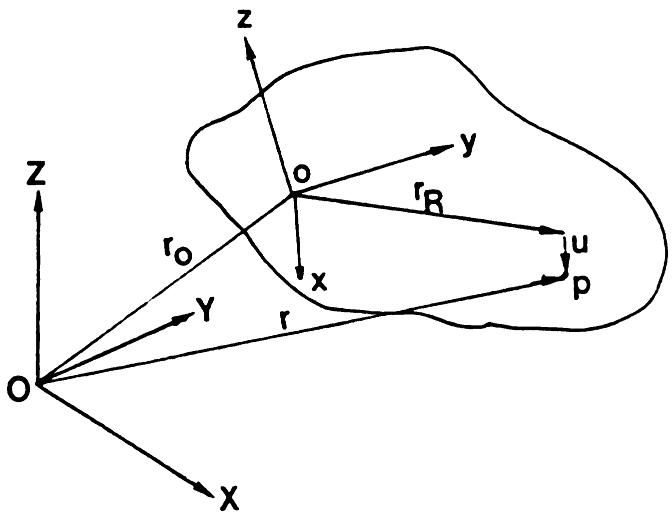

Figure 2.1 Definition of Axis Systems and Position Vectors

The absolute velocity associated with the time rate of change in r_i is written as p_i, ρ is the mass density, X_i is the body force per unit volume, W is the strain energy density, γ_{ij} is the nonlinear Lagrangian strain tensor and σ_{ij} is the associated stress tensor. Components of the angular velocity vector for the moving Lagrangian frame are represented by θ_j and e_{ijk} is the alternating tensor. The time rate of change with respect to oxyz is denoted by ($\tilde{}$) while the absolute rate of change is denoted by ($^\circ$). The comma represents the covariant derivative.

The definition of this class of mixed boundary value problems is completed by prescribing surface tractions $\bar{s}_i$ on region S_1, while surface displacements $\bar{u}_i$ are prescribed on region S_2. The surface region S_3 has a special constraint imposed upon it which models the kinematic action of a sliding joint, [172] and this constraint appears under the final integral in equation (2.1.1), where ϕ is the angle between the adjacent links at the joint. The constraint requires the direction of the resultant deformation vector at the joint to always be coincident with the axis of the guide. Hence, for example, the deformation components of the axial and flexural displacement fields must combine in the prescribed manner to ensure this.

The objective that follows is to develop from first principles a displacement finite element formulation for the analysis of the nonlinear vibrational behavior of linkages fabricated with straight slender flexible beam-shaped members. This is accomplished by first assuming that the flexural deformation field being modeled by the element is governed by the classical Bernoulli-Euler hypothesis.

The amount of detail sought by different analyses has resulted in a large number of theories being developed for predicting the nonlinear vibrational response of beam systems and many are cited in [136]. One of the principal reasons for this large variety of theories is due to the different assumptions employed to describe the elastic geometrical nonlinearity expression, which typically couples the axial and flexural modes of deformation. Other simplifying assumptions are also generally introduced into the equations of motion to make them mathematically tractable, or else reduce the computing effort, by neglecting higher-order terms. The presentation that follows is no exception.

The objective, herein, is to develop a displacement formulation for a single one-dimensional finite element with two exterior nodes, each having three nodal degrees of freedom. Two nodal variables W and θ describe the flexural displacement and slope respectively, while U describes the longitudinal displacement.

Defining the nodal displacement vector for the element by

$$[U]^T = [U_1 \; U_2 \; W_1 \; W_2 \; \theta_1 \; \theta_2] \qquad (2.1.2)$$

then the general displacements u(x,t) and w(x,t) at any point in the element may be related to [U] by

$$[u\ w]^T = [N][U] \tag{2.1.3}$$

where [N] contains the shape functions.

The axial displacement is defined by

$$u(x,t) = [N_1][U] + \int_0^x 1/2[U]^T[\acute{N}_{nl}]^T[\acute{N}_{nl}][U]dx \tag{2.1.4}$$

where $[N_1]$ is the shape function for the linear terms, $[N_{nl}]$ the shape function associated with the nonlinear terms, and (′) denotes spatial differentiation with respect to x. This notation has been adopted to clarify the linear and nonlinear terms in the subsequent mathematical development. The transpose is denoted by T. A more familiar formulation of equation (2.1.4) may be found in many works on nonlinear vibrations, such as [34], and this is

$$u_x = u_0 - z\partial w/\partial x + \int_0^x 1/2(\partial w/\partial x)^2 dx \tag{2.1.5}$$

where u_0 is the axial displacement, w(x,t) the transverse displacement, and x is the longitudinal spatial variable. The axial strain corresponding to (2.1.4) may be written as the sum of the linear and nonlinear terms. Thus,

$$[\gamma_{xx}] = [\gamma_{xx}]_1 + [\gamma_{xx}]_{nl} \tag{2.1.6}$$

or

$$[\gamma_{xx}] = [\acute{N}_1][U] + 1/2[U]^T[\acute{N}_{nl}]^T[\acute{N}_{nl}][U] \qquad (2.1.7)$$

which may be amplified to explicitly define $[\acute{N}_1]$ and $[\acute{N}_{nl}]$,

$$[\gamma_{xx}] = [\ \acute{N}_{11},\ \acute{N}_{12},\ -z\acute{N}_{13},\ -z\acute{N}_{14},\ -z\acute{N}_{15},\ -z\acute{N}_{16}\ ]$$

$$[\ U_1,\ U_2,\ W_1,\ W_2,\ \theta_1,\ \theta_2\ ]^T$$

$$+\ 1/2[\ U_1,\ U_2,\ W_1,\ W_2,\ \theta_1,\ \theta_2\ ]$$

$$[\ 0,\ 0,\ \acute{N}_{n13},\ \acute{N}_{n14},\ \acute{N}_{n15},\ \acute{N}_{n16}\ ]^T$$

$$[\ 0,\ 0,\ \acute{N}_{n13},\ \acute{N}_{n14},\ \acute{N}_{n15},\ \acute{N}_{n16}\ ]$$

$$[\ U_1,\ U_2,\ W_1,\ W_2,\ \theta_1,\ \theta_2\ ]^T \qquad (2.1.8)$$

Assuming that the constitutive equations have a very small dependence upon the rate of loading of the material, then the variational equation of motion (2.1.1) may be written as

$$\delta J = 0 = \int_{t0}^{t1} \Big[\int_V [\delta\gamma_{xx}]^T([\sigma_{xx}]-[C][\gamma_{xx}] - [C_1][\dot{\gamma}_{xx}])dV$$

$$- \int_V \rho[\delta P]^T([P]-[N_R][P_R]-[N][\dot{U}])dV$$

$$- \int_V \delta u_i(X_i+\sigma_{ij,j}-u_{i,kj}\sigma_{jk}+u_{i,k}\sigma_{jk,j}-\rho\dot{P}_i)dV$$

$$+ \int_V [\delta\sigma_{xx}]^T([\gamma_{xx}]-[\acute{N}_1][U] - 1/2[U]^T[\acute{N}_{nl}]^T [\acute{N}_{nl}][U])dV$$

$$+ \int_{S_1} [\delta U]^T[N]^T([\bar{g}]-[g]-[g]^T[\acute{N}][U])dS_1$$

$$- \int_{S_2}([\delta g]^T+[\delta g]^T[\acute{N}][U]+[g]^T[\acute{N}][\delta U])([\bar{U}] -[N][U])dS_2$$

$$+ \int_{S_3}([\delta g_z]^T+[\delta g]^T[\acute{N}][U_z]+[g]^T[\acute{N}][\delta U_z])$$

$$([U_x]\sin\theta-[U_z]\cos\theta)/\cos\theta \; dS_3 \Big]dt \qquad (2.1.9)$$

where [C] is the constitutive matrix, $[C_1]$ is a damping matrix providing stresses proportional to the strain rate, $[N_R]$ contains the shape functions approximating the rigid-body kinematics (to be described later) while $[P_R]$ is the column vector containing the nodal rigid body kinematic degrees of freedom. The nodal absolute velocity components are defined by [P] and the surface tractions by [g]. In addition, the terms $[U_x]$ and $[U_z]$ are defined by

$$[U_x]^T = [\; U_1 \quad U_2 \quad 0 \quad 0 \quad 0 \quad 0 \;] \qquad (2.1.10)$$

and

$$[U_z]^T = [\; 0 \quad 0 \quad W_1 \quad W_2 \quad \theta_1 \quad \theta_2 \;] \qquad (2.1.11)$$

Finally, because the rigid-body equations of motion are of no consequence here, they may be removed from the formulation by taking variations $[\delta r_{oi}]$ and $[\delta\theta_i]$ to be zero.

In order to complete the transformation of the variational theorem from an expression written in a Cartesian tensor notation to a matrix relationship appropriate for a finite element analysis, attention is focused upon the equations of equilibrium obtained from the second term in equation (2.1.9). The second term may be written

$$\int_V [\delta U]^T [N]^T \partial[\sigma_{xx}]/\partial x dV \qquad (2.1.12)$$

An integration-by-parts over x yields

$$\left[\int_A [\delta U]^T [N]^T [\sigma_{xx}] dA\right]_x - \int_V [\delta U]^T [\acute{N}]^T [\sigma_{xx}] dV \qquad (2.1.13)$$

The first term in equation (2.1.13) is a boundary term, to be evaluated on the cross-sectional area A, which will be manipulated later. For a homogeneous, isotropic material, the second term becomes, using the first and fourth integral expressions in equation (2.1.9),

$$- \int_V [\delta U]^T [\acute{N}_1]^T [\acute{N}_1] E [U] dV - \int_V [\delta U]^T 2 [\acute{N}_1]^T$$

$$[U]^T [\acute{N}_{nl}]^T [\acute{N}_{nl}]^T [U] E/2 dV$$

$$- \int_V 1/4[\delta U]^T[\acute{N}_{nl}]^T[\acute{N}_{nl}][U][U]^T[\acute{N}_{nl}][\acute{N}_{nl}]dV$$

$$- \int_V [\delta U]^T[\acute{N}_1]^T[C_1][\acute{N}][\mathring{U}]dV$$

$$- \int_V 1/2[\delta U]^T[U]^T[\acute{N}_{nl}]^T[\acute{N}_{nl}][C_1][\acute{N}][\mathring{U}]dV \qquad (2.1.14)$$

The first term in equation (2.1.14) yields the standard linear stiffness matrix $[K_1]$ defined by

$$[K_1] = \int_V [\acute{N}_1]^T E[\acute{N}_1]dV \qquad (2.1.15)$$

The second term in (2.1.14) defines $[K_2]$ which is one of several stiffness matrices incorporating elastic geometrical nonlinearity terms and is explicitly defined by

$$[K_2] = \int_0^L [F_x]_1[\acute{N}_{nl}]^T[\acute{N}_{nl}]dx \qquad (2.1.16)$$

where L is the length of the finite element and $[F_x]_1$ is the linear component of the axial force defined by

$$[F_x]_1 = EA[\acute{N}_1][U_x] \qquad (2.1.17)$$

since the antisymmetric terms in z disappear upon integration.

The third term in equation (2.1.14) is neglected, being of fourth order, while the fourth term is linearized to give a damping matrix

$$[D_1] = \int_V [\dot{N}_1]^T [C_1] [\dot{N}_1] dV \qquad (2.1.18)$$

The fifth term is also neglected because of higher-order derivatives.

Returning to the third integral expression in equation (2.1.9), the third and fourth terms may be combined as the derivative of a product, and upon subjecting this expression to Gauss' theorem they yield

$$\int_V \delta u_i (u_{i,k}\sigma_{kj})_{,j} dV$$

$$= \left[\int_A \sigma_{jk} n_j u_{i,k} \delta u_i dA\right]_x - \int_V \sigma_{kj} u_{i,k} \delta u_{i,j} dV \qquad (2.1.19)$$

where n_j is the unit-vector normal to the surface. The first term on the right-hand-side of (2.1.19) is a boundary term to be considered later, while the second term may be written

$$-\int_V [\delta U]^T \Big[\ [\dot{N}_1] + 1/2 [\dot{N}_{n1}]^T [\dot{N}_{n1} [U]\ \Big]^T [\sigma_{xx}]$$

$$- \Big[\ [\dot{N}_1] + 1/2 [U]^T [\dot{N}_{n1}]^T [\dot{N}_{n1}]\ \Big] [U] dV \qquad (2.1.20)$$

Upon substituting for $[\sigma_{xx}]$ from the first and fourth integrals in equation (2.1.9), only the following three lower-order terms are retained from the twelve terms obtained from the expansion of (2.1.20)

$$-[\delta U]^T[K_3][U]-[\delta U]^T[K_4][U]-[\delta U]^T[D_3][\dot{U}] \qquad (2.1.21)$$

Stiffness matrix $[K_3]$, depends upon the linear axial force and is defined by

$$[K_3] = \int_0^L [F_x]_1[\acute{N}_1]^T[\acute{N}_1]dx \qquad (2.1.22)$$

Matrix $[K_4]$, however, contains terms modeling the geometrically nonlinear elastic behavior and is defined by

$$[K_4] = 2\int_0^L 1/2[F_x]_1[U]^T[\acute{N}_1][\acute{N}_{nl}]^T[\acute{N}_{nl}]dx \qquad (2.1.23)$$

Matrix $[D_3]$ is a damping matrix, associated with the nonlinear behavior and is defined by

$$[D_3] = \int_0^1 [F_x]_1[\acute{N}_1]^T[C_1][\acute{N}_1]dx \qquad (2.1.24)$$

This completes the operations on the elastic terms governing the deformation throughout the volume V and attention is now focused on the boundary terms modeling surface tractions. The unit vectors on the ends of a one-dimensional element with plane faces, described relative to a Cartesian reference frame, are orthogonal. Consequently, upon incorporating the direction cosines into the fifth integral expression in equation (2.1.9) and adding it to the first term in equation (2.1.13) and also the boundary term in equation (2.1.19), terms cancel to yield

$$\int_{S_1} [\delta U]^T [N]^T [\bar{g}] \, dS_1 \qquad (2.1.25)$$

The manipulations of the elastic terms are now complete and attention is focused on the dynamic behavior of a link which is governed by the second integral expression in equation (2.1.9). This expression must be differentiated with respect to time and substituted into the final term in the second integral in equation (2.1.9). Instead of adopting this direct approach, an alternative method will be employed [172], in an effort to better demonstrate the parallels between classical methodology and a numerically-orientated formulation. Fundamental kinematical theory states that the absolute acceleration of one point, say B, on the link is the acceleration of point P relative to point B. Confining attention to the axial (ox) and flexural (oz) deformations u and w, respectively, the following statement may be readily developed [172]:

$$\ddot{P}_{px} = \ddot{P}_{Bx} + \ddot{u} + \ddot{\phi} w + 2\dot{\phi}\dot{w} - \dot{\phi}^2 (r+u)$$

$$\ddot{P}_{pz} = \ddot{P}_{Bz} + \ddot{w} - \ddot{\phi}(r+u) - 2\dot{\phi}\dot{u} - \dot{\phi}^2 w \qquad (2.1.26)$$

where r is the length of the position vector defining the position of point P, relative to B in the undeformed configuration, and $\dot{\phi}$ and $\ddot{\phi}$ are the angular velocity and acceleration of the link. It is assumed that

$\ddot{P}_{Bx}$ and $\ddot{P}_{Bz}$ may be approximated by classical rigid-body kinematic terms alone, but a more refined approach may be developed [172] where additional degrees of freedom are used to model the system.

The absolute rigid-body acceleration of point B may be written

$$[\ddot{P}_{RB}] = \begin{bmatrix} \ddot{P}_{RBx} \\ \\ \\ \ddot{P}_{RBz} \end{bmatrix} = \begin{bmatrix} \ddot{P}_{Bx} - r\dot{\phi}^2 \\ \\ \\ \ddot{P}_{Bz} - r\ddot{\phi} \end{bmatrix} = [N_R][\ddot{P}_R] \qquad (2.1.27)$$

where $[N_R]$ contains the shape functions modeling the linear distribution of the absolute rigid-body acceleration within the finite element and is the vector of nodal degrees of freedom. If, by using equations (2.1.10) and (2.1.11), equation (2.1.3) is rewritten as

$$\begin{bmatrix} u \\ \\ w \end{bmatrix} = \begin{bmatrix} u_x \\ \\ u_z \end{bmatrix} = \begin{bmatrix} N_x & 0 \\ & \\ 0 & N_z \end{bmatrix} \begin{bmatrix} U_x \\ \\ U_z \end{bmatrix} \tag{2.1.28}$$

then equation (2.1.26) may be reformulated as

$$[\ddot{P}] = [N_R][\ddot{P}_R] + [N][\ddot{U}] + 2\dot{\theta} \begin{bmatrix} 0 & N_z \\ & \\ -N_x & 0 \end{bmatrix} [\dot{U}] \begin{bmatrix} -\dot{\theta}^2 N_x & \ddot{\theta} N_z \\ & \\ -\ddot{\theta} N_x & -\dot{\theta}^2 N_z \end{bmatrix} [U] \tag{2.1.29}$$

Substituting (2.1.29) into the final term in the third integral in equation (2.1.9) yields the expression

$$-[\delta U]^T[M_R][\ddot{P}_R] - [\delta U]^T[M][\ddot{U}] - [\delta U]^T[M_{COR}][\dot{U}]$$
$$-[\delta U]^T[M_{IC}][U] \tag{2.1.30}$$

where $[M_R]$ is the mass matrix associated with the rigid-body motion and is defined by

$$[M_R] = \int_V \rho [N]^T [N_R] dV \tag{2.1.31}$$

the second matrix, $[M]$, is defined by

$$[M] = \int_V \rho [N]^T [N] dV \tag{2.1.32}$$

the third matrix, $[M_{COR}]$, is associated with the Coriolis acceleration, and is defined by

$$[M_{COR}] = \int_V 2\dot{\theta}\rho \begin{bmatrix} N_x & 0 \\ & \\ 0 & N_z \end{bmatrix}^T \begin{bmatrix} 0 & N_z \\ & \\ -N_x & 0 \end{bmatrix} dV \tag{2.1.33}$$

and the final matrix, $[M_{IC}]$, describes the inertial coupling between the gross rigid-body motion of the mechanism and the elastic deformation kinematic terms. It is defined by

$$[M_{IC}] = \int_V \rho \begin{bmatrix} N_x & 0 \\ & \\ 0 & N_z \end{bmatrix}^T \begin{bmatrix} -\dot{\theta}^2 N_x & -\ddot{\theta} N_z \\ & \\ -\ddot{\theta} N_x & -\dot{\theta}^2 N_z \end{bmatrix} dV \tag{2.1.34}$$

The variational equation of motion may now be written in the final form

$$\delta J = 0 = \int_{t0}^{t1} \Big[\int_V [\delta\gamma_{xx}]^T ([\sigma_{xx}] - E[\gamma_{xx}] - [C_1][\dot{\gamma}_{xx}]) dV$$

$$- \int_V \rho [\delta P]^T([P]-[N_R][P_R]-[N][\mathring{U}])dV$$

$$+ [\delta U]^T(([K_1]+[K_2]+[K_3]+[K_4]+[M_{IC}])[U]$$

$$+([D_1]+[D_2]+[M_{COR}])[\mathring{U}]+[M][\ddot{U}] - \int_V [N]^T[X]dV$$

$$- \int_{S_1} [N]^T[\bar{g}]dS_1-[M_R][\mathring{P}_R]) \qquad (2.1.35)$$

$$+ \int_V [\delta\sigma_{xx}]^T([\gamma_{xx}]-[\acute{N}_1][U] - 1/2[U]^T[\acute{N}_{nl}]^T [\acute{N}_{nl}][U])dV$$

$$- \int_{S_2} ([\delta g]^T+[\delta g]^T[\acute{N}][U]+[g]^T[\acute{N}][\delta U])([\bar{U}] -[N][U])dS_2$$

$$+ \int_{S_3}([\delta g_z]^T+[\delta g]^T[\acute{N}][U_z]+[g]^T[\acute{N}][\delta U_z])$$

$$([U_x]\tan\theta-[U_z])dS_3 \Big]dt$$

Equation (2.1.35) contains the field equations and displacement boundary conditions for one finite element and these governing equations may be obtained by taking arbitrary independent variations of the variables in this variational equation of motion. The resulting matrix formulation must be pre- and post-multiplied by standard transformation matrices in order that this general statement be used to develop a finite element model of a specific linkage. The matrices formulating the equations of motion, which are contained in the third term of equation (2.1.35), are presented explicitly in the Appendix of reference [180].

Having established the theory and the finite element formulation which provide a numerical scheme to theoretically predict the dynamic response of the high-speed flexible linkage mechanisms, an experimental study is necessary in order to prove the applicability of the theory. The experimental set-up and the procedures will be described in the following section.

2.2 Experimental Study

In the field of research dedicated to flexible mechanism systems there have been a number of combined theoretical and experimental studies, which include references [51,60,82,137,154,162,171,184,185]. Upon reviewing these publications and others, it is evident that most investigators have focused upon four-bar linkages and only a small number of papers have been dedicated to studying the flexural response of slider crank mechanisms incorporating bearings without clearance. Furthermore, there have been no combined experimental and finite element publications on flexible slider crank mechanisms, even though this is a very common linkage in industry.

Herein, the results of a comprehensive experimental study on the dynamic response of slider-crank linkages configured with the plane of the mechanism perpendicular to the gravitational field, and also four-bar linkages with the plane of the mechanism colinear with the gravitational field are presented. These kinematic chains were constructed with several link-length ratios and different link cross-sectional dimensions, and the systems operated over a wide-range of speed to generate a large variety of response histories for evaluating the predictive capabilities of the mathematical model developed above.

2.2.1 Experimental apparatus: Four-bar linkages

A photograph of the experimental four-bar linkage apparatus used in this study is presented in Figure (2.2) in page 47, from which it is clear that it incorporated two flexible members, the coupler and the rocker linkages. This apparatus was designed to accommodate a wide range of link lengths for the coupler, rocker and ground links, but the crank was always held constant at 63.5mm (2.5 inches). This member was assumed to be rigid since it was manufactured from steel bar stock of cross-sectional dimensions 25.4mm x 25.4mm (1 in. x 1 in.).

The depth of all of the flexible members used in this investigation was less than 25.4mm (1 in.) perpendicular to the plane of mechanism, and the thickness of the links in the plane of the mechanism was always less than 2.54mm (0.1 in.). These dimensions are clearly not representative of an industrial mechanism, but they were chosen in order to accentuate the flexural deformations in the plane of articulation, thereby creating the large signal-to-noise ratios desired by all experimentalists in all fields of scientific research.

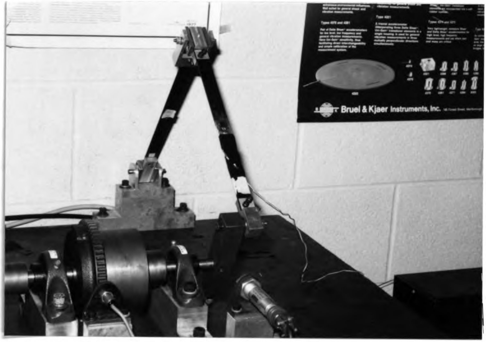

Figure 2.2   Experimental Four-Bar Linkage Mechanism

Naturally, the same signal-to-noise ratios could have been achieved using realistically proportioned links operating at much higher speeds, but this presents additional data-aquisition complexities when measuring the response of the links, and in addition, the response data may well be contaminated by accentuated elastodynamic effects at these higher speeds, due to linkage out-of-balance and other more subtle phenomena caused by manufacturing errors.

It is hypothesized that if mathematical models are capable of predicting the elastodynamic response of linkages fabricated with slender links operating at several hundred revolutions per minute, then they can also predict the response of industrial, realistically proportioned mechanisms with the same stiffness-to-loading ratios operating at higher speeds, because the two response histories are fundamentally governed by the same equations of motion.

The coupler and rocker links of the experimental four-bar linkage apparatus were both manufactured from strip steel material and the ends of each specimen were clamped to the respective bearing housings by two socket screws. The clamping loads were distributed over the ends by flat plates which are clearly visible on the coupler link in Figure (2.2) on page 47. These small clamping plates were found to be essential components of the mechanism since they ensured a smooth load transfer between the three principal components of each link.

Identical aluminum bearing housings were manufactured for the rocker link where it was retained on the ground-link/rocker joint, and also for the coupler where it was retained on the crank pin joint. The dimension of the housings in the longitudinal direction of their respective links was 38.1 mm (1.5 in.) from the end of the housing adjacent to the threaded holes for the socket screws and the centerline of the bearings. The masses of these components including bearings, socket screws and clamping plates was 0.05 kg (0.11 lbm).

The coupler and rocker links were supported on matched pairs of 6.4 mm (0.25 in.) bore R3 DB R12 instrument ball bearings supplied by FAG Bearings Limited. Each bearing housing in the mechanism was preloaded using a Dresser Industries torque limiting screw driver calibrated to ± 0.113 Nm (± 1 in-lb_f) which permitted bearing clearance to be eliminated since the impactive loading associated with bearing clearances would have resulted in larger link deflections. Conversely, if the bearings were subjected to large axial preloads, then the deflections would be attenuated.

The two flexible links articulated in the same plane in order to eliminate the complications of nonlinear torsional coupling terms which characterize co-planar flexible linkages. This was accomplished using a cleavage bearing design that is clearly visible in the top center of Figure (2.2). The housings were fabricated in an aluminum alloy and longitudinal dimension of the housing comprising part of the coupler was 38.1 mm (1.5 in.) from the bearing centerline to the end of the housing adjacent to the threaded holes used to clamp the link specimen. The mass of this assembly, including bearings, socket screws and clamping plate was 0.052 kg (0.114 lbm). The cleavaged component of the coupler-rocker joint was bolted to the rocker link. The axial dimension of this part from the bearing centerline was 44.5 mm (1.75 in) and the mass was 0.063 kg (0.138 lbm) including the spindle, washers and nuts.

The mechanism was bolted to a large cast-iron test stand which was bolted to the floor and also to the wall of the laboratory to provide a substantial rigid foundation. A 0.75 h.p. Dayton variable speed d.c. electric motor (model 2Z846) which was bolted to the test stand, powered the linkage through a 15.9 mm (0.625 in) diameter shaft supported by Fafnir pillow block bearings. A 100 mm (4 in) diameter flywheel was keyed to the shaft thereby providing a large inertia to ensure a constant crank frequency, when operating in unison with the motor's speed controller.

2.2.2 Experimental apparatus: Slider-crank mechanism

The experimental slider-crank linkage used in this study was also bolted to a test stand and a photograph of the apparatus is presented in Figure (2.3) on page 51. The length of the steel connecting rod was 292 mm (11.5 in) and the length of the crank, which was part of the flywheel, was 50 mm (2 in). The slider was a Micro Slides, Inc. type 2050-RW-118-5 linear crossed-roller slide assembly and this precision table was without bearing clearance. A photograph of this arrangement is presented in Figure (2.4) on page 51. A non-rotating spindle was fitted to the translating portion of the slide assembly and this supported the gudgeon pin bearings which were a matched pair of 6.35 mm (0.25 in) R4 DB 12 instrument bearings supplied by FAG Bearings Limited. A similar set of bearings were also used at the crank pin, and both bearing assemblies were preloaded using the technique described earlier.

Identical aluminum bearing housings were manufactured for the crank pin and gudgeon pin joints. These subassemblies each had a mass of 0.045 kg (0.098 lbm) including the mass of the socket screws and the clamping plate. The axial dimension of the housing from the bearing centerline to the extremity adjacent to the steel specimen was 31.75 mm (1.25 in).

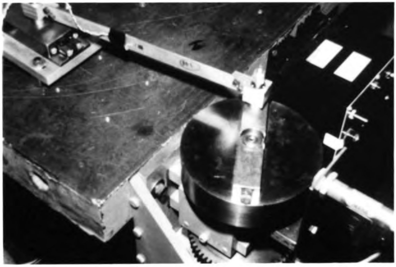

Figure 2.3 Experimental Slider-Crank Mechanism

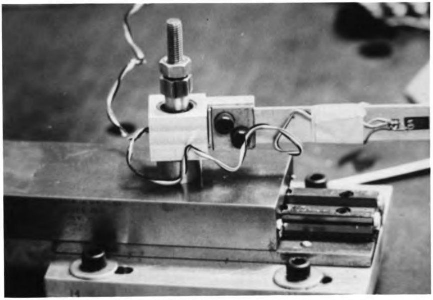

Figure 2.4 Slider Assembly for Experimental Slider-Crank Mechanism

The mechanism was again powered by 0.75 h.p. Dayton variable speed d.c. motor through a 19.05 mm (0.75 in) diameter shaft supported on a pair of Timken tapered roller bearings type TS4A-6. The action of the motor's speed controller was again augmented by a flywheel of 146.05 mm (5.75 in) diameter. Both of the experimental systems were covered by a safety enclosure fabricated from transparent Lexan sheeting of thickness 4.76 mm (0.1875 in).

2.2.3 Instrumentation

A schematic diagram of the instrumentation used in both experimental investigations is presented in Figure (2.5) on page 53. The rated speed of the electric motor was 2500 rpm and this was directly measured in revolutions per minute by a Hewlett Packard 5314A universal counter which was activated by an electro-magnetic pickup, model 58423, manufactured by Electro Corporation sensing a sixty tooth spur gear mounted on the drive shaft of each rig. This large gear is clearly visible in both Figures (2.2) and (2.3). The aforementioned arrangement provided visual feedback to the operator when the speed controller of the motor was being adjusted to establish a desired speed.

The flexural deflections at the midspan of each link specimen were monitored by Micromeasurements Groups Inc. type EA-06-125AD-120 strain gages bonded to each link at the midspan location. Bending half-bridge configurations were adopted, using one gage on each side of the specimen, and they were used in conjunction with a Micromeasurements Group Inc., strain gage conditioner/amplifier system, type 2100.

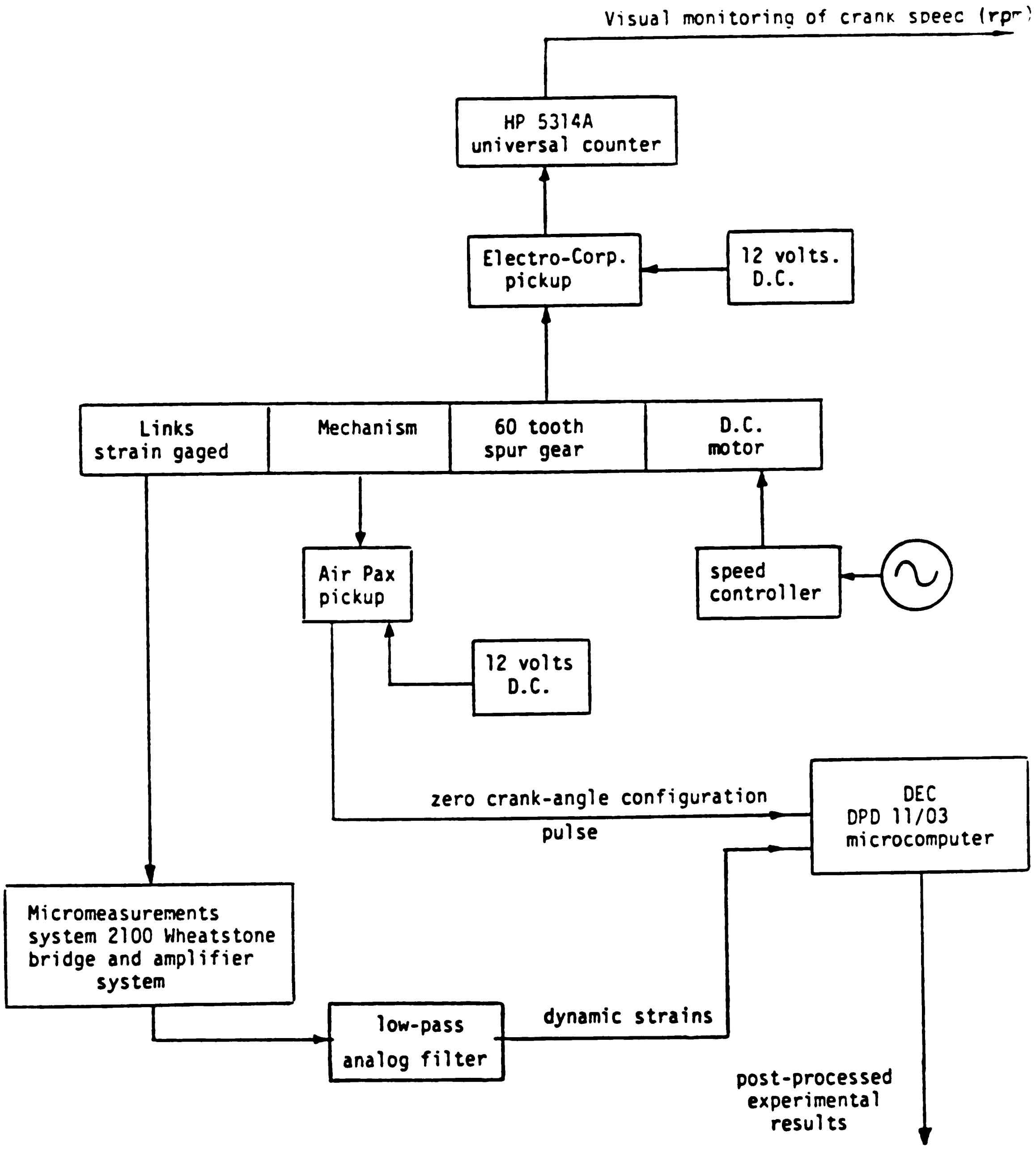

Figure 2.5 Schematic of Experimental Apparatus and Instrumentation.

In order to relate the strain gage signal to the configuration of the particular mechanism being studied, a third transducer arrangement was established. An Airpax type 14-0001 zero velocity digital pickup was employed to sense the bolt head at the end of the crank when the mechanism was in the conventional zero-degree crank angle position. This long hexagonal transducer is clearly visible in both Figures (2.2) and (2.3).

This mechanism configuration signal and the output from the gages were fed to a Digital Equipment Corporation PDP 11/03 microcomputer with a LSI 11/23 processor which is presented in Figure (2.6).

Figure 2.6 The Digital Data-Acquisition System in the Machinery Elastodynamic Laboratory

This digital-data-acquisition system featured 256 kB of memory for post-processing data and also two 5 mB hard disks for storage. A dual port floppy disk system was also available. The experimental response curves were displayed on a Digital Equipment Corporation VT100 terminal with retrographics enhancement.

The BNC cables from each experimental apparatus were connected to an input-output module, bolted to the cabinet of the computer, which was built by the Electronic and Computer Services Department at MSU. This instrument featured 16 analog-digital channels, 4 digital-analog channels and two Schmidt triggers. Using software developed specifically for digital data acquisition purposes, the flexural response signal was recorded from the zero crank angle position through 360 degrees by firing one of the Schmidt triggers. In order to activate the trigger, a 4 μF capacitor was used to modify the square-wave output from the Airpax pickup.

Experimental results were obtained by implementing the following procedure. The signal from the strain gage instrumentation was passed through a first-order analog low-pass filter with a cut-off frequency of 160 Hz in order to remove the electrically or mechanically induced noise prior to being digitized by the analog to digital converter and recorded by the PDP 11/03 microcomputer. This low-pass filter also prevented aliasing problems when employing a rectangular data window, and a sampling rate of $(2578)^{-1}$ seconds, which was considered to be at least twice the highest frequency component of the pure elastodynamic response signal [35,97,128,135]

The data was then post-processed by first multiplying the digitized response by a strain-deflection calibration factor for each link specimen. These factors were obtained by supporting each specimen at the ends on knife edges in a calibration fixture, prior to subjecting the midspan to a series of known monotonically increasing transverse deflections which were imposed and also measured by a micrometer attachment on the fixture. The bending strain corresponding to each midspan deflection was then recorded.

The second post-processing operation involved using a fast fourier transform (FFT) algorithm to convert the time-domain signal to the frequency domain and this was motivated by the need to reinforce the operation of the analog filter by removing induced noise from the strain-gage signal. Using an FFT algorithm, the frequency spectrum of the signal was constructed to determine the frequency range and amplitude of the noise relative to the desired signal. This noise was then removed by simulating a digital low-pass filter prior to transforming the modified data back into the time-domain for presentation of the response on a graphics terminal.

Figures (2.7), (2.8), and (2.9) demonstrate the aforementioned post-processing operations. The experimental results are for the midspan transverse deflection of a four bar linkage with a rigid crank length of 63.5mm (2.5 in), a ground link length of 406.4mm (16 in) and the coupler and rocker links were both 304.8mm (12 in) long with a thickenss in the plane of the mechanism of 1.575mm (0.062 in) and a width perpendicular to the mechanism of 19.05mm (0.75 in). The crank

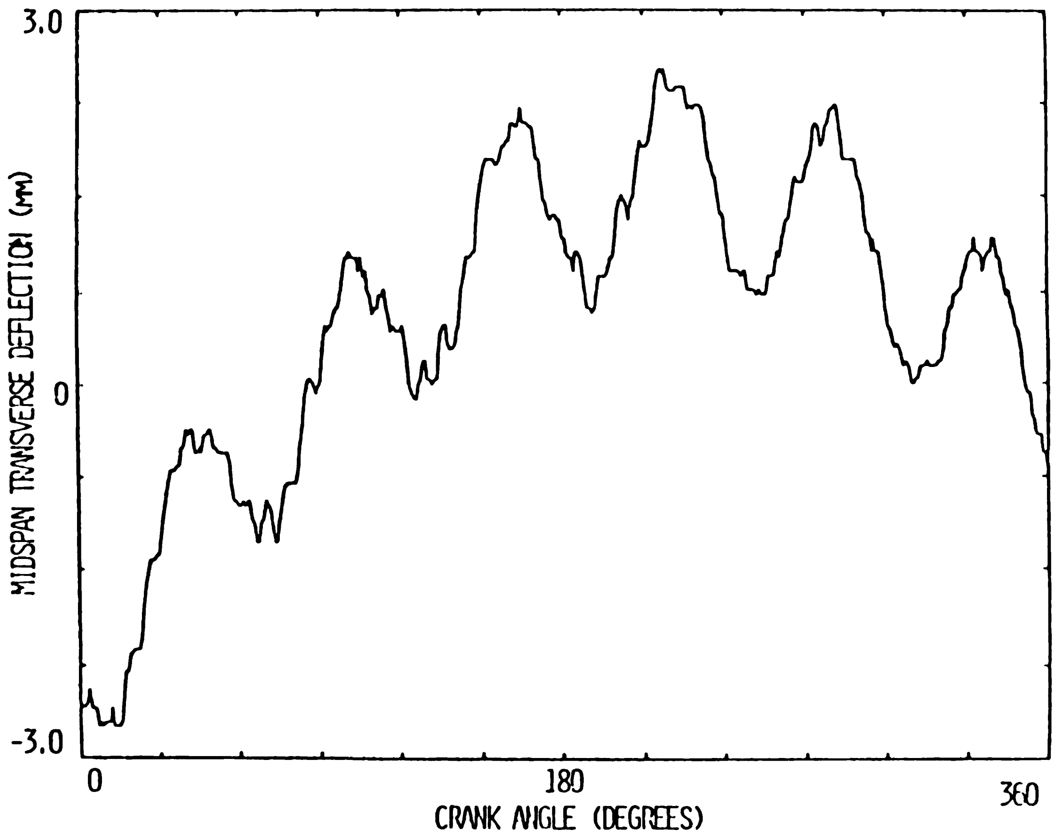

Figure 2.7 **Four-Bar Linkage: Rocker Midspan Transverse Deflection at 254 rpm before Digital Filtering**

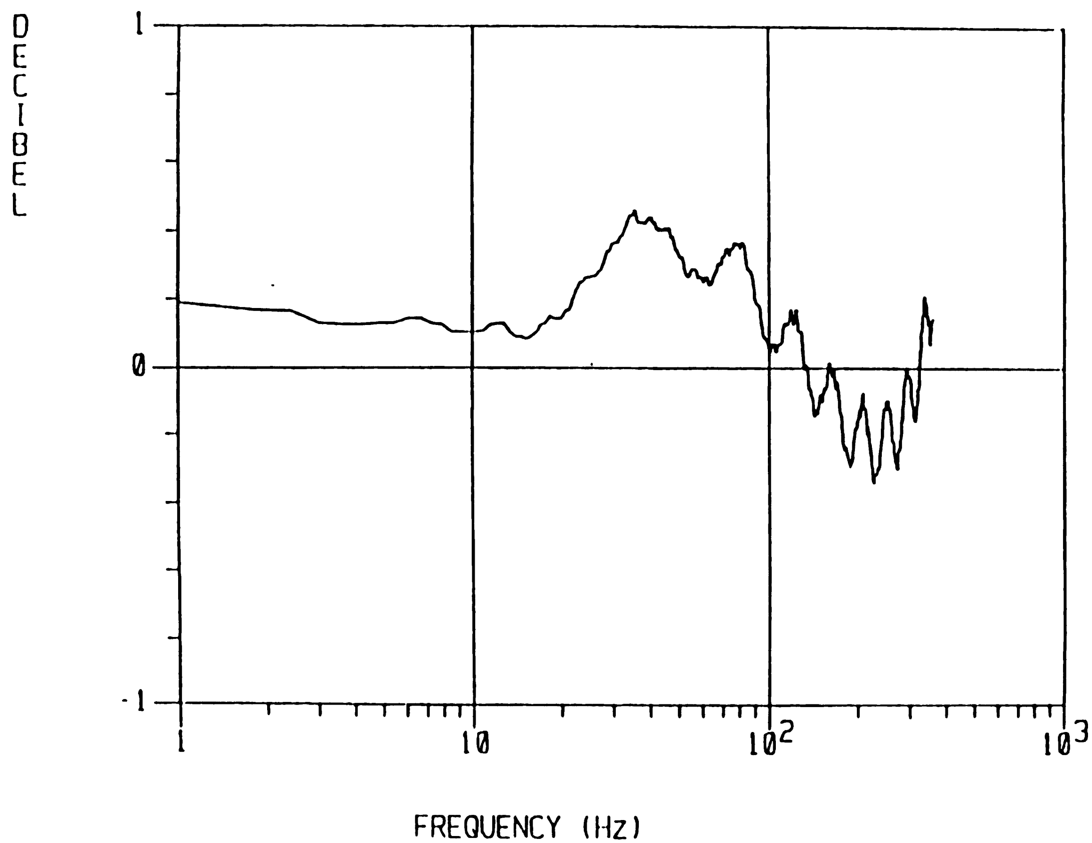

Figure 2.8 **Four-Bar Linkage: Frequency Spectrum of Rocker Midspan Transverse Deflection at 254 rpm**

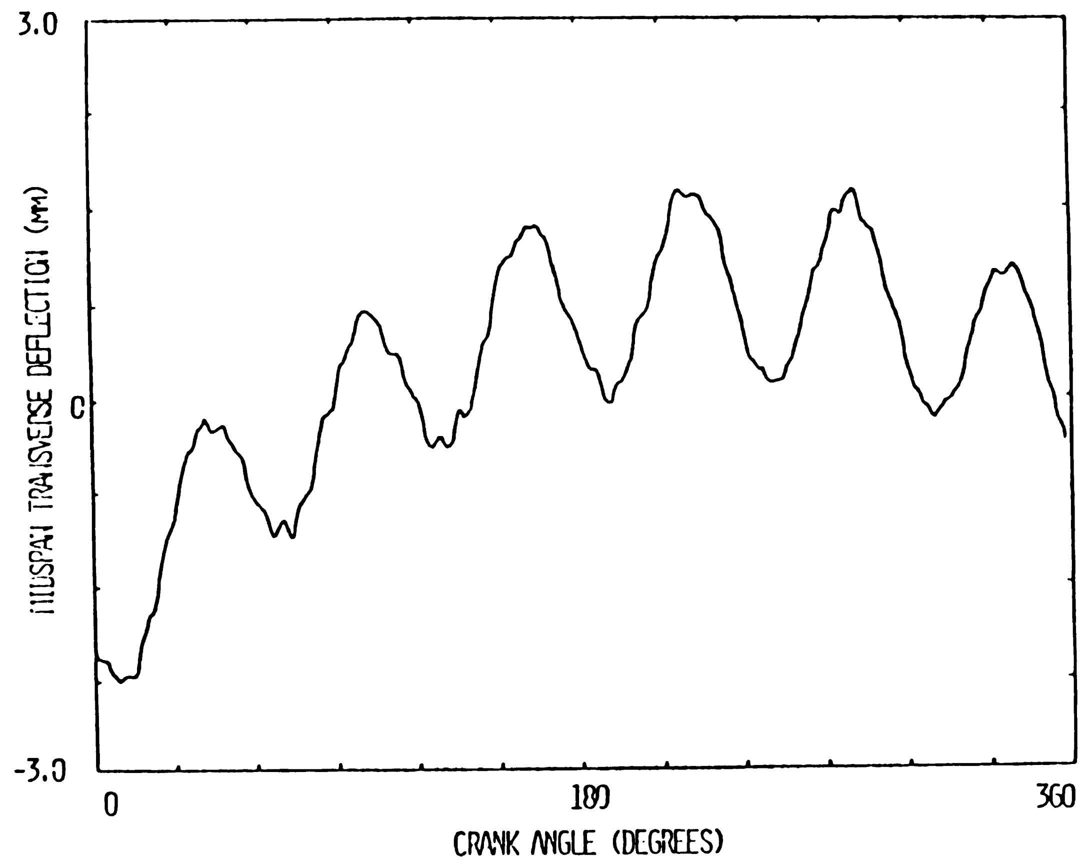

Figure 2.9 Four-Bar Linkage: Rocker Midspan Transverse Deflection of 254 rpm after Digital Filtering

frequency was 254 rpm.

Figure (2.7) presents the experimental data following analog filtering, digitization and post-processing for converting the strain gage signal to midspan deflections. The noise content of the signal is clearly evident. Figure (2.8) presents the frequency spectrum and bandwidth of the same signal presented in Figure (2.7). The natural frequency of the rocker link in a simply-supported beam configuration was experimentally measured to be 41.1 Hz and this response is evident in Figure (2.9). This frequency-response data also indicates mains noise at 60 Hz and higher harmonics. The frequency content above 160 Hz is attributed to roll-off in the circuitry of the analog filter. Using an FFT software package the data was then subjected to digital low-pass filtering with a cut-off frequency of 55 Hz to yield the response presented in Figure (2.9).

2.3 Computer simulations

Multi-element general purpose finite element programs were written for both of the experimental mechanisms described previously and each code had the versatility of permitting the analyst to arbitrarily specify the number of elements to be employed for modeling each link. A parametric study revealed that a six element model of each link provided adequate convergence capabilities when comparing the computer generated results with the experimental results.

The steel specimens were assumed to have a Young's modulus, E, of 207 MPa (30 x 10^6 lb_f/in^2) and a density of 8310 kg/m^3 (0.3 lb_f/in^3).

The bearing housings, however, were assumed to posses the elastic characteristics of aluminum (Young's modulus of 73.14 MPa (10.6×10^6 lb_f/in^2) but the density of the assembly was obtained using the mass and dimensional data. The cleavaged sub-assembly of the coupler-rocker joint, which is part of the coupler, was assumed to have a constant second moment of area of 18272.56 mm^4 (0.0439 in^4) while the mating assembly, which is part of the rocker link, had a second moment of area of 1194.58 mm^4 (0.00287 in^4).

The magnitude of the reciprocating table mass of the slide-crank mechanism, which was required as a input parameter for the simulations, was obtained by configuring the table so that it reciprocated in the vertical direction, prior to resting the reciprocating portion on a laboratory weighing balance while holding the normally fixed portion of the table. The laboratory balance was then activated and the instrument employed to weigh the total mass of the cast-iron table top, the steel spindle and the nuts of the gudgeon-pin assembly. The resulting value was 0.35 kg (0.77 lbm).

The complex phenomenon of system damping was treated in an approximate manner, using the philosophy adopted in references [154,185]. Namely, transient response studies and logarithmic decrement calculations were undertaken for each mechanism in a large number of different system configurations. An average value of the damping ratio was then determined and then distributed uniformly throughout all of the finite elements modeling the particular mechanism under investigation. A mean value of 0.029 was employed to model the slider crank mechanism and 0.031 for the four bar linkage.

The global equations of motion for the two experimental mechanisms were developed using the local element equations of motion obtained from the variational equation of motion (2.1.35), by taking variations of $[\delta U]^T$. The model of the four-bar linkage incorporated gravitation loading using [X] and surface tractions $[\bar{g}]$ were taken to be zero. Figure (2.10) presents the model of the four-bar linkage system and indicates the global degrees of freedom. In this formulation, region S_s in the variational equation of motion, was assumed to be zero.

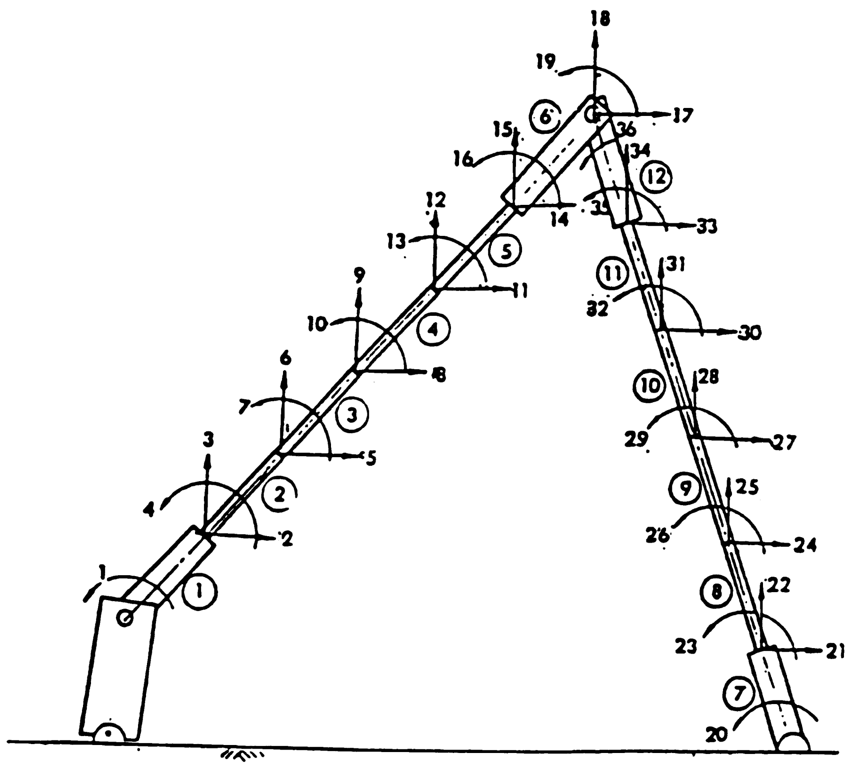

Figure 2.10 Finite Element Model of Experimental Four-Bar Linkage

This was not the case for the slider-crank model, where region S_3 was employed to incorporate the rectilinear kinematic constraint at the gudgeon pin. By utilizing this condition, the transverse deformation was replaced by a function of the axial deformation at the end of the connecting rod thereby reducing the nodal degrees of freedom from three to two. The inertial loading imposed upon the flexible link at the gudgeon pin by the reciprocating table was incorporated into the finite element model as a surface traction $[\bar{g}_x]$ in the axial direction. This was defined by the approximation,

$$[\bar{g}_x] = m[\ddot{p}_{rx} + \ddot{p}_{rz}\tan(-\phi)] \qquad (2.3.1)$$

where m is the total mass of the reciprocating portion of the sliding table and the bearing assembly, and $\ddot{p}_{rx}$ and $\ddot{p}_{rz}$ are the absolute rigid-body accelerations in the axial and transverse directions respectively at the gudgeon pin. The angle ϕ denotes the angle between the centerline of the reciprocating table and the undeformed configuration of the connecting rod. Upon formulating the global equations of motion, these equations were then solved by the Newmark method of direct integration using a step-size governed by the highest frequency anticipated in the response, which in this case was dictated by the axial mode. Several of the matrices modeling nonlinear terms contain an axial force component. For an analysis at time step t_n the axial loading at the previous time step, t_{n-1}, was employed in the simulation algorithm in order to effectively model this dynamical term.

2.4 Results and Discussion

Figures (2.11)-(2.14) on pages 65-68 present the results of combined experimental and analytical investigations on a flexible four-bar linkage with a ground link length of 406.4mm (16 in), a crank length of 63.5mm (2.5 in) and both the coupler and rocker links were 304.8mm (12 in) long. The depth of both flexible links in the plane of the mechanism was 1.4mm (0.055 in) and the width perpendicular to the plane of the mechanism was 19.05mm (0.75 in). The operating speed of the mechanism and also the time-step employed in the simulations are indicated in the legend for each figure.

It is evident from an evaluation of the experimental data and the results of the simulation that the mathematically nonlinear formulation has a very favorable predictive cpability for both frequency content and also amplitude response of the strain-gage signals over the experimental speed range from 193 rpm to 342 rpm. While there are indeed portions of the response where the analytical and experimental results diverge, when this discrepancy is viewed in the context of a peak deflection of only 1.5mm in a very flexible linkage then the results are certainly impressive.

Figure (2.15) on page 69 presents the results of a combined analytical and experimental study of a four-bar linkage with different

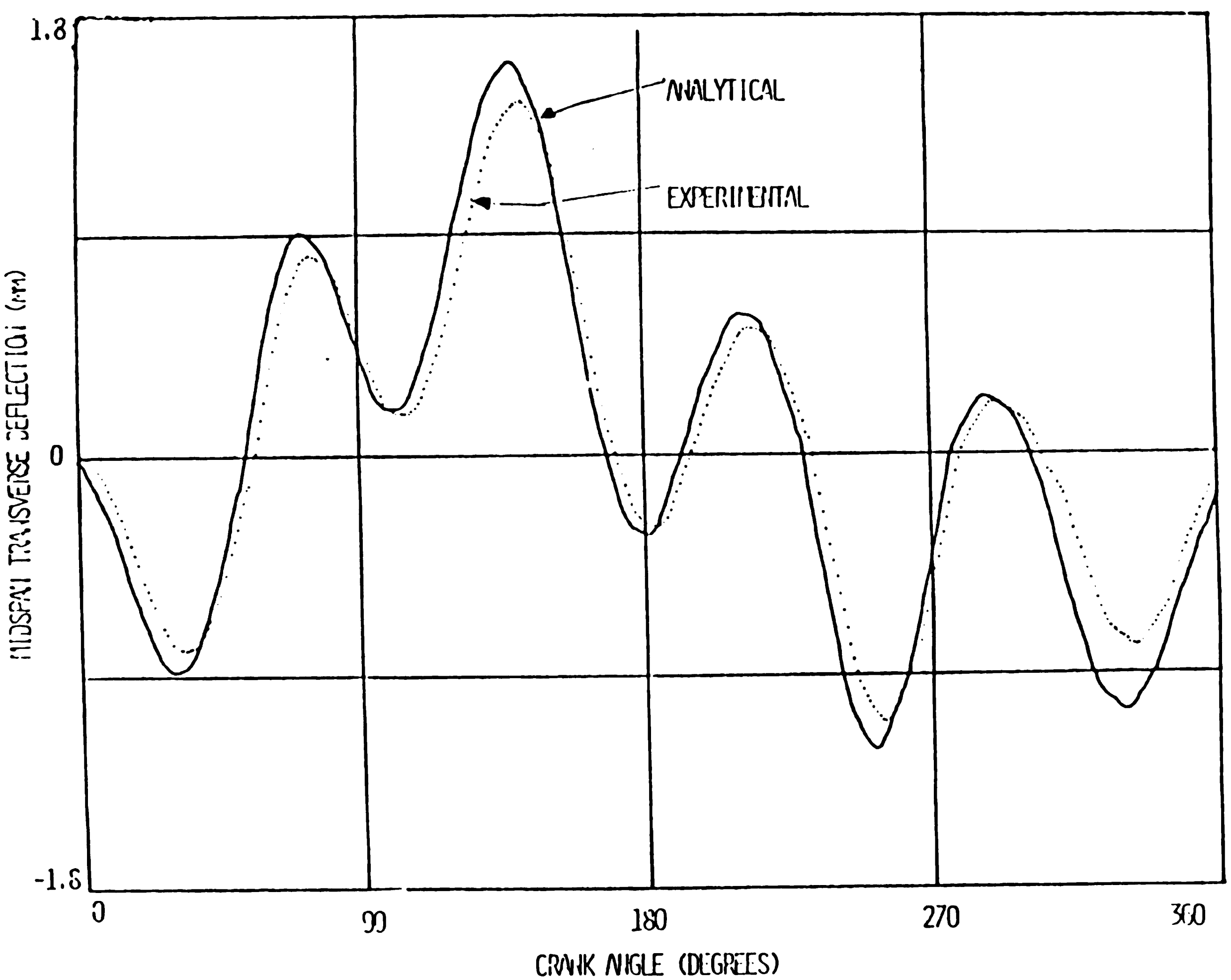

Figure 2.11 **Four-Bar Linkage: Coupler Midspan Transverse Deflection at 342 rpm, Integration Time-Step 0.00048733 Seconds**

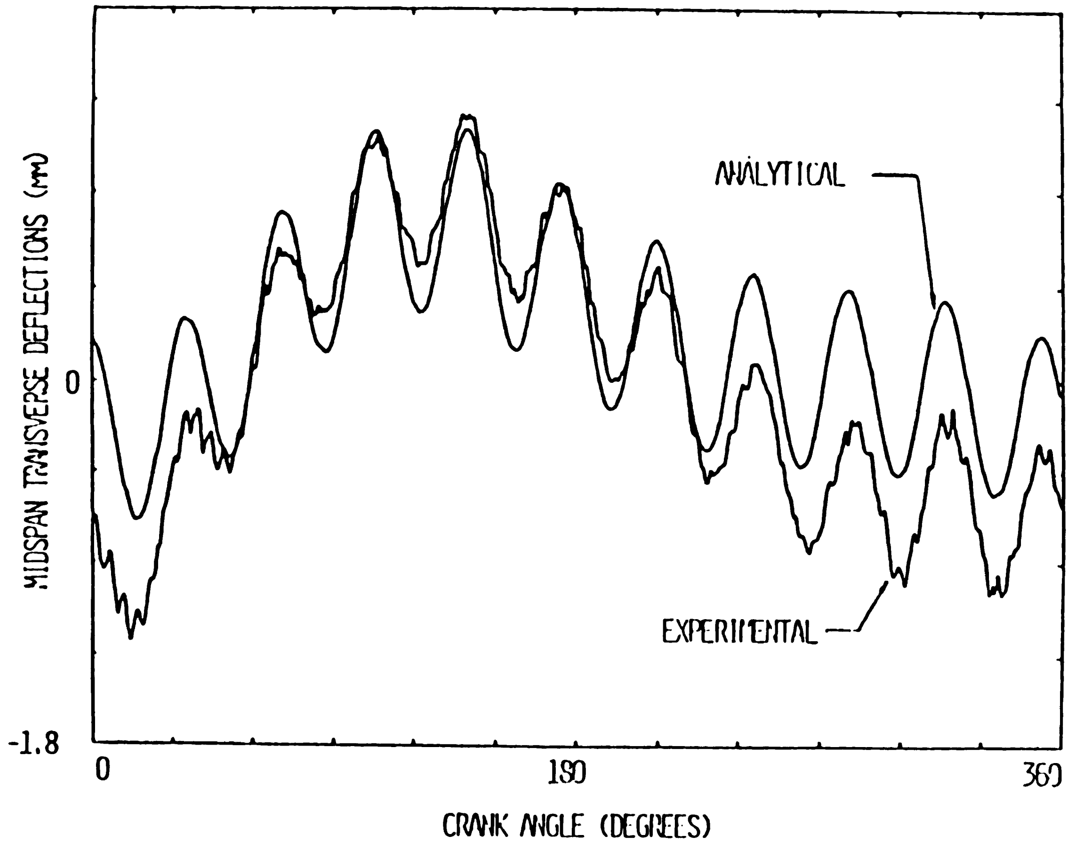

Figure 2.12 **Four-Bar Linkage: Coupler Midspan Transverse Deflection at 193 rpm, Integration Time-Step 0.00086356 Seconds**

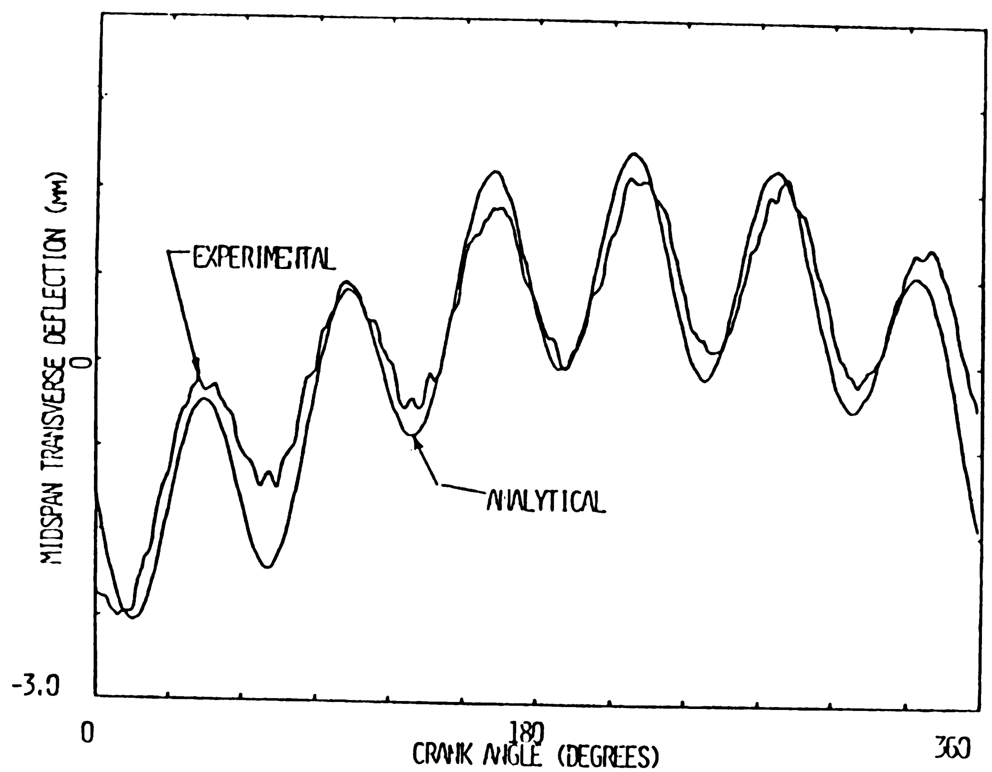

Figure 2.13 Four-Bar Linkage: Rocker Midspan Transverse Deflection at 254 rpm, Integration Time-Step 0.00065617 Seconds

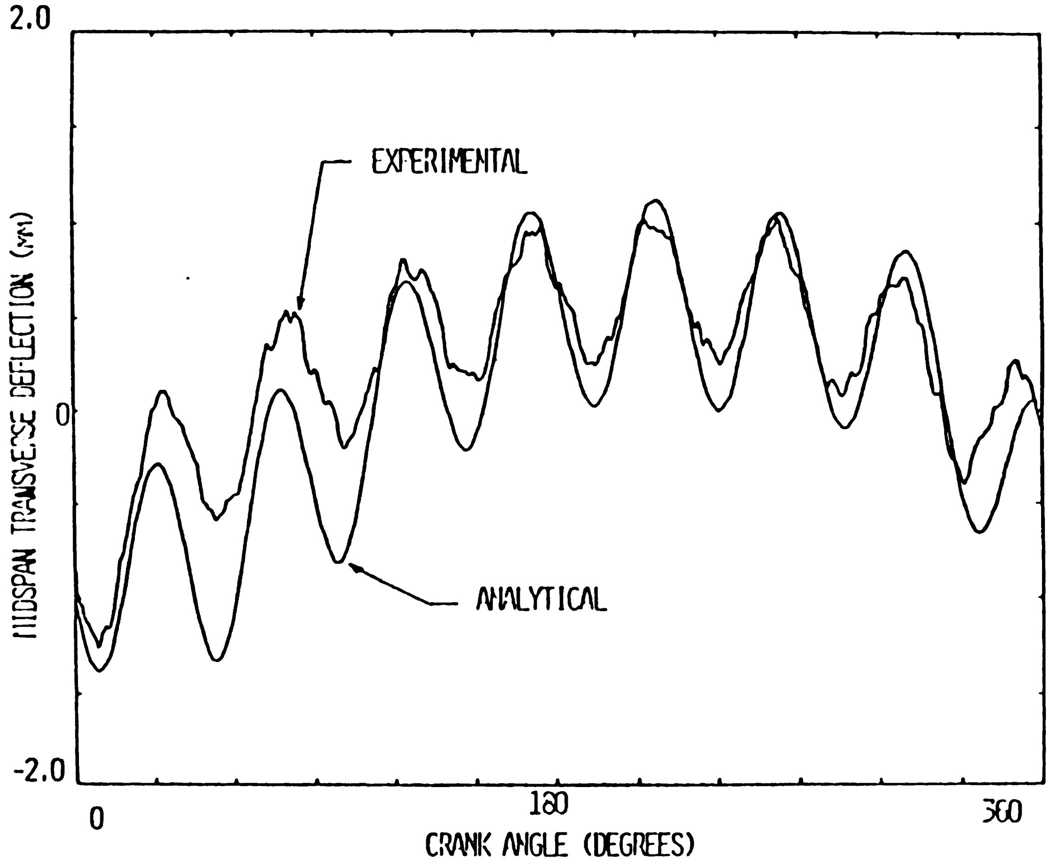

Figure 2.14 Four-Bar Linkage: Rocker Midspan Transverse Deflection at 205 rpm, Integration Time-Step 0.00081301 Seconds

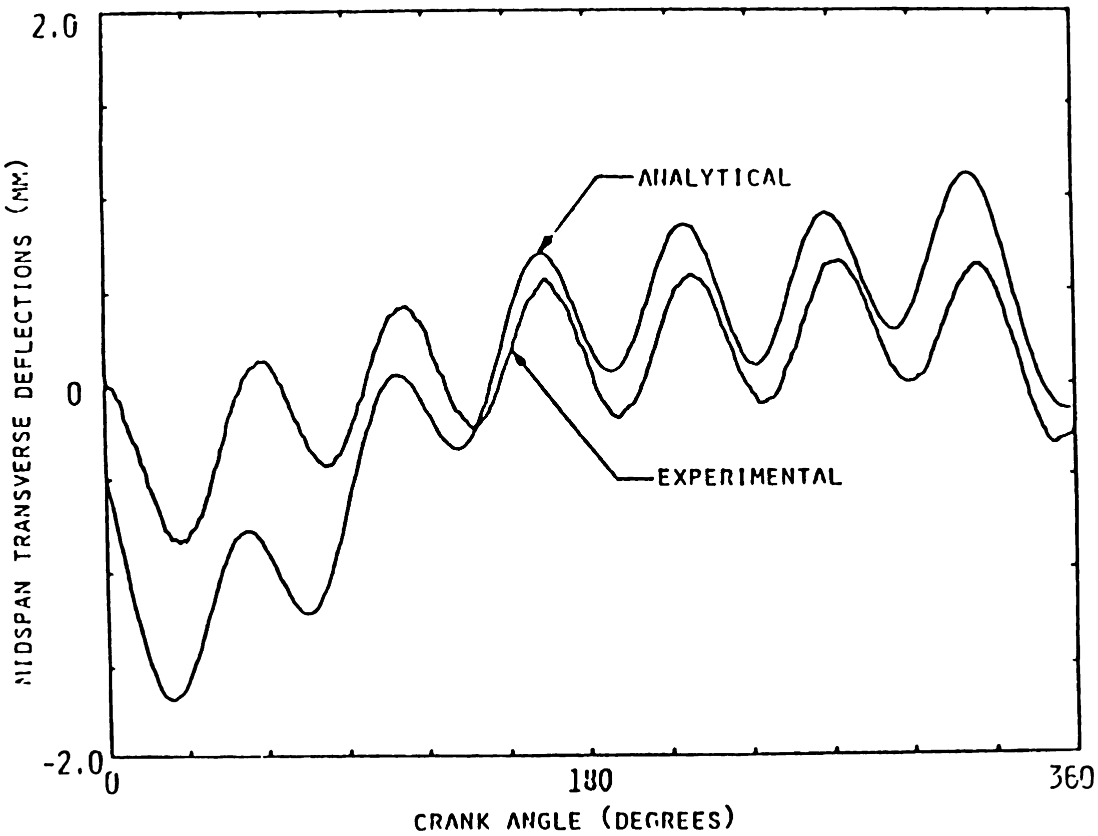

Figure 2.15 Four-Bar Linkage: Rocker Midspan Transverse Deflection at 290 rpm, Integration Time-Step 0.00057471 Seconds

cross-sectional dimensions and link lengths to the system previously investigated, thereby providing a totally different set of test conditions for evaluating the nonlinear formultion developed in [180]. The crank length of the coupler was 228.6mm (9 in) and the length of the rocker was 304.8mm (12 in). Furthermore, the depth of the coupler and rocker links in the plane of the mechanism were 1.17mm (0.046 in) and 1.57mm (0.062 in) respectively, while the width of these links in the plane perpendicular to the plane of the mechanism were 25.4mm (1 in) and 19.05mm (0.75 in) respectively. Figure (2.15) again demonstrates a favorable comparison between the experimental and theoretical responses since the maximum amplitude deviation between the two waveforms is 0.2mm and the frequency correlation is quite good.

Figures (2.16) and (2.17) on pages 71 and 72 present the results of combined experimental and analytical studies of the slider crank apparatus photographed in Figure (2.4). Both systems operated with a constant crank length of 50mm (2 in) and a connecting rod of length 292mm (11.5 in). The depth of the steel connecting rod in the plane of the mechanism was 1.4mm (0.055 in) and the width perpendicular to the plane of the mechanism was 19.05mm (0.75 in). Correlation is again very favorable between the two responses considering the maximum deflections are both less than one millimeter.

All of the response data presented in Figures (2.11)-(2.17) were obtained by modeling the mechanisms using the complete formulation developed in reference [180] as part of a mathematical modeling exercise. However, in industry, the designer is often content with

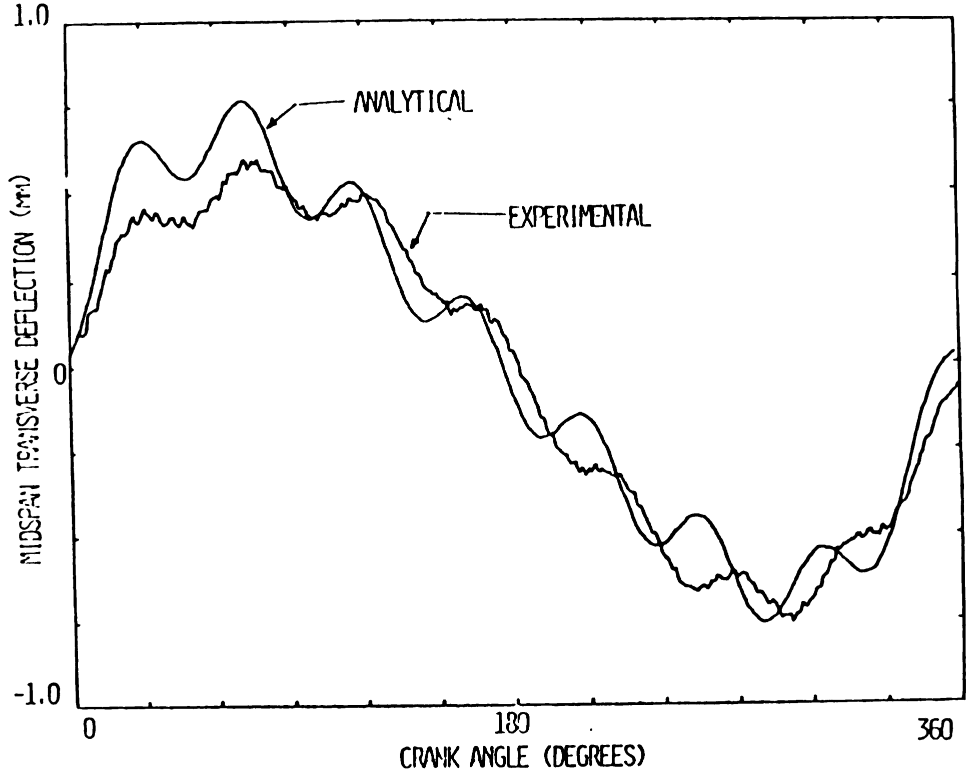

Figure 2.16 **Slider-Crank Mechanism: Connecting-Rod Midspan Transverse Deflection at 235 rpm, Integration Time-Step 0.00070922 Seconds**

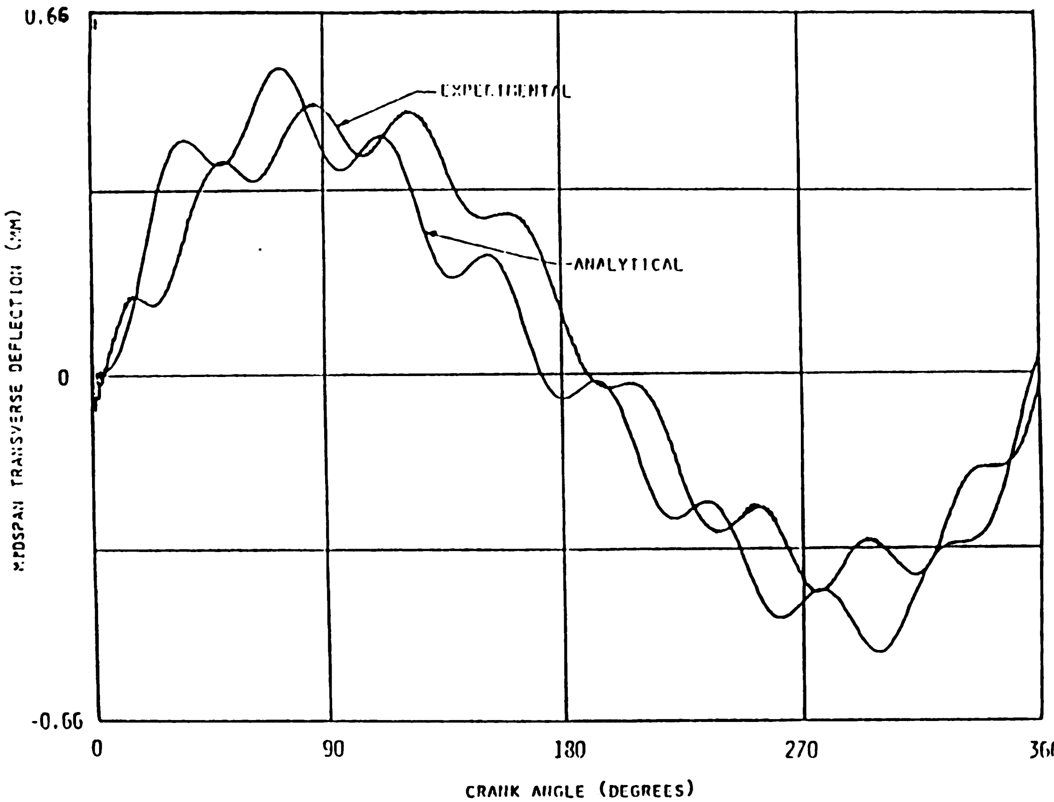

Figure 2.17 **Slider-Crank Mechanism: Connecting-Rod Midspan Transverse Deflection at 274 rpm, Integration Time-Step 0.00060827 Seconds**

results from a simplified formulation if this is more cost-effective. This observation catalyzed an investigation in which several simplifying assumptions were made in the formulation and the system was again simulated prior to examining the correlation between the experimental and computer simulation results. This approach also provides a useful test for determining the significance of the terms in the formulation developed in [180].

Firstly, the matrices modeling the inertial coupling terms in equations (2.4.1) and (2.4.3),

$$[M_{IC}]_1 = \rho AL\ddot{\theta}[\bar{N}] \qquad (2.4.1)$$

where

$$[\bar{N}] = \begin{bmatrix} -1/3 & -1/6 & 0 & 0 & 0 & 0 \\ -1/6 & -1/3 & 0 & 0 & 0 & 0 \\ 0 & 0 & 13/35 & 9/70 & 11L/210 & -13L/420 \\ 0 & 0 & 9/70 & 13/35 & 13L/420 & -11L/210 \\ 0 & 0 & 11L/210 & 13L/420 & L^2/105 & -L^2/140 \\ 0 & 0 & -13L/420 & -11L/210 & -L^2/140 & L^2/105 \end{bmatrix} \qquad (2.4.2)$$

$$[M_{IC}]_2 = \rho AL\dot{\theta}^2[\bar{N}] \qquad (2.4.3)$$

and also the matrix modeling the coriolis' effect, equation (2.4.4)

$$[M_{COR}] = 2\rho AL[\tilde{M}] \qquad (2.4.4)$$

were removed from the equations of motion. The simulation results for the four-bar linkage were found to be only altered by an insignificnt, almost imperceptible, amount thereby demonstrating that for these extremely flexible mechanisms operating in this specific range of speeds, that these terms can be neglected. Of course at higher speeds, and for stiffer systems, this statement may no longer be valid.

Secondly, the stiffness matrices $[K_2]$, $[K_3]$ and $[K_4]$ in equation (2.1.35) were removed from the simulation to generate a formulation based on a linear theory of elsticity. The consequences of this action on the results of the simulations were much more significant causing a deviation of about eight percent in the amplitude response and four percent in the frequency content of the coupler response, when compared with the results based on the nonlinear formulation. This is to be anticipated from the comprehensive literature on the nonlinear response of beams and beam systems (see for example reference [34,132,198]).

These deviations appear to be of smaller magnitude than those in reference [185], which is to be anticipated because the latter publication concerns a mechanism with three, rather than two, flexible links. Thus a cumulative effect concerning the magnitudes of the midspan deflections can be anticipated as the number of flexible links increases.

In conclusion, a theoretical and experimental study has been undertaken in order to investigate the dynamic response of the high-speed flexible linkages fabricated from elastic materials, and good correlations between the computer simulations and the experimental results have been achieved. Attention now focuses on the fabrication of mechanisms with composite materials. The subsequent chapter describes an experimental study in which a comparative study is undertaken between linkage mechanisms fabricated with two commercial metals and two fibrous composite laminates.

CHAPTER 3

AN EXPERIMENTAL STUDY TO DEMONSTRATE THE SUPERIOR RESPONSE CHARACTERISTICS OF MECHANISMS CONSTRUCTED WITH COMPOSITE MATERIALS

References [158,173,176,177,178] suggest that composite materials should be employed to replace the commercial metals in mechanism design because of the high stiffnesses-to-mass ratio, the high strength-to-mass ratio and the high damping characteristics. However there is no experimental validation for the theoretical prediction. In this chapter an experimental study is performed to validate the theoretical predictions made in references [158,173,178,179].

3.1 Theoretical Motivation for This Experimental Study

In chapter 1, the equation of motion governing the general behavior of a high-speed flexible mechanism is described by equation (1.2) which is rewritten here for convenience

$$[I][\ddot{U}] + [M_G]^{-1}[C_G][\dot{U}] + [M_G]^{-1}[K_G][U] = -[I][\ddot{R}] \quad (3.1)$$

The significance of equation (3.1) is that an examination of terms suggests that the elastodynamic response is governed by the energy dissipation per unit mass and the stiffness to mass ratio of the mechanism links. Two design philosophies have been proposed by the mechanism design community for designing high-speed mechanisms. The first, [44], advocates that links with high stiffness-to-weight ratios can be synthesized in the commercial metals by employing optimization techniques to develop special cross-sectional geometries and tapers. The second philosophy, [158,173,179], requires links be fabricated in modern fibrous composite laminates which possess stiffness-to-weight ratios superior to both carbon steels and aluminum alloys [83,183].

References [176,177] reported on the investigations of linkages fabricated in composite laminates, and the comparative theoretical studies [158,160,178,179] demonstrated the superior dynamic response of linkages constructed with composite materials rather than the commercial metals. These theoretical papers predict that the stress levels and dynamic deflections of linkages are inversely proportional to the stiffness-to-weight ratios of the links, and also that these elastodynamic effects are considerably attenuated when a linkage is fabricated with a graphite/epoxy laminate. However, experimental comparative studies to validate the above predictions have not appeared in the literature.

3.2 Objectives and Material Characterization

The objectives of this chapter are not only to experimentally validate the hypothesis that the stiffness-to-weight ratio governs the dynamic response at a prescribed operating speed, but also to demonstrate that the response of a linkage fabricated in a graphite/epoxy laminate is superior to a similar linkage fabricated in a carbon steel or an aluminum alloy.

These objectives were accomplished by monitoring the experimental dynamic responses of mechanisms with identical link lengths operating at specified speeds and constructed with link specimens possessing the same flexural rigidity but fabricated in four different materials. Hence the only variables for each set of tests were the link materials, which affected the inertial loading on the links, and also the damping properties of each system. In order to expose these link specimens to service conditions typically experienced in practice, a comprehensive experimental program was undertaken using both slider-crank and four-bar mechanisms which permitted a wide variety of loading conditions and speed ranges to be imposed upon them.

A link of a flexible mechanism principally deforms in the bending, or flexural mode and the associated deformation fields are governed by the flexural rigidity, which is the product of the Young's modulus (E) of the material and the second moment of area (I) of the link cross-section. Thus, in the context of evaluating how the dynamic response of a flexible mechanism is affected by the type of link material, an appropriate rationale is to fabricate several links of the same length and flexural rigidity (EI) from several different materials and use them, in turn, to construct a flexible linkage. Upon operating the mechanism at a specific speed and comparing the associated responses of the different link materials, design criteria can then be deduced.

This is the philosophy of the study presented herein.

The materials selected for the tests were a low carbon steel, an aluminum alloy, a unidirectional 16-ply graphite-epoxy laminate 3501-6/AS-4 manufactured by Hercules Inc, and a 16-ply graphite epoxy laminate of the same material with a symmetrical ply layup of [±45] degrees relative to the longitudinal axis of the link. These laminates were selected to demonstrate something of the different responses attainable using this class of material. Clearly this limited investigation cannot do justice to the large variety of different fibers and matrices employed commercially, or even to the different types of graphite fibers or epoxy resins currently available.

The modulus of elasticity of the steel and aluminum links were obtained from supplier's data sheets, and because the quality control of the commercial metals is so good, specimens were not subjected to mechanical testing. This is not the case with composite materials, where there is a greater variability of the mechanical properties and furthermore, the constitutive behavior of the laminates needs to be carefully determined. While the commercial metals are sensibly elastic materials at room temperatures, composites may exhibit elastic, viscoelastic, visco-plastic or plastic behavior under these conditions depending upon the material being examined.

The first task in the testing of these composite materials was to determine the shape and dimensions of the specimens. The literature on this subject was reviewed [73,126,193] but there appeared to be no consensus of opinion as to whether a dogbone or parallel sided specimen should be employed. Since there were no major criticisms of using a parallel-sided specimen, and this class of specimen is more easily manufactured, a total of four specimens, were cut from the two 16-ply thick plates of graphite-epoxy laminate using a thin grinding wheel. The dimension of the unidirectional specimens were 2.06mm x 12.5mm x 165.1mm (0.081 in x 0.5 in x 6.5 in.), while the $[\pm 45]_s$ specimens were 2.34mm x 12.5mm x 165.1mm (0.092 in x 0.5 in x 6.5 in.). These dimensions are dictated by the maximum size of specimen that the testing machine could acommodate and also an edge-effect criterion associated with the application of St. Venant's principle to heterogeneous, anisotropic materials [77].

These latter characteristics of composite laminates complicates the mechanical testing of these materials because bending moments and shear forces imposed upon a misaligned specimen being gripped in a tensile testing machine could generate erroneous results [126]. To avoid these pitfalls an alignment fixture was fabricated using a design developed by the composites group at Virginia Polytechnic Institute and State University [73]. Figure (3.1) on page 81 presents a photograph of the fixture and also the pin-jointed grips which screw into the ram and anvil of a electro-hydraulic MTS mechanical testing machine. Figue (3.2) on page 81 presents a photograph of a specimen being tested. The motion of the ram was pre-programmed and during the ensuing motion the output from the two-inch clip-gage fixed to the specimen was recorded automatically on the x-y plotter shown on the right ofthe photograph.

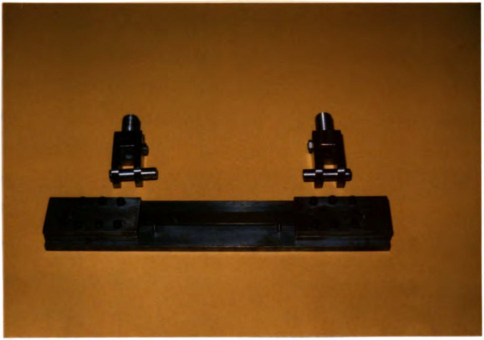

Figure 3.1 Alignment Fixture and Mechanical Arrangement for Testing Graphite/Epoxy Specimens

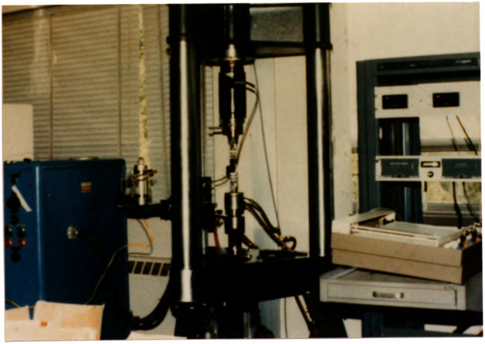

Figure 3.2 The Mechanical Testing of Graphite/Epoxy Laminates in a MTS Testing Machine

The objective for the mechanical testing was to classify the behavior of the unidirectional and $[\pm45]_s$ graphite-epoxy laminates. Initially the specimens were subjected to dynamic testing. This involved prescribing a maximum load, or stress, and requiring the specimen to attain this load over a range of time intervals. Figure (3.3) on page 83 presents the results of these tests performed on the unidirectional AS-4/3501-6 laminate and maximm stress level of 0.258 MPa (37.5×10^3 lb_f/in^2) was reached in 1, 10, 100 and 1000 seconds during the four tests. The responses during the loading and unloading phases of the tests are superimposed. All specimens were stored in a controlled hygrothermal environment for two weeks prior to testing to ensure some degree of thermodynamic equilibrium.

The results presented in Figure (3.3) suggest that the unidirectional laminate is an elastic material because all of the gradients of the response histories are identical. However this is not true for the $[\pm45]_s$ AS-4/3501-6 specimens whose test results are presented in Figure (3.4) on page 84. The behavior of the material is certainly dependent upon the rate of application of the load (and hence strain rate) and this is clearly demonstrated by the two plots on the extreme right of the figure which are for specimens subjected to a prescribed load during time intervals of 1 second and 100 seconds. These results indicate that the $[\pm45]_s$ liminate is a viscoelastic material, and moreover, it is nonlinear as evidenced by the shape of the response curves.

In order to verify the deductions made from these test data a

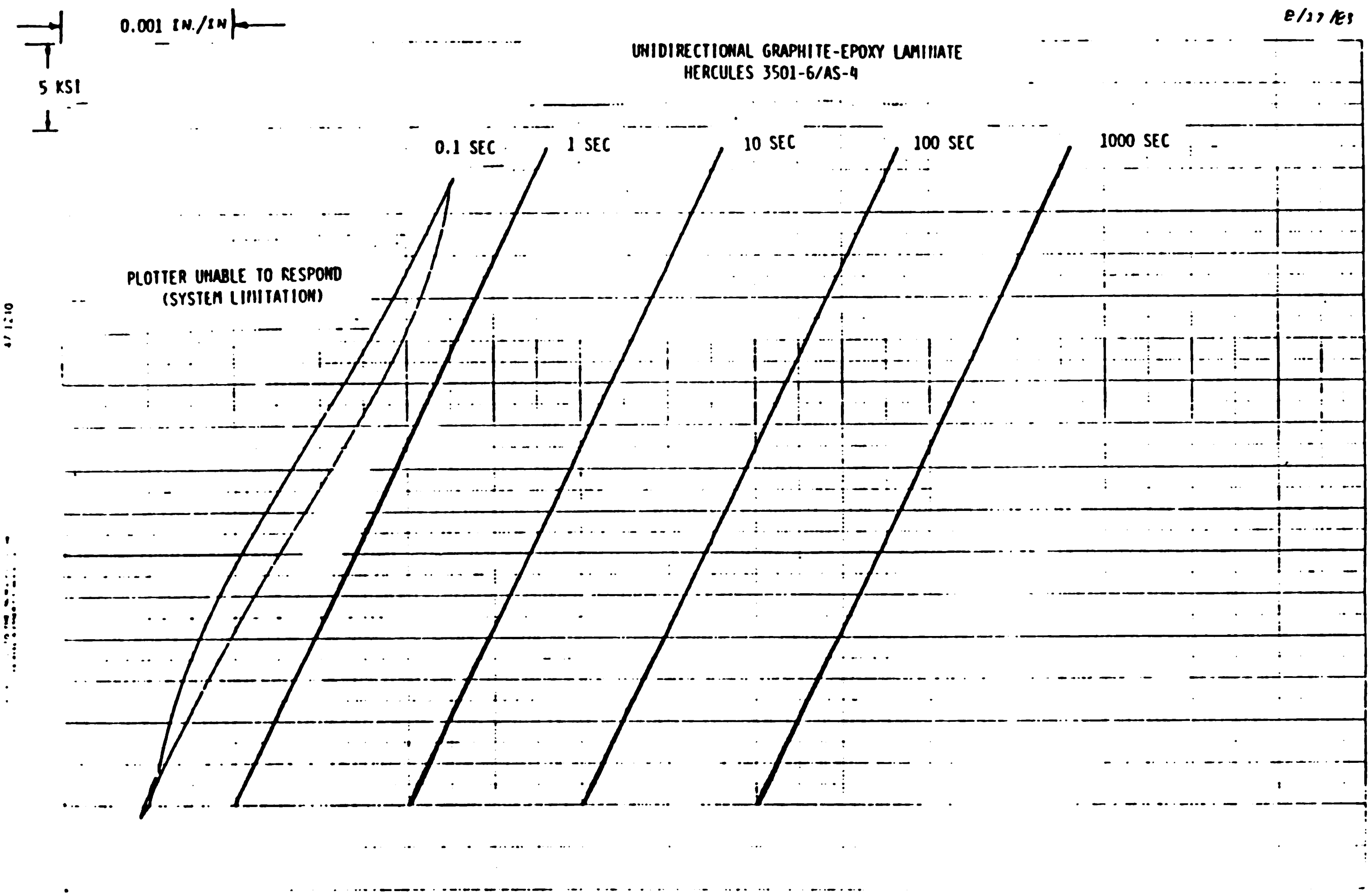

Figure 3.3 Dynamic Test Results for Unidirectional AS-4/3501-6 Laminate

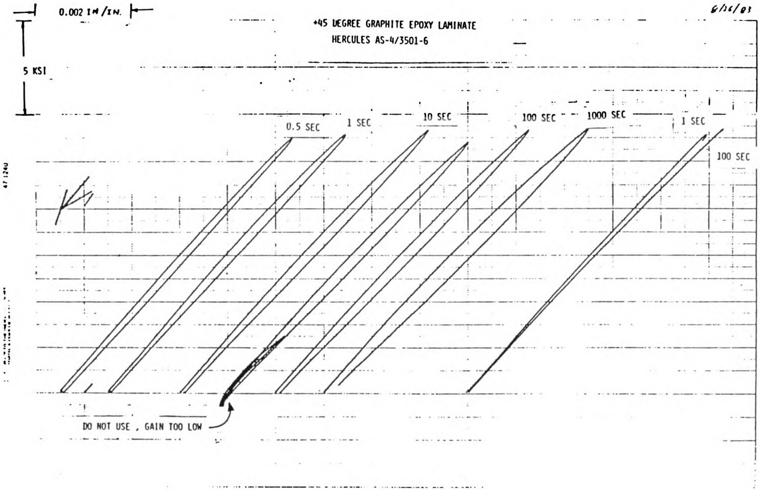

Figure 3.4 Dynamic Test Results for $[\pm 45]_s$ AS-4/3501-6 Laminate

second set of tests were initiated to study the creep response of the materials. The results are presented in Figures (3.5) and (3.6) on pages 86 and 87. Time is the abscissa for both plots and the pen on the x-y plotter was programmed for the different speeds indicated. In addition, the pen was programmed to quickly return to the left hand edge of the paper in the stand-off mode upon reaching the limit of travel at the right hand edge. This procedure permitted each creep response to be presented in one compact figure rather than several feet of paper from a strip recorder.

The response presented in Figure (3.5) verifies that the unidirectional laminate is an elastic material, while the creep data in Figure (3.6) indicates that the $[\pm45]_s$ composite is viscoelastic.

Having completed the dynamic and creep testing of the laminates, the response data presented in Figures (3.3)-(3.6) provides the basis for a number of different investigations. In the context of this paper the effective modulus of the unidirectional laminate can be readily calculated from Figure (3.3). The $[\pm45]_s$ laminate has a more complex response because the stress-strain history is not linear, and moreover, the gradient depends upon the strain rate. Clearly a wide range of different Young's moduli could be deduced from the experimental data depending upon the assumptions deemed to be relavant by the investigator. Because a link of any mechanism experiences rapidly fluctuating stress levels, the response curve on the extreme left of Figure (3.3) was selected to provide the basis for the Young's modulus calculation because this records the highest strain rate of any

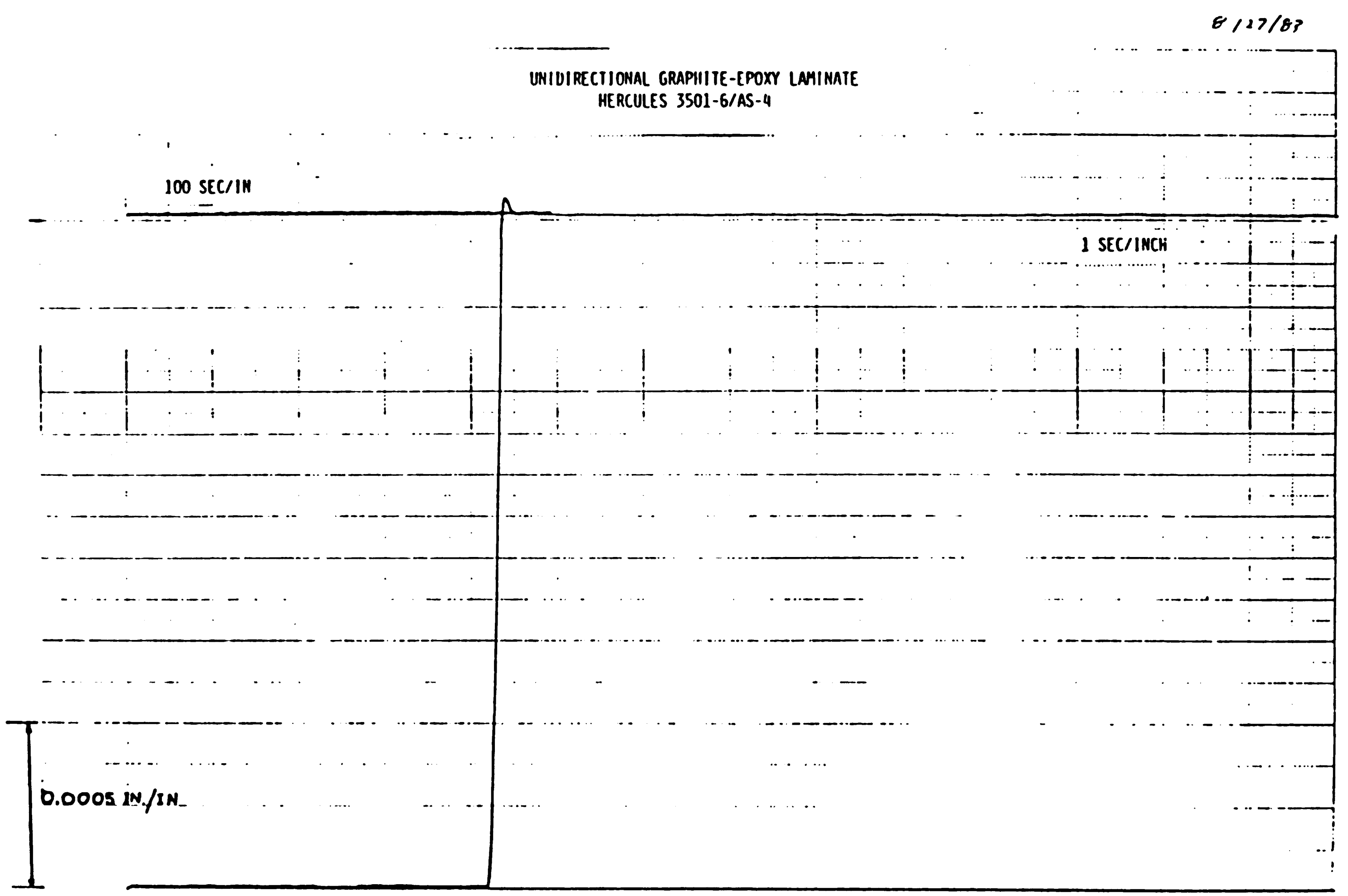

Figure 3.5 Creep Response for Unidirectional AS-4/3501-6 Laminate

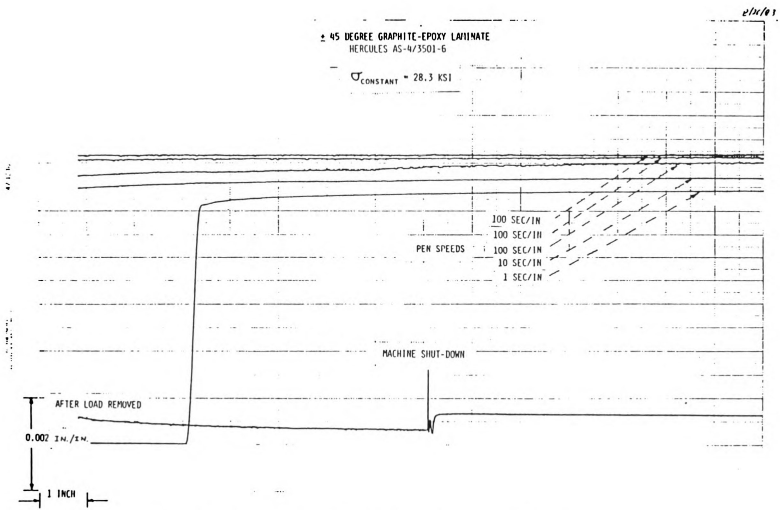

Figure 3.6 Creep Response for $[\pm 45]_s$ AS-4/3501-6 Laminate

specimen. Higher strain rates could not be achieved with the experimental testing equipment available.

The approach adopted was to draw a tangent to the response curve at the lower end of the curve in the region recording the initial response immediately following load application. The effective Young's modulus for this viscoelastic material was calculated to be 21.7 MPa (3.143×10^6 lb_f/in^2) while a mean value of 19.6 MPa ($2.834 \times 10^6 lb_f/in^2$) was calculated for the line joining the points defining the maximum and minimum stress levels.

Having established the effective Young's moduli for the four link materials, the cross sectional dimensions were calculated so that the flexural rigidity of each link was identical and the link specimens were then manufactured. The data are presented in Figure (3.7) on page 89. The members were designed to principally deform in flexure in the plane of the mechanism due to the inertial loading associated with the articulation of the mechanism. The steel and aluminum specimens were cut from sheet material and the depths indicated in Figure (3.7) are standard American stock sizes.

The objective for the final phase of the material characterization studies was to determine the material damping of each member. This involved clamping each specimen at one end to develop a cantilever configuration prior to deflecting and releasing the other end and recording the ensuing transient vibration (using instrumentation to be described later). Simple logarithmic decrement calculations yielded the

MATERIAL	WIDTH (mm)	DEPTH (mm)	EFFECTIVE MODULUS (MPa)	SPECIFIC STIFFNESS (MPa/kg)
Steel	29.0	1.168	207	1,959
Aluminum	16.3	2.02	71.1	6,049
[0]	9.1	1.93	147.1	18,924
$[\pm 45]_s$	34.7	2.34	21.7	4,132

Figure 3.7 Link Stiffness Characteristics

damping ratio (ξ) for each specimen. The results are presented in Figures (3.8), (3.9), (3.10) and (3.11) on pages 91 and 92 for the steel, aluminum, $[\pm 45]_s$ and [0] specimens respectively. The corresponding values of material damping are 0.002, 0.0048, 0.006 and 0.0018. Upon reviewing the data in Figure (3.7), it is apparent that the unidirectional graphite-epoxy specimen is much stronger than the specimen but it has a much lower damping ratio. Since most machinery applications require links to possess a high stiffness and be manufactured in materials with high damping, a hybrid design utilizing both fiber configurations can be readily proposed to achieve this objective.

This serves to illustrate one of the many benefits obtained through designing components in composite laminates that is unobtainable when employing conventional materials. By changing the stacking sequence, fiber volume-fraction, fiber orientation, matrix characteristics and type of fiber, these design parameters enable the designer to synthesize link materials with the desired properties. These typically include impact resistance, fatigue resistance, stiffness, strength, mass and material damping; and these properties in turn govern the linkage response characteristics such as natural frequencies, dynamic deflections and acoustical radiation [142]. This philosophy is presented in more detail in the introductions to references [76] and [77]. This versatility is not available to the design engineer when designing in the commercial metals because the only design variables are material selection and the cross sectional geometry.

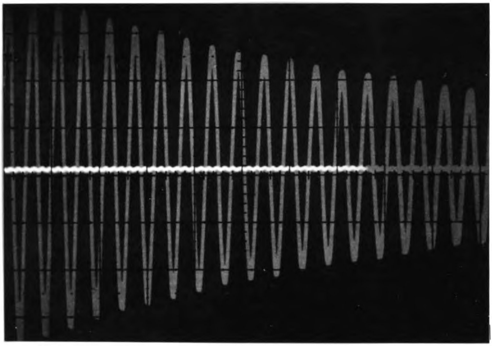

Figure 3.8 Steel Specimen Transient Response. Horizontal Scale 20mS/div, Vertical Scale 0.1V/div

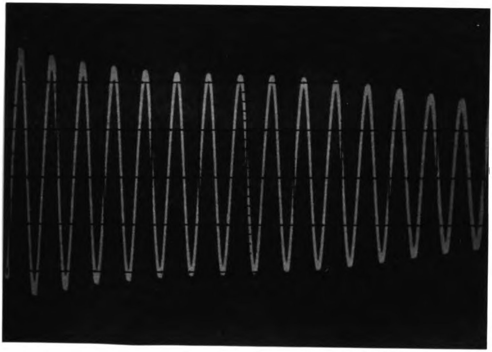

Figure 3.9 Aluminum Specimen Transient Response. Horizontal Scale 50mS/div, Vertical Scale 0.1V/div

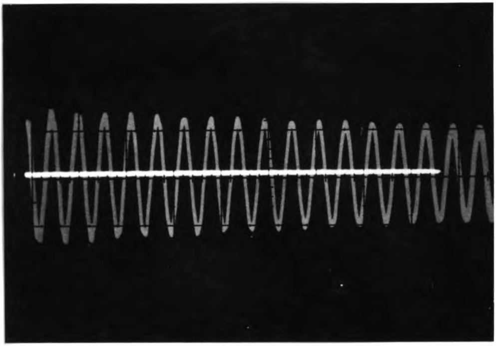

Figure 3.10 [±45]$_s$ Specimen Transient Response. Horizontal Scale 20mS/div, Vertival Scale 0.1V/div

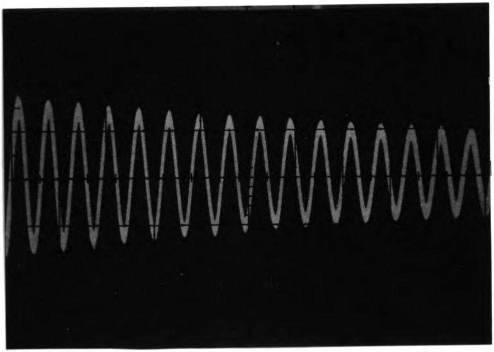

Figure 3.11 [0] Specimen Transient Response. Horizontal Scale 20mS/div, Vertical Scale 50mV/div

3.3 Results and Discussion

Eight link specimens were prepared to form four matched pairs in the four test materials. At the end of each specimen two clearance holes were drilled. These accomodated the socket screws which clamped each specimen to the bearing housings and enabled two experimental mechanisms to be constructed: a four bar linkage with the plane of the mechanism coincident with the gravitational field and a slider crank mechanism operating in a plane perpendicular to the gravitational field.

The experimental setups employed in this study, include a four-bar linkage, a slider-crank mechanism and the related instruments, are the same as those mentioned in chapter 2 and will not be described here.

Figures (3.12), (3.13), (3.14) and (3.15) on pages 94-97 present the dynamic bending strain responses of the mechanism systems studied, and each features a comparative study among different materials and all of them are under the premise of constant EI value and same operational condition (i.e. speed, alignment and environment etc.). The relative magnitudes of the deflections may be obtained from the oscilloscope photographs by using the calibration data in the legend of each figure. The calibration coefficient for the $[\pm 45]_s$ composite material is a mean value since the calibration curve is nonlinear, however, this nonlinear characteristic was employed to accurately present the results in Figures (3.14) and (3.15) which were recorded by the digital data acquisition system.

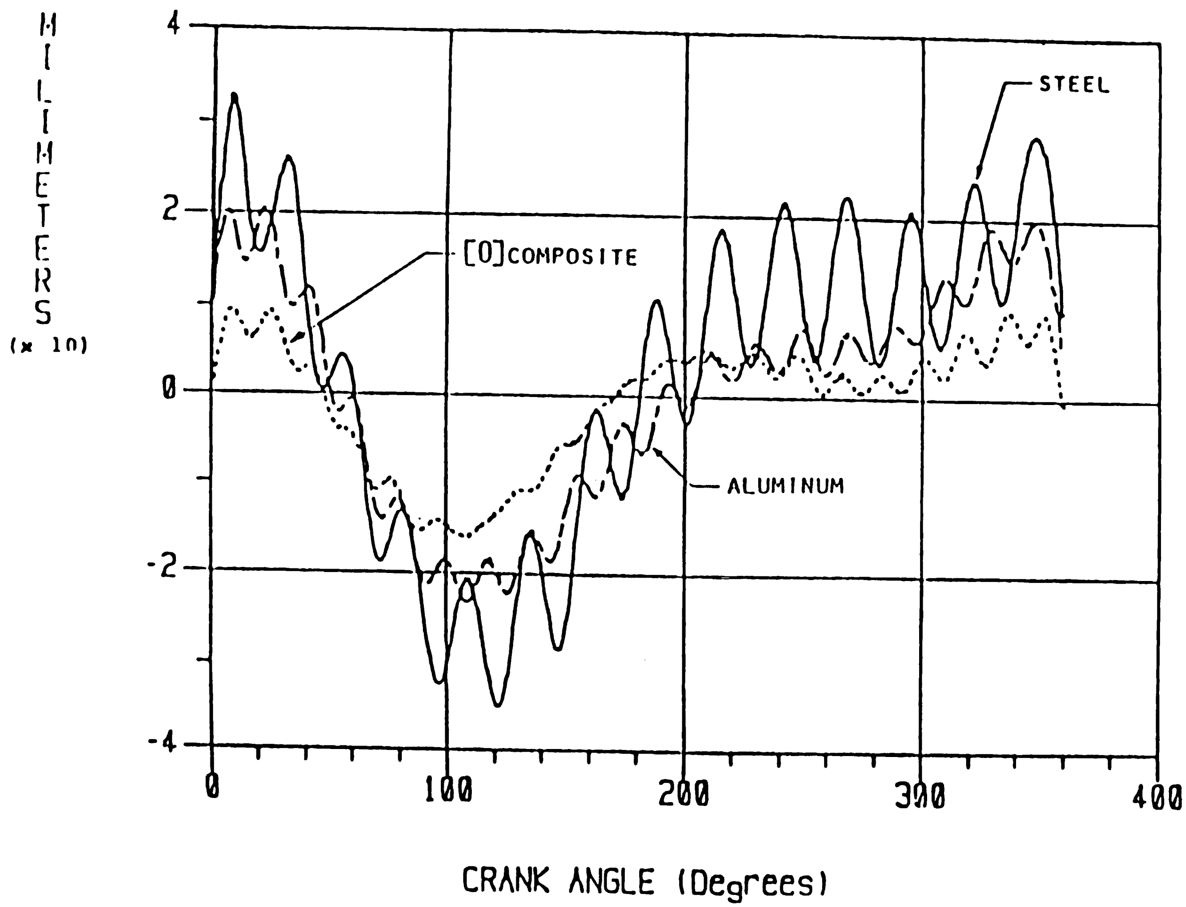

Figure 3.12 Coupler Midspan Bending Deflections: 280 rpm

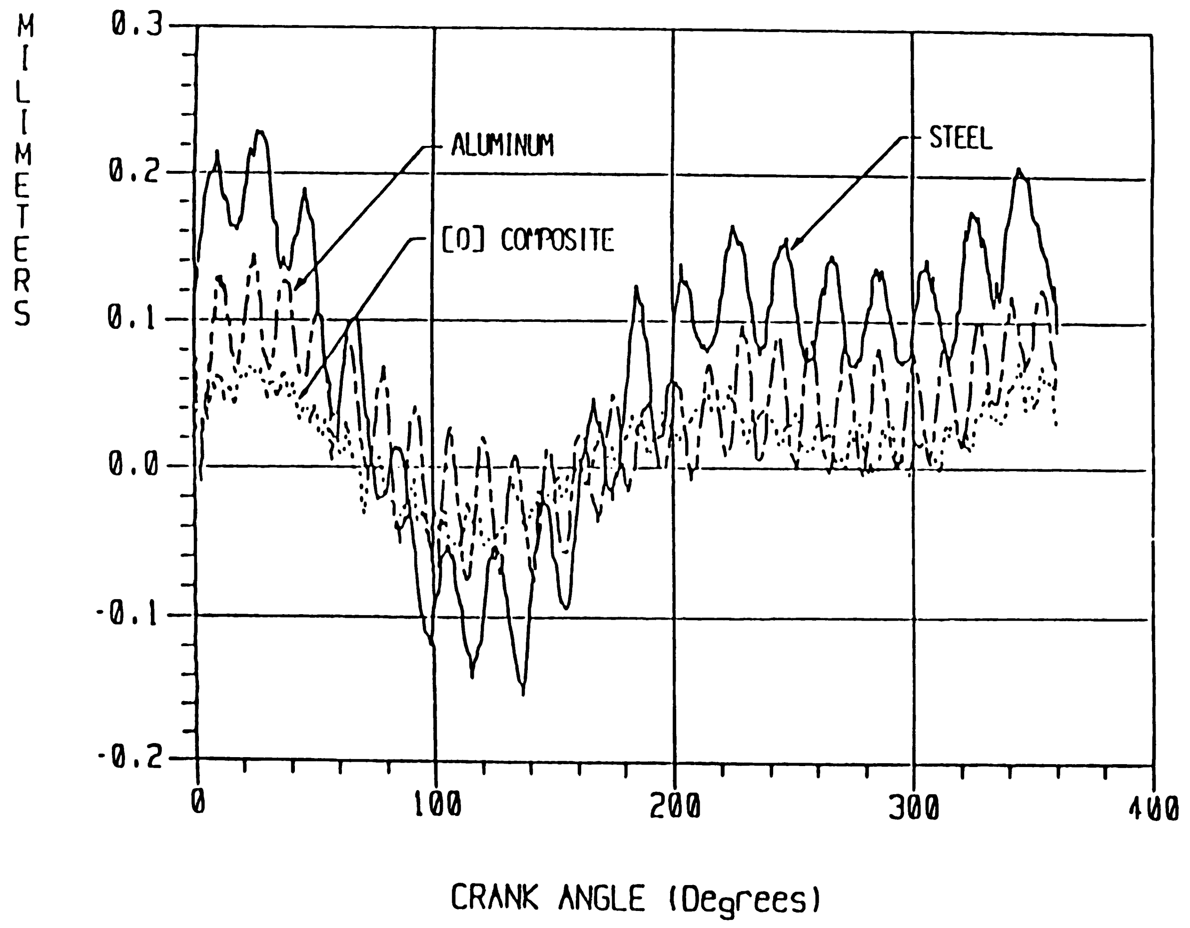

Figure 3.13 Coupler Midspan Bending Deflections: 198 rpm

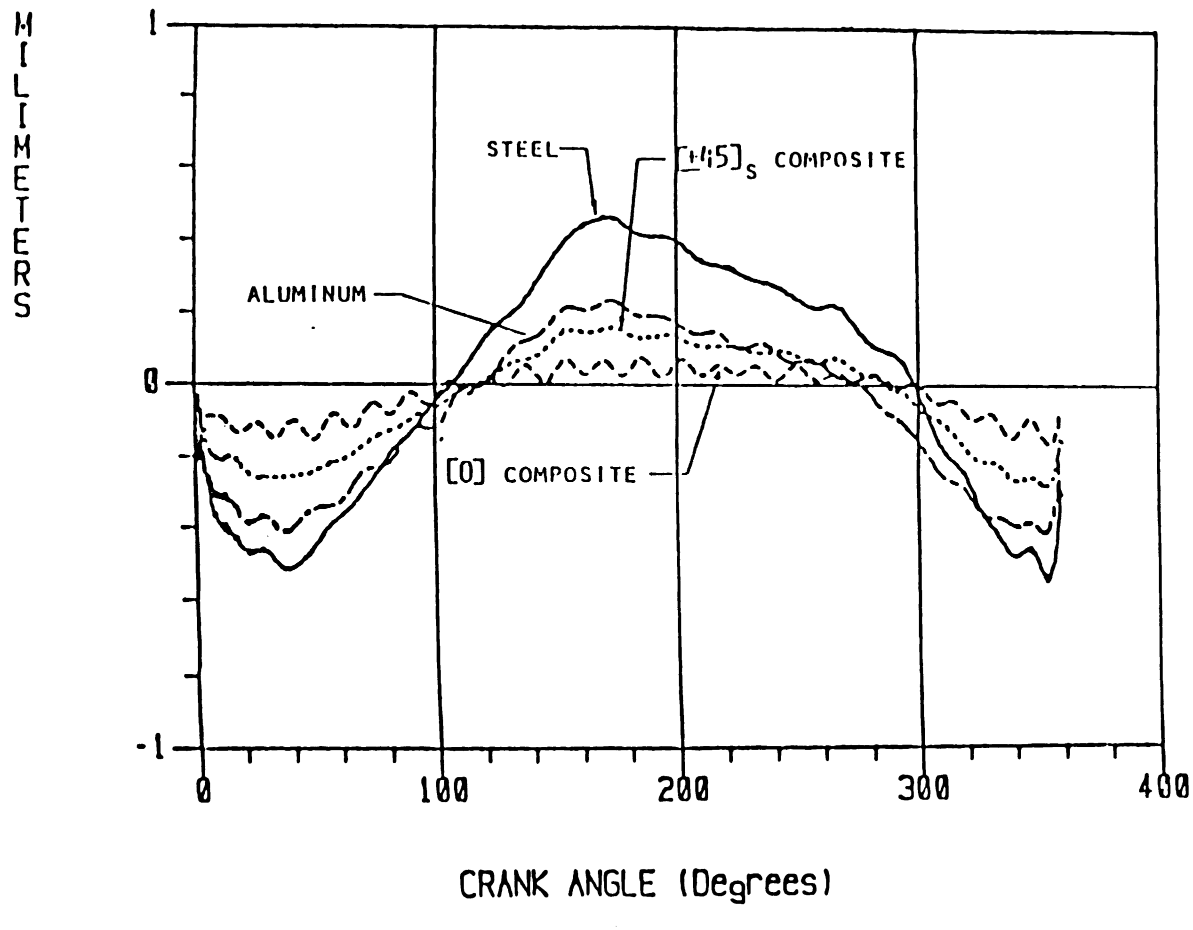

Figure 3.14 Rocker Midspan Bending Deflections

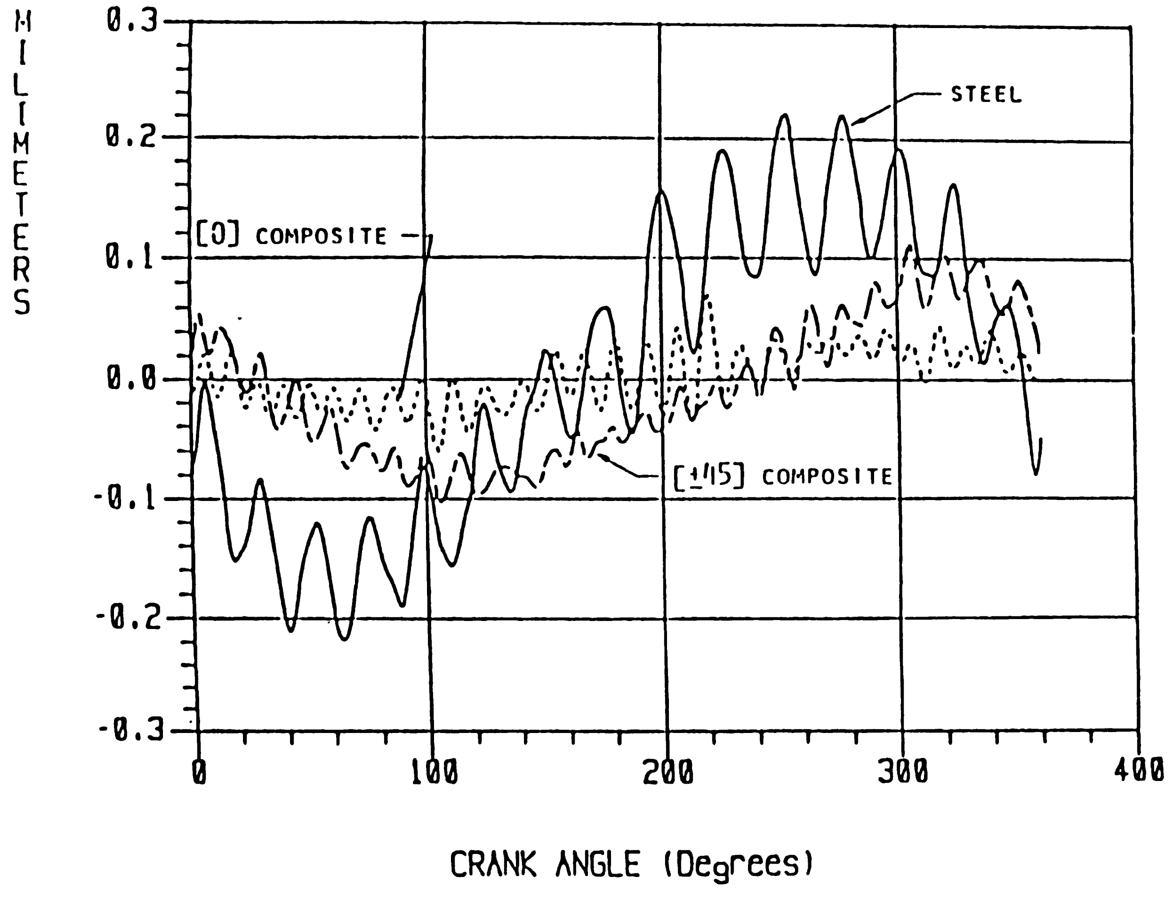

Figure 3.15 Connecting-Rod Midspan Bending Deflections

The calibration data mentioned previously was obtained by supporting each link in the calibration-fixture presented in Figure (3.16). The midspan of each link specimen was subjected to a series of monotonically increasing transverse deflections which were accurately measured by the micrometer attachment on the central support structure. The corresponding voltages from the strain gages bonded to each link specimen were also recorded to complete the calibration procedure.

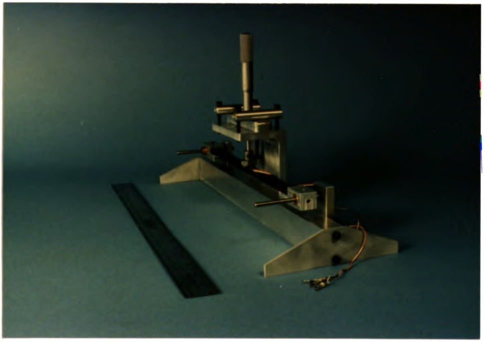

Figure 3.16 Link Calibration-Fixture

The fixture accommodated links of different lengths by subjecting the central support structure and also the supports for the bearing housings to a translational motion in a dove-tailed slot which was machined parallel to the longitudinal axis of the base member. These translating components were then locked in the desired locations by grub-screws.

Figure (3.13) contains a set of results similar to those presented in Figure (3.12), The principal difference between these results is that one set of mechanisms was operating at 280 rpm while the other operated at 198 rpm. These results indicate that the phenomenon evident in Figure (3.12) is not restricted to that particular speed range, but is in fact governed by the universal relationship hypothesized in the beginning of this chapter.

Figure (3.15) presents the results for the midspan deflections of the rocker links of the four-bar linkages. Upon comparing Figures (3.12) and (3.14), it is clear that while the responses of Figure (3.14) closely follow the relative values ofthe stiffness-to-weight ratios presented in Figure (3.7), this characteristic is not quite so evident in Figure (3.12). The much higher response frequencies of the composite links is again clearly demonstrated in these figures, and furthermore, these response data indicate that the polymeric members do not develop maximum deflections in the same mechanism configuration as the steel or aluminum linked systems. This characteristic is probably due to the different damping phenomena of the composites.

Figure (3.15) presents the midspan transverse deflections of connecting rods of slider-crank mechanisms constructed with the carbon steel and the composite laminates. The superior responses of the composite materials is again clearly evident, and furthermore, the maximum deflections, and hence stresses, are again inversely proportional to the stiffness-to-weight ratio of the links for this completely different mechanism system. This experimental study demonstrates that the advanced composite materials not only offer strength and stiffness characteristics superior to metallic designs, high material damping and excellent fatigue life, but furthermore, the designer may be able to synthesize the required material properties from a large number of design variables.

CHAPTER 4

A THEORETICAL AND EXPERIMENTAL INVESTIGATION ON THE DYNAMIC RESPONSE OF FLEXIBLE MECHANISMS MADE FROM COMPOSITE MATERIALS OPERATING UNDER ISOTHERMAL CONDITIONS

4.1 Introduction

The experimental comparison study performed in the last chapter clearly demonstrates that composite materials not only offer strength and stiffness characteristics superior to metallic designs, and also high material damping [23,83], but furthermore, since the engineer has a large number of design variables available for the synthesis process, composite materials may be innovatively fabricated in order to satisfy specific design specification for each particular application.

These chapter presents a theoretical, computational and experimental study of two flexible linkage mechanisms fabricated from two different composite laminates with a variety of combinations of link lengths and geometries. In this study, the mechanical material test results of these two composite laminates were obtained from the last chapter and the constitutive behaviors of the material were then modeled mathematically by employing least-square curve fitting software and a variational theorem was derived for the dynamic analysis of flexible linkages fabricated from viscoelastic composite laminates. Subsequently, a finite element formulation was developed and then implemented to predict the response of both experimental slider-crank mechanisms and four-bar linkages. The experimental program permitted a wide variety of loadings and speed ranges to be imposed on the link specimens under service conditions so that the predictive capability of the mathematical models could be thoroughly evaluated.

4.2 Material Characterization study

The materials selected for this study were a unidirectional 16-ply graphite/epoxy laminate AS4/3501-6 manufactured by Hercules Inc., and a 16-ply laminate with the same constitutents which was fabricated with a symmetrical ply layup of ±45 degrees relative to the longitudinal axis of the beam-like specimen. The mechanical testing of these materials was described in chapter 3 and the experimental results were presented in Figures (3.3) and (3.4) on pages 83 and 84. The results shown in Figure (3.3) suggest that the unidirectional laminate is an elastic material because all of the stress-time gradients are identical. The effective modulus of the unidirectional laminate can be readily calculated from Figure (3.3) because all the responses are linear and of the same gradient. The $[\pm 45]_s$ laminate, however, has a more complex response because the stress-strain history is not linear, and moreover, the gradient depends upon the strain-rate. In order to verify the deductions made from these test data, another test was undertaken to study the creep response of the materials. The results are presented in Figure (3.6) on page 87 and it does show that the $[\pm 45]_s$ composite is truly a viscoelastic material.

There are two types of constitutive relationship expressions for modeling the material characteristics from experimental material testing of viscoelastic materials. These are the creep function and the stress relaxation function. The creep function is obtained by retaining the uniaxial stress constant, then measuring the relation between the strain and time. However, the stress relaxation function is obtained by keeping the uniaxial strain constant and then measuring the relation between the stress and time. This latter method was adopted in order to develop a mathematical model which incorporates the data from the material characterization studies. The objective was to determine the stress relaxation function relating stress and time. Firstly, the maximum strain was measured on the curve on the extreme left of Figure 3.4. This corresponded to a stress of 0.258 MPa (37.5×10^{3} lb_f/in^2) at 0.5 second after the load was initially applied.

Then using this magnitude of strain, a horizontal line was measured from the point of load initiation on each of the response curves in Figure (3.4) and a vertical line was drawn until it intersected each response curve on the upper portion of the curve. This permitted the stress to be obtained and assuming that the rate of application of load was constant (the MTS testing machine was programmed to be constant). This operation permitted a stress-time curve to be plotted and this is presented in Figure (4.1) on page 104.

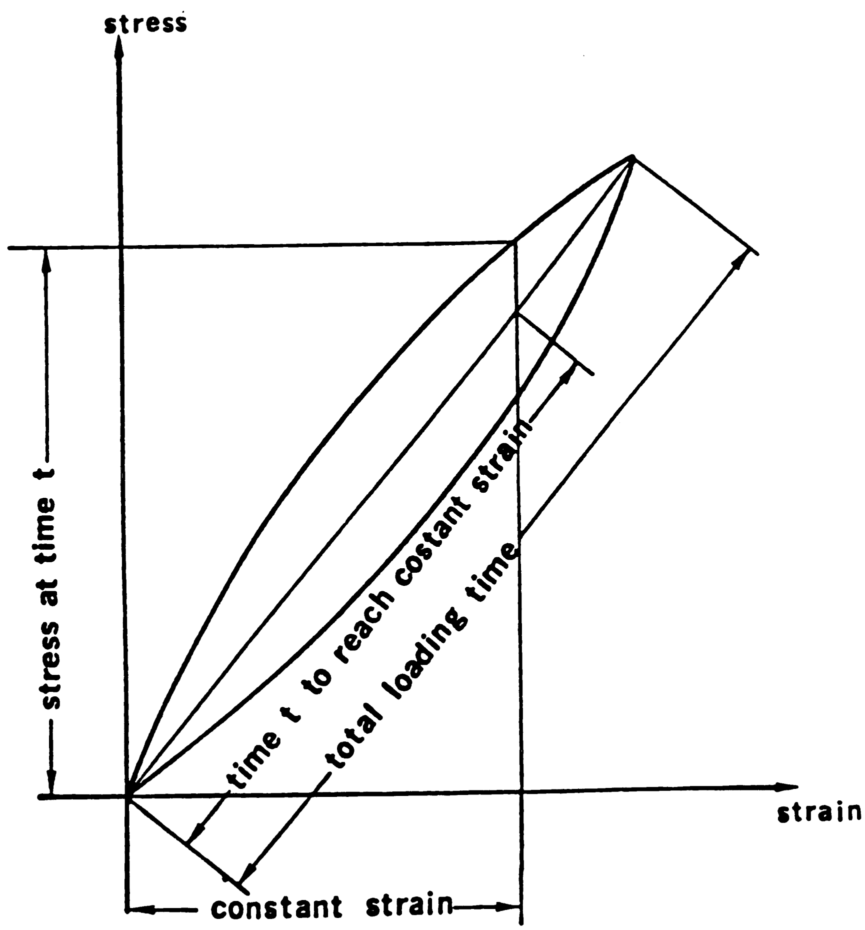

Figure 4.1 Method of Obtaining the Stress Relaxation Function.

The data presented in Figure (4.2) on page 106 is obtained according to the method described above and the constitutive relation was modelled as a standard linear solid viscoelastic model for simplicity. This model may be represented by a spring-dashpot combination shown in Figure (4.3) on page 107 consisting of two springs E_1 and E_2, and a single dashpot η_2.

The constitutive equation may be expressed by

$$\dot{\sigma} + [(E_1+E_2)/\eta_2]\sigma = E_1\dot{\gamma} + (E_1 E_2/\eta_2)\gamma \tag{4.2.1}$$

Let μ be the relaxation time $\mu = \eta_2/(E_1+E_2)$ and multiply both sides of equation (4.2.1) by $\exp(\tau/\mu)$ and integrate this equation from initial state at time zero to the present time t, by assuming that there is zero stress and strain at the initial state, equation (4.2.1) becomes

$$\sigma(t) = [E_1 E_2/(E_1+E_2)]\gamma(t) + \alpha q(t) \tag{4.2.2}$$

$$q(t) = \int_0^t \exp[-(t-\tau)/\mu]\dot{\gamma}(\tau)d\tau \tag{4.2.3}$$

where $\alpha = E_1 - E_1 E_2/(E_1+E_2)$ and the stress relaxation function G(t) is

$$G(t) = E_1 E_2/(E_1+E_2) + \alpha \exp(-t/\mu) \tag{4.2.4}$$

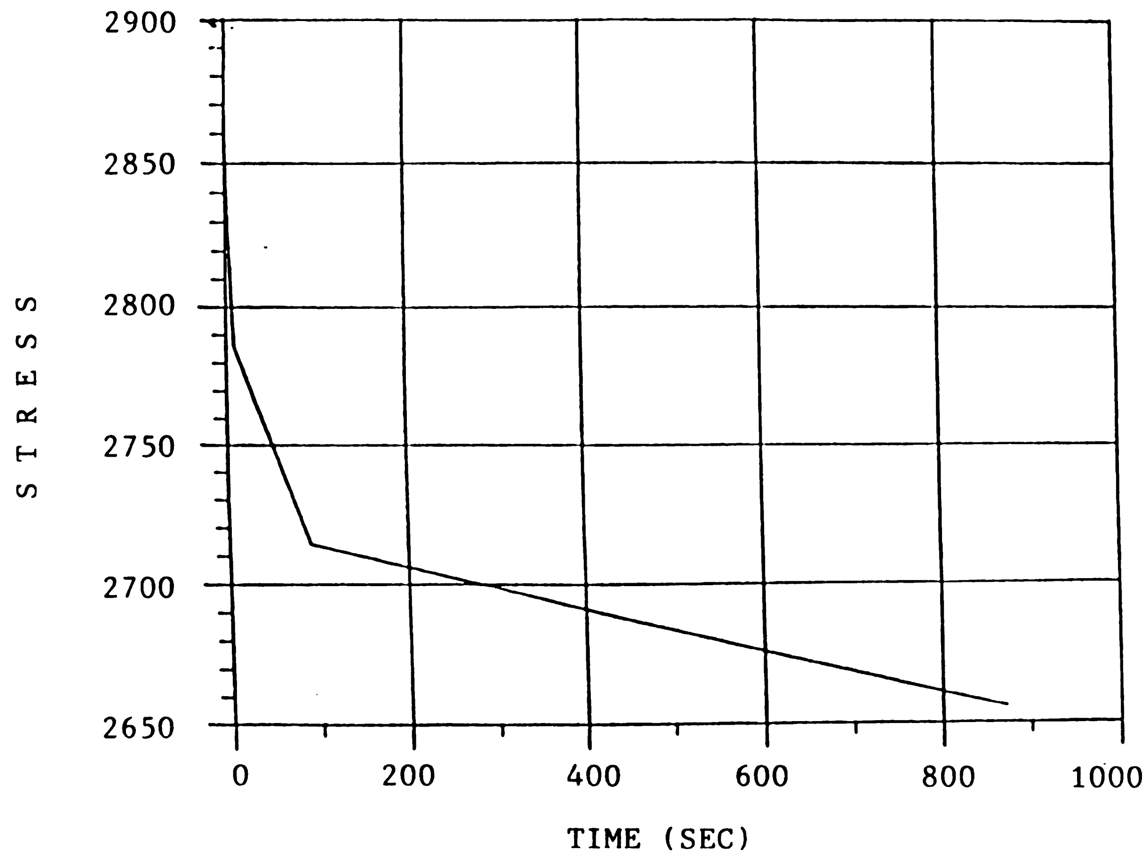

Figure 4.2 Stress Relaxation Function Obtained from Material Testing

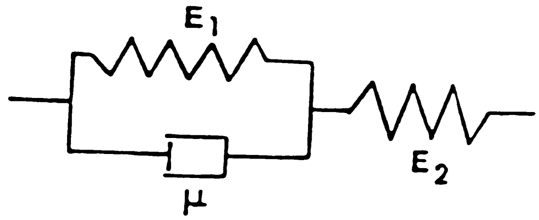

Figure 4.3 Standard Linear Solid Model

By employing a least-square curve-fitting software package to determine the parameters E_1, E_2 and η_2, the graph of the curve-fitted stress relaxation function is presented in Figure (4.4) on page 108. Then the constitutive equation for this class of material may be represented by

$$\sigma_{ij} = \int_0^t G_{ijkl}(t-\tau)\partial\gamma_{kl}(\tau)/\partial\tau \, d\tau \tag{4.2.5}$$

or

$$\sigma_{ij} = G_{ijkl}{*}d\gamma_{kl} \tag{4.2.6}$$

where σ_{ij} is the Lagrangian stress tensor, γ_{kl} is the associated strain tensor, τ is the time variable and t is the current time and the Stieltjes convolution, $\theta{*}d\phi$ of two functions $\theta(t)$ and $\phi(t)$ is defined by

$$\theta{*}d\phi = \int_{-\infty}^{t} \theta(t-\tau)d\phi(\tau) \tag{4.2.7}$$

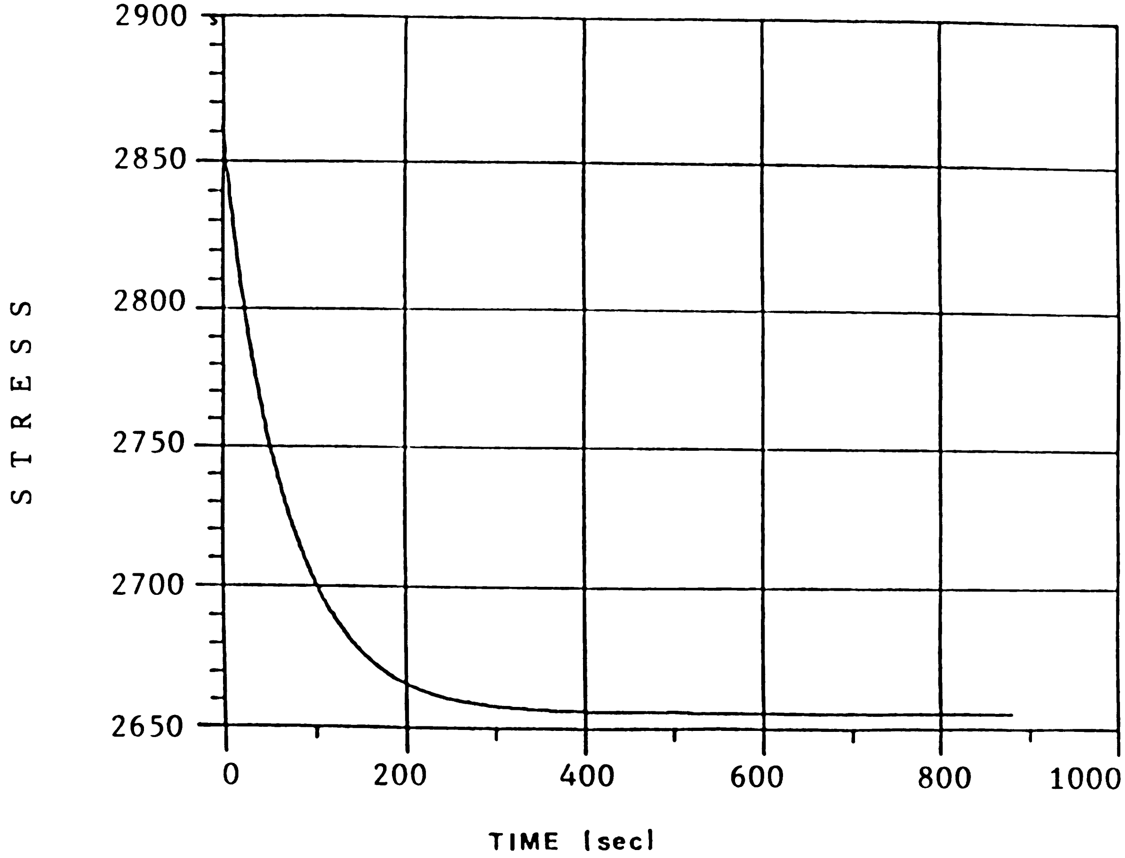

Figure 4.4 Stress Relaxation Function Obtained from Curve-Fitting.

where $\phi(t) \to 0$ for $t \to \infty$ and $\Theta(t)$ is continuous for $0 \leq t < \infty$. Assuming further that $\Theta(t)=0$ for $t<0$, then equation (4.2.7) may be shown to satisfy the commutivity, associativity and distributivity properties of Stieltjes computations [62,63,64].

4.3 Variational Principle

The same methodology is adopted as the variational development in the previous chapters. In this chapter, the variational principle incorporated a variety of auxilary conditions such as the constitutive equation, the strain-displacement equation and the geometrical boundary conditions. Hamilton's Principle is presented using the Stieltjes convolution integral notation.

The dynamical problem of a viscoelastic body of volume V and surface area S describing a general spatial motion relative to an inertial frame OXYZ is considered. In Figure (2.1) page 30, oxyz are Lagrangian coordinates fixed in the body in a reference state containing zero deformations, strains and stresses. Furthermore, it is also assumed that these parameters have been zero throughout the previous time history. Employing a Cartesian tensor notation, at time t, a general point P in the continuum has the position vector

$$r_i = r_{oi} + r_{Ri} + u_i \qquad (4.3.1)$$

where r_{oi} is the position vector of the origin of the body axes relative to the origin of the inertial frame, r_{Ri} represents the position vector of point P in the undeformed reference state relative to the origin of the body axes and u_i is the deformation displacement vector. Equation (4.3.1) may be differentiated with respect to time to yield the velocity rate-of-change of displacement expression

$$P_i = \tilde{r}_{oi} + \tilde{u}_i + e_{ijk}\dot{\theta}_j(r_{oi} + r_{Rk} + u_k) \qquad (4.3.2)$$

where P_i is the absolute velocity associated with r_i. In addition, e_{ijk} is the alternating tensor, $\dot{\theta}_j$ is the angular velocity defining the rotation of the Lagrangian frame oxyz, $(\tilde{\ })$ represents the time rate-of-change with respect to the moving frame oxyz and $(^\circ)$ represents the absolute rate-of-change.

In order to provide the basis for analyzing flexible linkage mechanisms fabricated with viscoelastic materials, the stationary conditions are sought for the functional

$$F_* = \int_V \left[1/2\delta_{ij}\rho P_i * dP_j + X_i * dr_i - 1/2G_{ijkl} * dr_{ij} * dr_{kl}\right] dV$$
$$+ \int_{S_1} \bar{g}_i * dr_i dS_1 \qquad (4.3.3)$$

subject to the constraints imposed by equations (4.2.6) and (4.3.2), and also the following field equation

$$\gamma_{ij} = 1/2(u_{i,j} + u_{j,i}) \qquad (4.3.4)$$

which is the linear strain-displacement relationship. In these equations, a comma denotes spatial differentiation, δ_{ij} is the Kronecker delta, ρ is the mass density of the material, g_i is the surface traction vector and the overbar ($^{-}$) denotes a prescribed quantity.

The total surface area of the continuum is denoted by S which is the summation of regions S_1 and S_2. Tractions are prescribed on S_1, while on S_2, the prescribed deformation displacement boundary condition

$$\bar{u}_i = u_i \tag{4.3.5}$$

is imposed.

Equations (4.2.6), (4.3.2), (4.3.4) and (4.3.5) may be incorporated within functional F_0 using Lagrange multipliers to create a free variational problem defining a new functional F. The first variation is then generated using the standard rules of the variational calculus, and this procedure involves utilizing the divergence theorem and also the symmetric properties of the tensors where appropriate. Upon setting the first variation equal to zero, the Lagrange multipliers may be expressed in terms of the system parameters leading to the following variational equation of motion:

$$\delta F = 0 = \int_V \Big[(\sigma_{ij} - G_{ijkl} * d\gamma_{kl}) * d\delta\gamma_{ij}$$

$$-(\sigma_{ij,j} + X_i - \rho \dot{P}_i) * d\delta u_i$$

$$-(\gamma_{ij} - 1/2[u_{i,j} + u_{j,i}]) * d\delta\sigma_{ij}$$

$$-(P_i - \rho[\tilde{r}_{oi} + \tilde{u}_i + e_{ijk}\dot{\emptyset}_j(r_{ok} + r_{Rk} + u_k)] * d\delta P_i \;)\Big] dV$$

$$+ \int_{S_1} [(g_i - \bar{g}_i) * d\delta u_i] dS_1 + \int_{S_2} [(\bar{u}_i - u_i) * d\delta g_i \;] dS_2$$

$$+ \Big[\int_V X_i dV + \int_{S_1} \bar{g}_i dS_1 - \int_V \rho \dot{P}_i dV\Big] * d\delta r_{oi} \qquad (4.3.6)$$

$$+ \Big[\int_V e_{ijk} X_i (r_{ok} + r_{Rk} + u_k) dV + \int_{S_1} e_{ijk} \bar{g}_j \; (r_{ok} + r_{Rk} + u_k) dS_1$$

$$- \int_V e_{ijk} \dot{P}_i \rho (r_{ok} + r_{Rk} + u_k) dV\Big] * d\delta\emptyset_j$$

Independent arbitrary variations of the deformation displacement, strain, stress, absolute velocity, and the kinematic parameters defining the rigid-body motion enable equation (4.3.6) to yield, as Euler equations, the field equations and boundary conditions for this class of dynamic viscoelastic problem. This variational statement represents a generalization to the theory of viscoelasticity of the elastodynamic variational theorem presented in chapter 2. In fact if the body being subjected to the analysis were elastic, then the time integrations in equation (4.3.6) could be evaluated and the resulting theorem would distill to the formulation developed in chapter 2.

The characteristic equations obtained from equation (4.3.6) precisely define the dynamic viscoelastic problem associated with the analysis of mechanisms fabricated with linear viscoelastic materials.

However an exact solution for these equations is beyond current mathematical means, and in any case would probably contain too much information to be useful to an industrial design engineer for solving practical problems. Simplifying assumptions are therefore needed, and these center upon which model to be adopted to represent the material constitutive relationship, equation (4.2.5).

A variety of approaches have been developed for this task. Numerical viscoelastic analyses have been undertaken by Laplace transform techniques [76], by numerical integration of the constitutive equations [37], by step-by-step procedures used in conjunction with mechanical models for the constitutive equations [204], by using complex-modulus forms of the relaxation functions [201], and also by finite-difference formulations [98,212]. Thus, a wide variety of techniques have been proposed, but there is no consensus of opinion as to which is the best approach. In order to simplify this viscoelastic problem, a one-dimensional linear-solid model is assumed herein and a finite-difference approach is adopted [98,212].

The constitutive equation (4.2.5) is to be used in a numerical analysis scheme by changing the integration form into a summation of discretized time increments for obtaining the dynamic response of the mechanism systems. For example, the strain-rate $\dot{\gamma}(\tau)$ in equation (4.2.5) may be represented by a linear interpolation function over each increment:

$$\dot{\gamma}(\tau) = \dot{\gamma}(t-h) + (h-t+\tau/h)[\dot{\gamma}(t)-\dot{\gamma}(t-h)] \qquad (4.3.7)$$

in which $t-h \leq \tau \leq t$ and h represents the integration increments.

Separating equation (4.2.3) into two parts, it can be shown that

$$q(t) = \exp(-h/\mu)q(t-h) + \int_{t-h}^{t} \exp[-(t-\tau)/\mu]\dot{\gamma}(\tau)d\tau \tag{4.3.8}$$

Then substituting equation (4.3.7) into equation (4.3.8) and explicitly carrying out the integration leads to

$$q(t) = \beta q(t-h) + \lambda_1\dot{\gamma}(t-h) + \lambda_2\dot{\gamma}(t) \tag{4.3.9}$$

in which

$$\lambda_1 = \mu[-\beta+\mu/h\ (1-\beta)] \tag{4.3.10}$$

$$\lambda_2 = \mu[1-\mu/h\ (1-\beta)] \tag{4.3.11}$$

$$\beta = \exp(-h/\mu) \tag{4.3.12}$$

Equation (4.3.9) is a recurrence formula for the value of the present stress in terms of its value at the previous time step and the value of the strain rate at both the previous and the present time steps; it is used in conjunction with equation (4.2.2) to characterize a linear viscoelastic material. It is seen that this approach permits characterization of the hereditary nature of the material by retaining strain history information at only the immediately proceeding time step.

The appearance of both the relaxation moduli of the material, μ, and the integration step size, h, in the parameters of the recurrence formula for q indicates an interaction between the mechanism system, the material, and the solution procedure. In general the step size is governed by the highest frequency among the natural frequencies of the system and the dominant forcing frequency. If the step size, h, is determined from the system considerations, an examination of the numerical behavior of the coefficients in equation (4.3.9) as a function of the material parameter, μ, it is expected to provide some insight of the system behavior. For small values of the dimensionless parameter h/μ, utilizing (4.3.10), (4.3.11) and (4.3.12)

$$\beta \simeq 1$$

$$\lambda_1 \simeq \lambda_2 \simeq h/2 \tag{4.3.13}$$

and for large values of h/μ,

$$\beta \simeq \lambda_1 \simeq 0$$

$$\lambda_2 \simeq \mu \tag{4.3.14}$$

In the former case the behavior is primarily that of an elastic element, in the latter that of a viscous element.

4.4 Finite Element Formulation

The variational equation of motion (4.3.6) may be employed as the basis for a variety of finite element models depending upon the geometrical shape of the body being analyzed, the type of deformation theory assumed to be appropriate, the information sought from the analysis, and the accuracy of the model for the constitutive equations. Herein, a displacement finite element model is developed for analyzing the flexural response of the beam-shaped links of planar linkage mechanisms deforming in the plane of the mechanism. This is accomplished by first assuming that the flexural deformation field is governed by the classical Euler-Bernoulli hypothesis. The constitutive equation is obtained by material testing, and the deformation of the link is assumed to be so small that it is not necessary to model geometrically nonlinear deformations. The objective, herein, is to develop a linear displacement formulation for a single one-dimensional finite element with two exterior nodes, each having three nodal degrees of freedom. Two nodal variable W and θ describe the flexural displacement and slope respectively, while U describes the longitudinal displacement as shown in Figure 4.5.

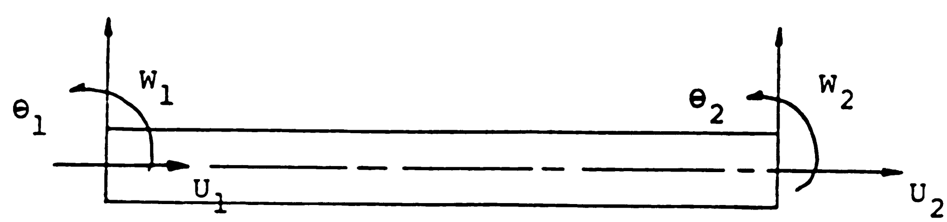

Figure 4.5 The Deformation of a Beam Element

Defining the nodal displacement vector for the element by

$$[U]^T = [U_1 \quad U_2 \quad W_1 \quad W_2 \quad \theta_1 \quad \theta_2] \tag{4.4.1}$$

the general displacements $u(x,t)$ and $w(x,t)$ at any point in the element may be related to $[U]$ by

$$[u \quad w]^T = [N][U] \tag{4.4.2}$$

where $[N]$ contains the shape functions.

The axial displacement is defined by

$$u_x = u_o - z\partial w/\partial x \tag{4.4.3}$$

where $u_o(x,t)$ is the axial displacement, $w(x,t)$ the transverse displacement and x is the longitudinal spatial variable. The axial strain corresponding to equation (4.4.3) may be written as

$$[\gamma_{xx}] = [N'][U] \tag{4.4.4}$$

where $(')$ denotes spatial differentiation with respect to x.

The finite element representation of the constitutive equation (4.2.2) of the viscoelastic material is

$$[\sigma_{xx}(t)] = [E_1 E_2/(E_1+E_2)][\gamma_{xx}(t)] + \alpha\Big[\exp(-h/\mu)[q(t-h)] + \lambda_1[\dot{\gamma}_{xx}(t-h)] + \lambda_2[\dot{\gamma}_{xx}(t)]\Big] \qquad (4.4.5)$$

The variational equation of motion (4.3.6) may be written as

$$\begin{aligned}
\delta F = 0 = &\int_V [\delta\gamma_{xx}(t)]^T \Big[[\sigma_{xx}(t)] - (E_1 E_2/(E_1+E_2))[\gamma_{xx}(t)] \\
&- \alpha\Big[\exp(-h/\mu)[q(t-h)] + \lambda_1[\dot{\gamma}_{xx}(t-h)] + \lambda_2[\dot{\gamma}_{xx}(t)]\Big]\Big]dV \\
&+ \int_V \rho[\delta P]^T\Big[[P] - [N_R][P_R] - [N][\dot{U}]\Big]dV \\
&- \int_V [\delta U]^T[N]^T\Big[\partial[\sigma_{xx}(t)]/\partial x + [X] - \rho[\dot{P}]\Big]dV \\
&+ \int_V [\delta\sigma_{xx}]^T\Big[[\gamma_{xx}] - [N'][U]\Big]dV \qquad (4.4.6) \\
&+ \int_{S_1} [\delta U]^T[N]^T([\bar{g}] - [g])dS_1 \\
&- \int_{S_2} [\delta g]^T([\bar{U}] - [N][U])dS_2
\end{aligned}$$

where $[N_R]$ contains the shape functions approximating the rigid-body kinematics while $[P_R]$ is the column vector containing the nodal rigid-body velocities. The nodal absolute velocity components are defined by $[P]$ and the surface tractions by $[g]$. Finally, because the rigid-body equations of motion are of no consequence here, they may be removed from the formulation by taking variations $[\delta r_{oi}]$ and $[\delta\phi_i]$ to be zero.

In order to express the finite element formulation in terms of deformation of the links, attention is now focused upon the equation of equilibrium. The first term may be written as

$$\int_V [\delta U]^T[N]^T \partial[\sigma_{xx}(t)]/\partial x \; dV \tag{4.4.7}$$

An integration-by-parts over x yields

$$\left[\int_A [\delta U]^T[N]^T[\sigma_{xx}(t)]dA \right]_x - \int_V [\delta U]^T[\acute{N}]^T \, [\sigma_{xx}(t)]dV \tag{4.4.8}$$

The first term in equation (4.4.8) is a boundary term, to be evaluated on the cross-sectional area A, at the extremes of the one-dimensional element, and this is identical to the manipulation in chapter 2. Therefore, it will not be discussed in this chapter. The second term becomes, using the first and fourth volume integral expressions in equation (4.4.6),

$$-\int_V [\delta U]^T[\acute{N}]^T\Big[\, (E_1 E_2/(E_1+E_2))[\acute{N}][U(t)] + \alpha\Big[\, \exp(-h/\mu)[q(t-h)]$$
$$+ \lambda_1[\acute{N}][\mathring{U}(t-h)] + \lambda_2[\acute{N}][\mathring{U}(t)] \, \Big] \Big]dV \tag{4.4.9}$$

The first term in equation (4.4.9) yields the standard linear stiffness matrix [K] defined by

$$[K] = \int_V [\dot{N}]^T (E_1 E_2/(E_1+E_2))[\dot{N}]dV \qquad (4.4.10)$$

The second and third terms in equation (4.4.9), which feature the hereditary nature of the material, are defined as

$$[F_h] = \int_V [\dot{N}]^T \alpha \; \exp(-h/\mu) q(t-h)dV + \int_V [\dot{N}]^T \lambda_1 \; \alpha [\dot{N}][\dot{U}(t-h)]dV$$

$$(4.4.11)$$

From equation (4.4.11) $[F_h]$ is known as a force term which is contributed from the stresses and viscous strains of the previous time step. The fourth term of equation (4.4.11) is recognized as a damping matrix [C]

$$[C] = \int_V [\dot{N}]^T \lambda_2 \alpha [\dot{N}]dV \qquad (4.4.12)$$

Substituting equations (4.4.10), (4.4.11) and (4.4.12) into equation (4.4.9) leads to

$$-[\delta U]^T \Big[\; [k][U] + [F_h] + [C][\dot{U}] \; \Big] \qquad (4.4.13)$$

According to the derivation in chapter 2, the variational equation of motion may now be written in the final form

$$
\begin{aligned}
\delta F = 0 = &\int_V [\delta\gamma_{xx}]^T\Big[[\sigma_{xx}(t)] - (E_1 E_2/(E_1 + E_2))[\gamma_{xx}] \\
&- \alpha(\exp(-h/\mu)[q(t-h)] + \lambda_1[\dot{\gamma}_{xx}(t-h)] + \lambda_2[\dot{\gamma}_{xx}(t)])dV \\
&- \int_V \rho[\delta P]^T([P]-[N_R][P_R]-[N][\dot{U}])dV \\
&+ [\delta U]^T\Big[([K][U]+[C][\dot{U}]+[M][\ddot{U}]+[F_h])-\int_V [N]^T[X]dV \\
&- \int_{S_1} [N]^T([\bar{g}]dS_1 - [M_R][\dot{P}_R]) \Big] \\
&+ \int_V [\delta\sigma_{xx}]^T([\gamma_{xx}]-[\acute{N}][U])dV \qquad (4.4.14) \\
&- \int_{S_2}[\delta g]^T([\bar{U}]-[N][U])dS_2
\end{aligned}
$$

When independent arbitrary variations of the system variables in equation (4.4.14) are permitted, this equation yields the field equations and displacement boundary conditions for one finite element. This formulation provides the basis for developing a finite element model of a general planar flexible mechanism in order to investigate the dynamic linear viscoelastic response.

The experimental apparatus of four-bar linkage, slider-crank mechanism and related intrumentations are the same as those used in chapters 2 and 3. The only difference is the dimension of the linkage specimens employed in this study. These data will be introduced later.

4.5 Comparison between Theoretical and Experimental Result

A solution for these equations will be sought using the Newmark method of direct integration which uses the following statements to update the kinematic terms as the response is discretized,

$$\dot{U}_{t+\Delta t} = \dot{U}_t + [(1-\beta)\ddot{U}_t + \beta\ddot{U}_{t+\Delta t}]\Delta t \qquad (4.5.1)$$

$$U_{t+\Delta t} = U_t + \dot{U}_t\Delta t + [(1/2-\alpha)U_{Ut} + \alpha\ddot{U}_{t+\Delta t}]\Delta t^2$$

$$(4.5.2)$$

where $\beta \geq 0.5$ and $\alpha \geq 0.25(0.5+\beta)^2$ for stability of solution [21]. The algorithm models the system by considering the continuous motion of the mechanism to be discretized. Thus, the inertial loading from the rigid-body analysis is used to continually update the force funtion for a series of time intervals, and the response is determined for each time increment to give a set of discrete values for the link deformation.

With all direct integration methods, solution instability must be considered carefully, and it was avoid here by choosing $\beta=0.5$. Under these conditions the system is unconditional stable. Finally, a numerical value must be assigned to the step-size Δt which is determined by choosing $\Delta t \leq T/10$, where T is the smallest period in the response [21]. Thus the step-size is governed by the higher modes of vibration presented in the response and for stiff systems this may necessitate a small step size.

Figures (4.6)-(4.11) on pages 124-129 present computer-generated experimental response curves superimposed upon the results of computer simulations for the dynamic response of the midspans of the links of the flexible four-bar linkages and slider crank mechanisms tested. The predictive capabilities of the mathematical models were tested by running the mechanisms at different operating speeds, which inherently imposes different loading on the links; mechanisms with different link-length combinations and a variety link materials, and link cross-sections were also employed in this investigation.

Figures (4.6) and (4.7) present the midspan transverse deflections of a 304.8 mm long connecting-rod of the slider-crank mechanism fabricated with a $[\pm 45]_s$ laminate. The thickness of the link in the plane of the mechanism was 2.34mm, the width perpendicular to the plane of the mechanism was 19.05mm and the length of the composite specimen was 228.6mm. It is evident from the figures that there is reasonably good correlation between both the amplitude and phase components of the response at both operating speeds for these viscoelastic links.

Figures (4.8), (4.9) and (4.10) present the midspan transverse deflections of the coupler and rocker links of a four-bar linkage in which both links were fabricated with a unidirectional laminate, and operated at three different crank frequencies. The coupler and rocker links had the same overall length of 304.8mm long. The thickness of the laminate in the plane of the mechanism was 1.93mm and the width perpendicular to the plane of the mechanism was 19.05mm. Again there is good correlation between the theoretical and experimental responses for

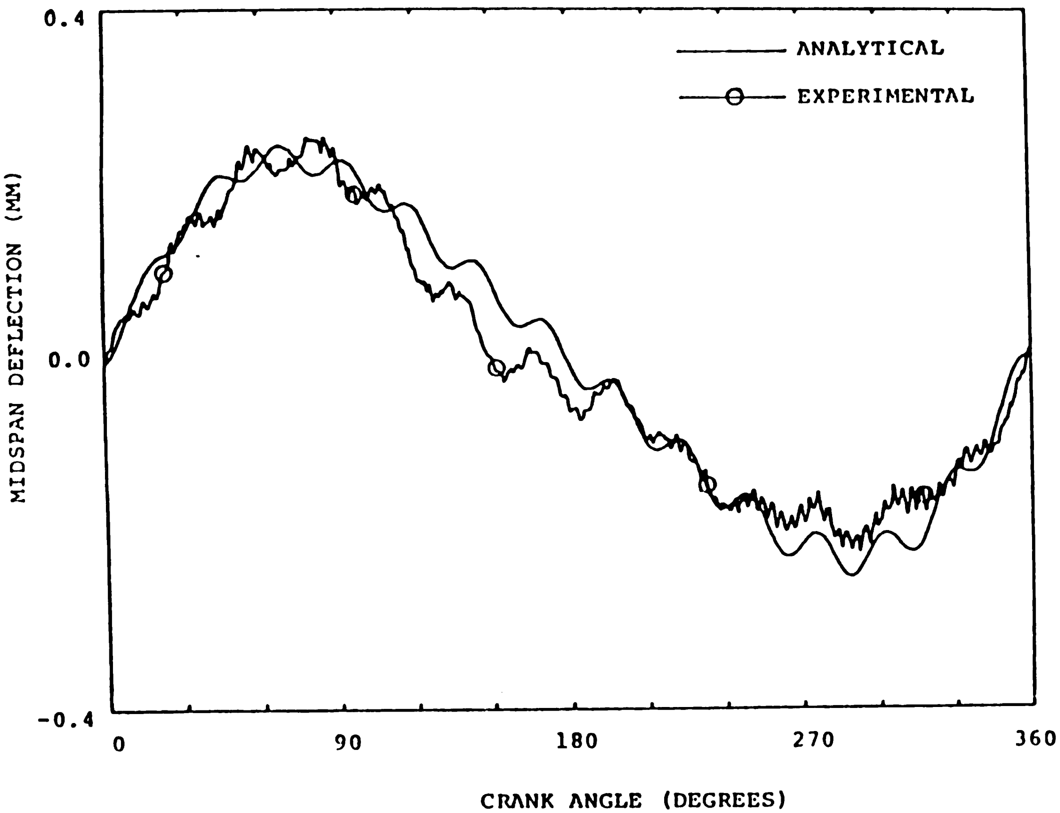

Figure 4.6 Slider-Crank Mechanism: $[\pm 45]_s$ Connecting-rod Midspan Trans. Deflection at 154 rpm, time-step 1.80375×10^{-5} s

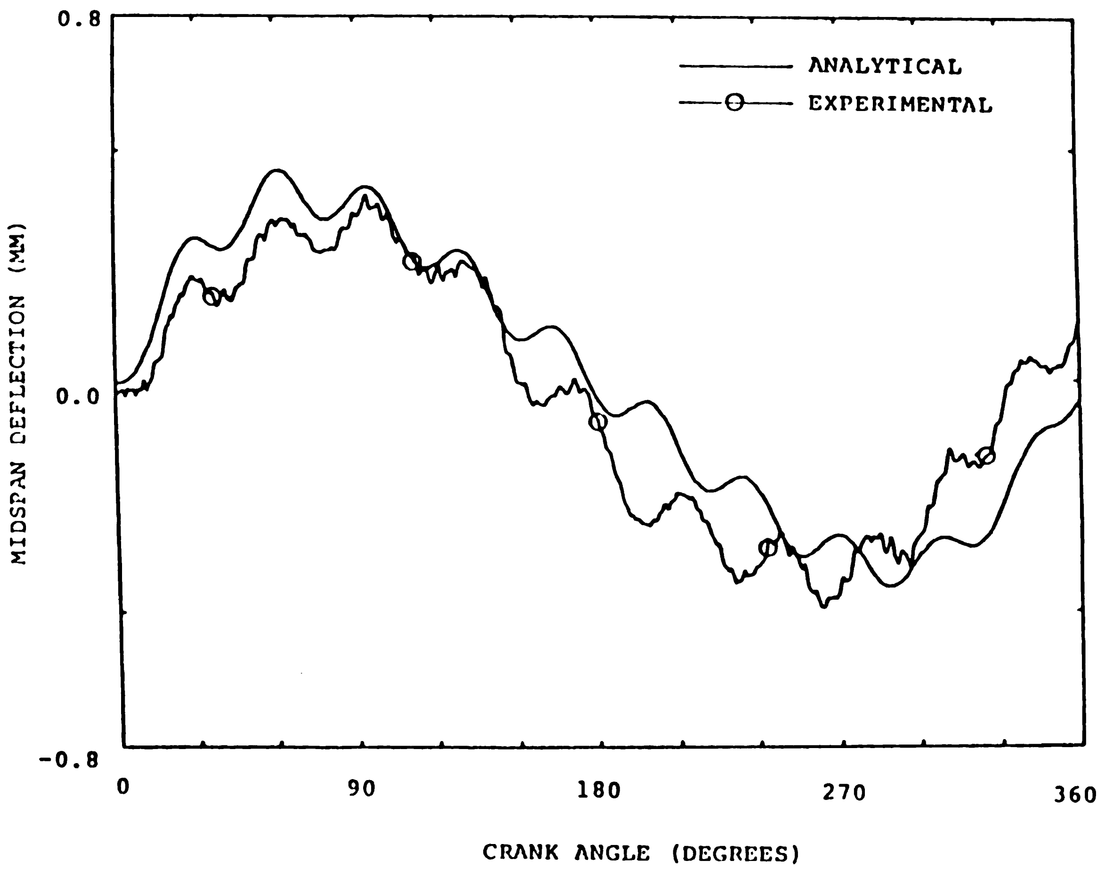

Figure 4.7 Slider-Crank Mechanism: $[\pm 45]_s$ Connecting-rod Midspan Trans. Deflection at 212 rpm, time-step 1.31027×10^{-3} s

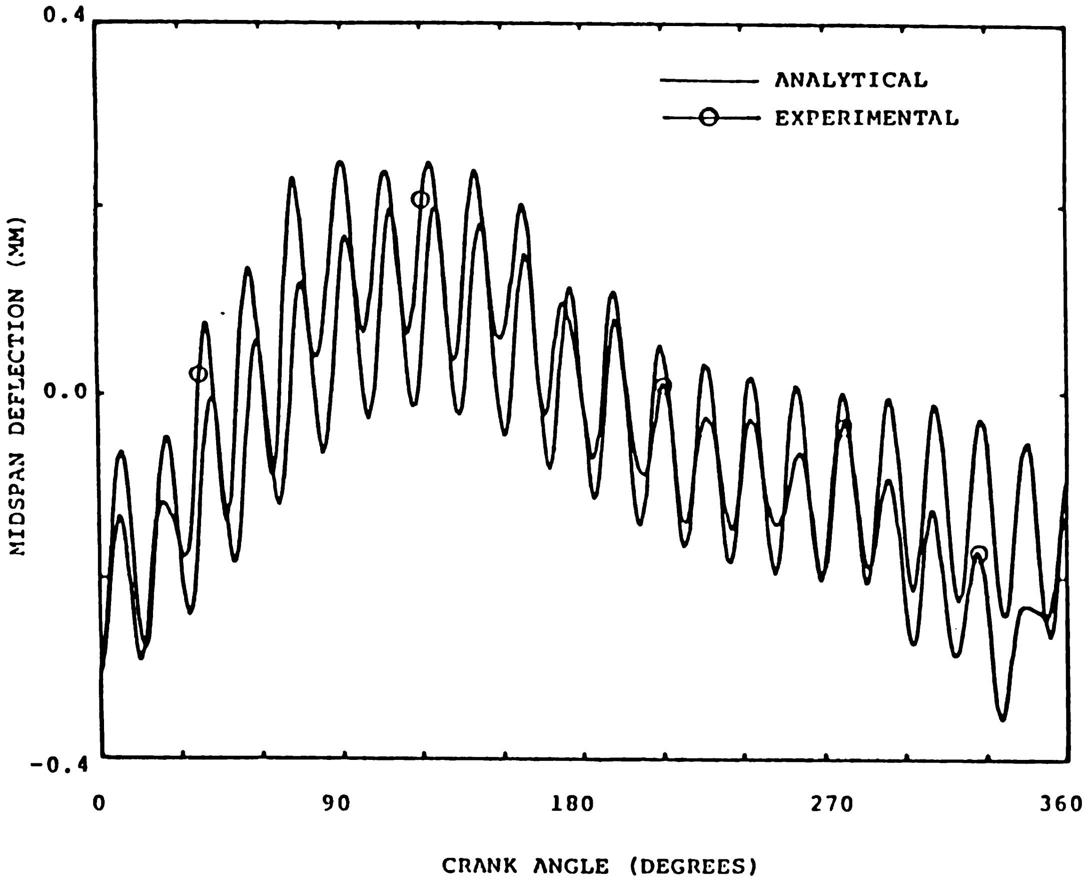

Figure 4.8 **Four-Bar Linkage: Unidirectional Coupler Link Midspan Trans. Deflection at 212 rpm, time-step 1.31027×10^{-5}s**

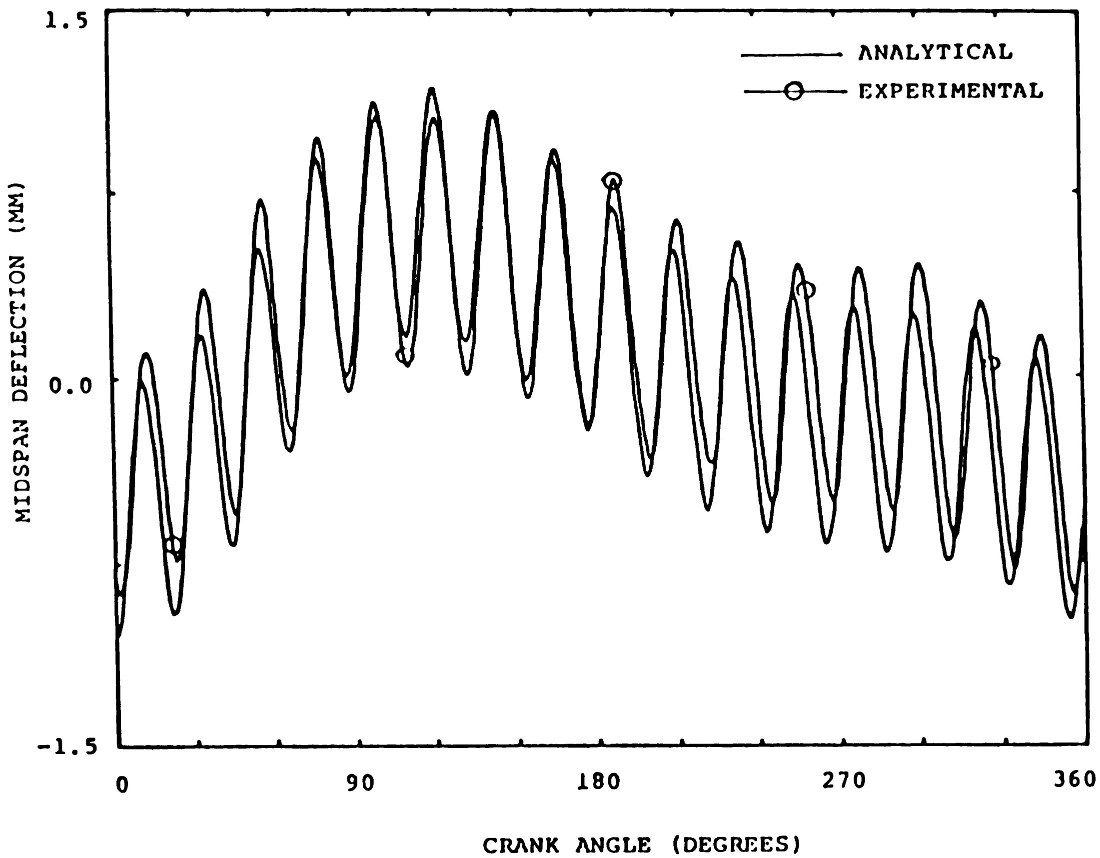

Figure 4.9 **Four-Bar Linkage: Unidirectional Coupler Link Midspan Trans. Deflection at 278 rpm, time-step 0.9992×10^{-5} s**

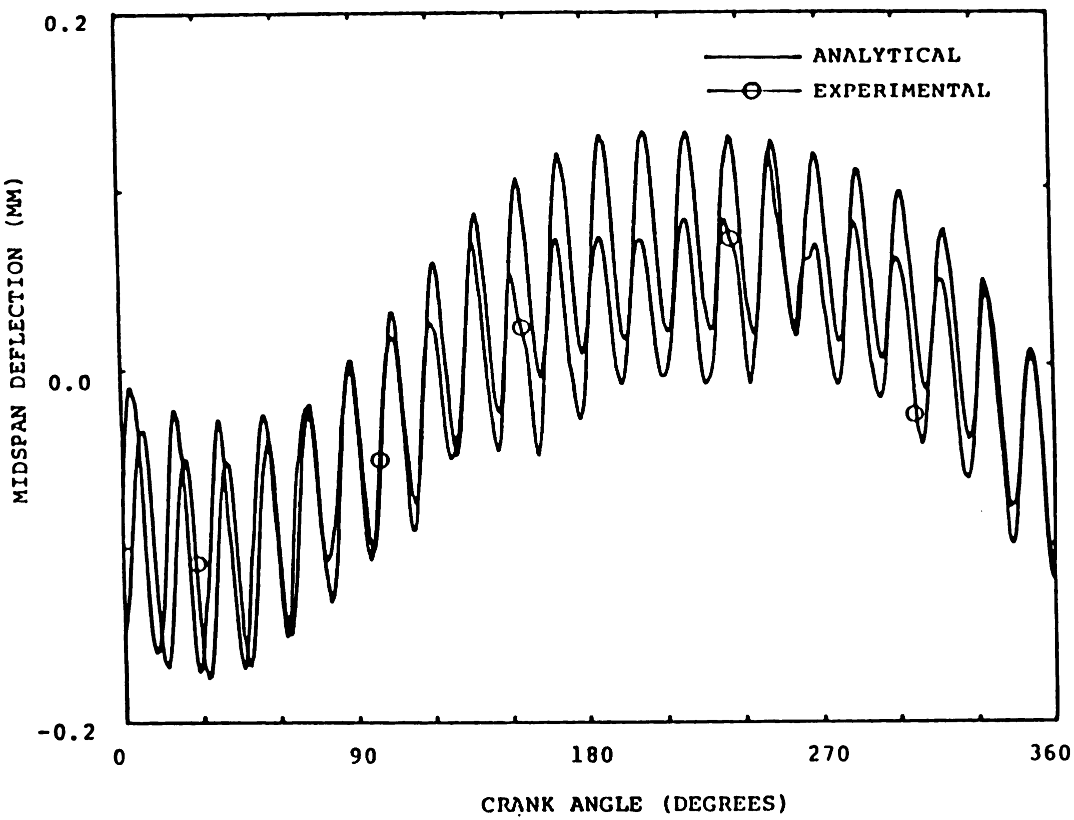

Figure 4.10 **Four-Bar Linkage: Unidirectional Rocker Link Midspan Trans. Deflection at 187 rpm, time-step 1.48544x10^{-5}s**

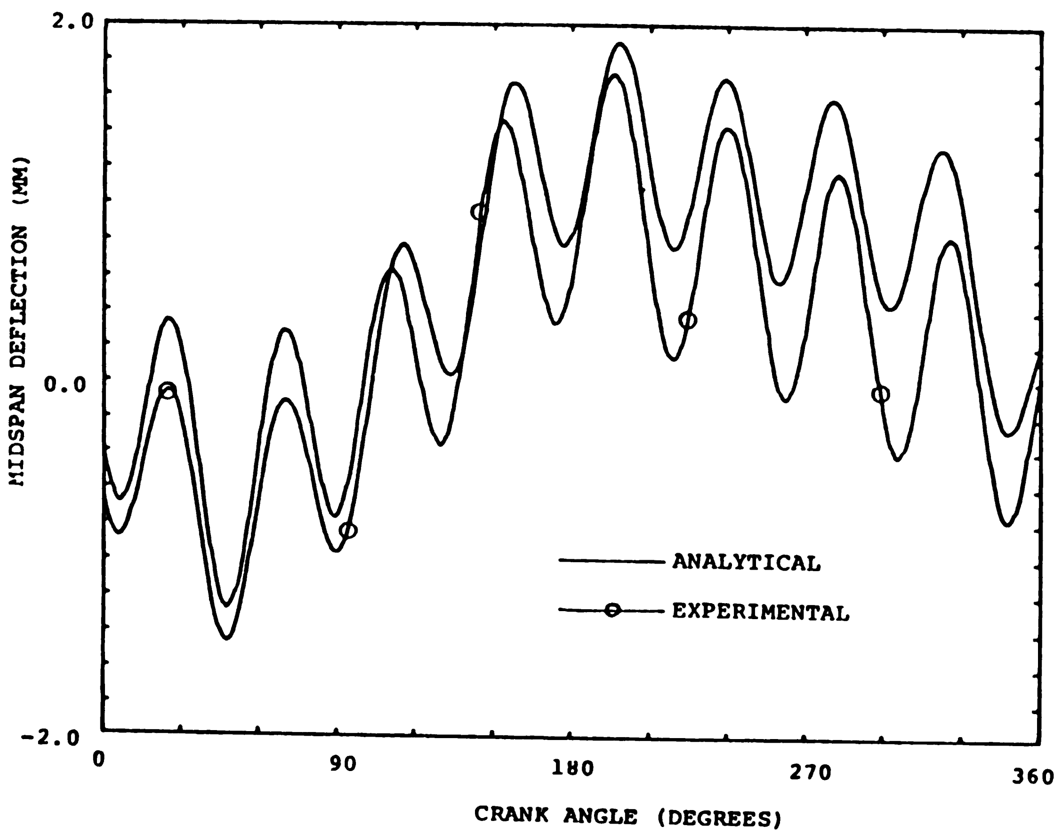

Figure 4.11 Four-Bar Linkage: $[\pm 45]_s$ Rocker Link Midspan Transverse Deflection at 223 rpm, time-step 1.24564×10^{-5}s

this different kinematic chain in which two links, rather than one, was flexible.

Figure (4.11) presents the transverse midspan response of the rocker link of a four bar mechanism operating at 223 rpm. This link was fabricated with a $[\pm 45]_s$ graphite-epoxy specimen of dimensions 19.05mm x 2.337mm x 152.4mm to form a link of length 228.6mm between bearing centre-lines. The coupler link, however, was fabricated with a unidirectional graphite-epoxy laminate of dimensions 9.09mm x 1.93mm x 304.8mm to form a link of length 304.8mm between bearing axes. Again, the mathematical model readily captures the frequency content of the experimental response but there is a small amplitude error (about 10%)between the two waveforms.

Hence it is apparent that the mathematical model developed herein for analyzing the dynamic response of linkage fabricated with commercial graphite epoxy laminates is capable of predicting the response of a variety of mechanism systems with the one or more flexible links fabricated with different combinations of link materials, link geometries and link lengths for a number of different operating speeds. The discrepancy between the experimental results and computer simulations is 10 percent which may suggest the need for an improved modeling of the constitutive equation because the material is subjected to changing environmental conditions.

CHAPTER 5

A THEORETICAL ANALYSIS FOR HYGROTHERMOVISCOELASTICITY

5.1 Thermoviscoelasticity: A Background Review

The field of non-equilibrium thermodynamics provides a general framework for the macroscopic description of irreversible processes. It is a branch of macroscopic physics, and it has been connected with macroscopic solid mechanics in the investigation described herein. The thermodynamics of irreversible processes should be set up from the start as a continuum theory, treating the state parameters of the theory as field variables, (i.e., as continuous functions of space coordinates and time). Moreover, the basic equations of the theory are formulated in such a way that they contain quantities referring to a single point in space at one time (i.e. in the form of local equations). However in equilibrium thermodynamics such a local formulation is generally not needed, since the state variables are usually independent of the space coordinates.

In non-equilibrium thermodynamics, the so-called balance equation for entropy plays a central role. This equation expresses the fact that the entropy of a volume element changes with time for two reasons. First it changes because entropy flows in or out of the volume element, and second because there is an entropy source due to irreversible pheonomena inside the volume element [66]. The domain of validity of non-equilibrium thermodynamics is essentially the one for which local equilibrium is attained and the phenomenological equations are linearly defined. Therefore, the entropy source vanishes for reversible thermodynamics and this is the local formulation of the second law of thermodynamics. The main aim is to relate the entropy source explicitly to the various irreversible processes that occur in a system. To this end, the macroscopic conservation laws of mass, momentum and energy in local (i.e.differential) form are necessary for further development. These conservation laws contain a number of quantities such as the diffusion flows, the heat flow and the stress tensor, which are related to the transport of mass, energy and momentum, respectively.

The general form of the magnitudes of the entropy source may then be determined by the thermodynamic Gibbs relation which connects the rate-of-change of entropy in each mass element to the rate-of-change of energy, the rate-of-change of moisture content, and the dissipation work. The entropy source has a very simple appearance being a sum of terms. Each term being a product of a flux characterizing an irreversible process, and a thermodynamic force, which is related to the spatial non-uniformity of one or more of the system properties (the gradient of temperature for instance). The entropy source strength can then serve as a basis for the systematic description of the irreversible processes occurring in a system. For example, each flux function may be derived from the general form of the entropy source strength by the Onsager and Casimir law of reciprocity [49 ,66]. And then the governing equations of the irreversible processes are obtained by substituting the flux functions into the balance equation of mass, equation of motion and energy equation. The detailed derivation is presented in the remaining part of this chapter.

As yet the set of conservation laws together with the entropy balance equation and the equations of state are to a certain extent incomplete, since this set of equations contains the irreversible fluxes as unknown parameters and can therefore not be solved with given initial and boundary conditions for the state of the system. Hence, at this stage it is necessary to supplement the equations by an additional set of phenomenological equations which relate the irreversible fluxes and the thermodynamic forces appearing in the entropy source strength term. In the first approximation the fluxes are linear functions of the thermodynamic forces such as Fourier's law of heat conduction and Fick's law of diffusion. These two laws also contain additional possible *cross-effects* between various phenomena, since each flux may be a linear function of all thermodynamic forces which are needed to characterize the entropy source strength. Together with the phenomenological equations the original set of conservation laws may be said to be *complete* in the sense that the set of partial differential equations may be solved with proper initial and boundary conditions.

5.2- Problem Definition

The problem proposed herein is to explore the dynamic response of a high-speed flexible mechanism made from graphite/epoxy composite laminates and operating in a varying environment where both temperature and relative humidity fluctuate. The links are modelled as several anisotropic continuous media which are perfectly hinged without bearing clearance. This mechanism is also regarded thermodynamically as an open system, (i.e., system may exchange heat as well as matter with its surroundings), subjected to both mechanical and hygrothermal loads. Furthermore, all the boundary conditions are assumed to be uncoupled. Namely there is no interaction between each load over the boundary, in order to simplify the formulation. Since the composite laminates have been characterized as viscoelastic materials, a heat source term (by way of the dissipation in the viscous nature of the material) is also considered. This problem formulation is described in the following pages.

Consider a three-dimensional anisotropic body of volume V bounded by a surface S which describes a general spatial motion while being subjected to mechanical and hygrothermal loads. The total surface area S is divided into regions S_σ, S_u, S_H, S_θ, S_m and S_c on which surface tractions, displacements, heat flux, temperature, mass flux, and moisture concentration, respectively, are prescribed. Figure 5.1 defines the inertial frame OXYZ and also the body axes oxyz, which is a lagrangian frame fixed on the body in a reference state of temperature T_o, moisture concentration C_o, zero stresses and strains. Employing a subscript notation and the summation convention, at time t, a general point, P, in the continuum has the position vector

$$r_i = r_{oi} + r_{Ri} + u_i \qquad (5.2.1)$$

where r_{oi} are the components relative to oxyz of the position vector of the origin of the body axes relative to the origion of the initial frame. Similarly, r_{Ri} represents the position vector of point P in the reference state relative to the origin of the body axes and $u_i(m)$ is the deformation displacement vector.

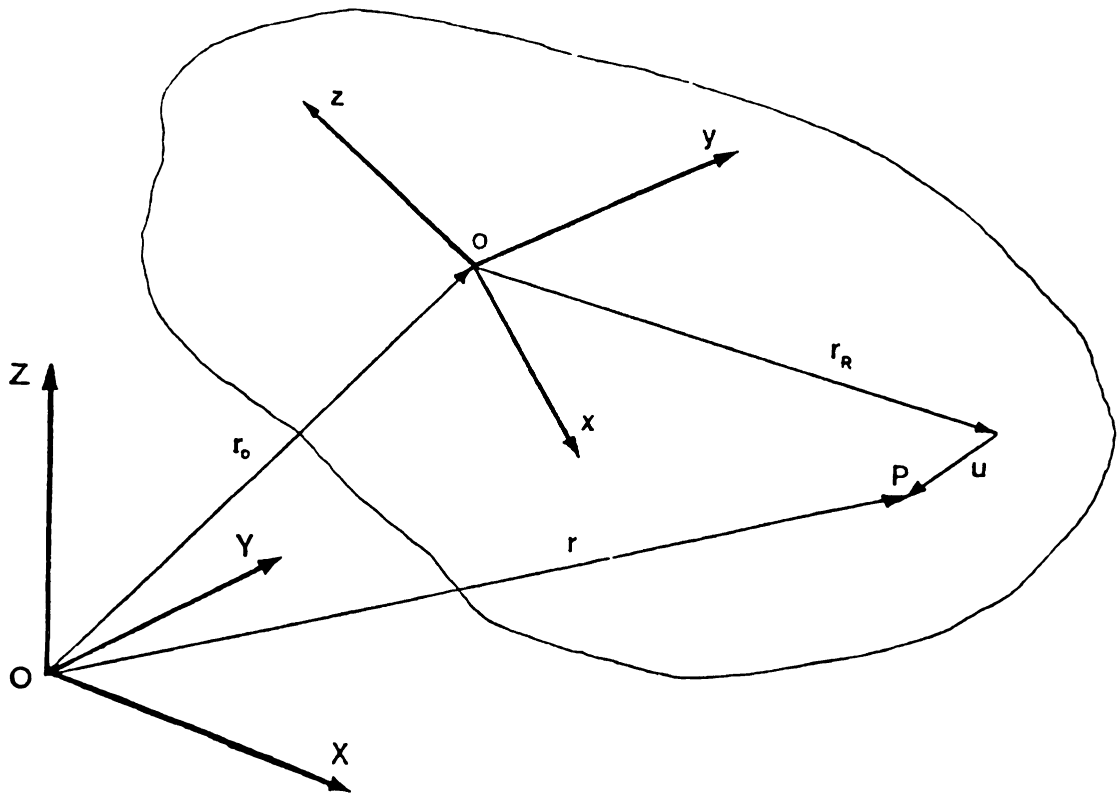

Figure 5.1   Definition of Axes System and Position Vectors

In this formulation the transient response as well as the response of two equilibrium states are studied. The first equilibrium state is defined by the same conditions of temperature and moisture concentration as the initial conditions for the system, and the second equilibrium state is defined by the temperature and moisture conditions in a steady-state situation at any position in the volume V after a sudden change of the environment. These two states are assumed to be equilibrium conditions for both thermal and ambient moisture concentrations.

5.3- Conservation laws

Thermodynamics is based on two fundamental laws: the first law of thermodynamics or law of conservation of energy, and the second law of thermodynamics or entropy law. A systematic macroscopic scheme for the description of non-equilibrium processes (i.e. the scheme of thermodynamics of irreversible processes) must also be built upon these two laws. In order to develop a theory applicable to systems of which the properties are continuous functions of space coordinates and time, the local formulations of the laws of conservation of mass, momentum and energy should be given sequentially.

5.3.1- Conservation of mass

Consider an open system which exchanges mass with its surroundings through the boundary by diffusion driven by a concentration gradient. In the study of the hygrothermal behavior of composite materials the specific moisture concentration C (Kg/Kg) defined by

$$C = M_c/\rho \qquad (5.3.1.1)$$

is frequently used. Physically, M_c (Kg/m^3) representing the moisture concentration is defined by

$$M_c = \lim_{\Delta V \to 0} \text{mass of moisture in } \Delta V/\Delta V \qquad (5.3.1.2)$$

so M_c is a measure of the amount of moisture at a point. However, C represents the amount of moisture as a fraction of the dry mass of the composite material, i.e.

$$C = \lim_{\Delta V \to 0} \text{mass of moisture in } \Delta V/\text{mass of dry material of volume } \Delta V \qquad (5.3.1.3)$$

The rate of change of mass within a given volume V due to diffusion is

$$\rho dC/dt = -q^{(M)}_{i,i} \qquad (5.3.1.4)$$

where d/dt is the Lagrangian time derivative,

$q_i^{(M)}$ ($Kg/m^2 sec$) is a component of the mass flux,

ρ (Kg/m^3) is the density of dry composite material.

The equilibrium specific moisture concentration C_∞ (Kg/Kg) is the environmental moisture concentration. In humid air it may be related to the relative humidity ϕ in percent by a power law [218]

$$C_\infty = a(\phi/100)^b \qquad (5.3.1.5)$$

where a and b are material constants [183]. This expression is inferred from the response data presented in Figure 8.6 of Reference [183] for graphite/epoxy composite AS/3501, manufactured by Hercules Inc.

For the purpose of simplification, several assumptions are made as follows :

(1) Vapor is the only phase involved in the mass transfer process, in other words the liquid phase is not taken into consideration.

(2) The kinetic energy caused by the transport phenomena of diffusive matter is neglected because the transport velocity is very slow, and the mass of transported matter is very small compared with the mass of the medium.

(3) The system is in chemical equilibrium, hence there is no mass transfer caused by a chemical reaction.

5.3.2- Conservation of momentum and energy

According to the principle of conservation of energy, the total energy content within an arbitrary volume V can only change if there are energy flows in or out of the volume through its boundary S and energy is generated or destroyed inside the volume because of energy change or energy supply accompanied by the mass supply.

The conservation of energy [42,43] may be expressed by

$$Q^{(H)} + Q^{(M)} = \dot{U} + \dot{K} - R \qquad (5.3.2.1)$$

where ($^{\bullet}$) represents taking the Lagragian derivative with respect to time, the heat transfer $Q^{(H)}$ (N-m/sec), the energy transfer $Q^{(M)}$ (N-m/sec) due to mass transfer, internal energy U (N-m), macroscopic kinetic energy K (N-m) and the mechanical power R (N-m/sec) are defined as

$$Q^{(H)} = -\int_S q^{(H)}{}_i n_i dS + \int_V \rho h^{(H)} dV \qquad (5.3.2.2)$$

$$Q^{(M)} = -\int_S \mu q^{(M)}{}_i n_i dS \qquad (5.3.2.3)$$

$$U = \int_V \rho e dV \qquad (5.3.2.4)$$

$$K = 1/2\int_V \rho p_i p_i dV \qquad (5.3.2.5)$$

$$R = \int_V \rho X_i p_i dV + \int_S \sigma_{ij} n_j p_i \, dS \qquad (5.3.2.6)$$

where p_i (m/sec) is the velocity associated with the time rate of change of r_i is defined by

$$p_i = r'_{oi} + u'_i + e_{ijk}\dot{\theta}_j(r_{oi} + r_{Ri} + u_i) \qquad (5.3.2.7)$$

where ($'$) represents the time rate of change with respect to the moving frame oxyz, ($\dot{}$) defines the absolute rate of change, e_{ijk} is the alternating tensor, and components of angular velocity vector for the moving axes are represented by $\dot{\theta}_j$, $h^{(H)}$ (N-m/Kgsec) is the heat source, $q^{(H)}{}_i$ (N-m/m²sec) is the heat flux in or out of the system and the influx is considered to be positive, n_i is the component of the unit outward vector normal to the boundary surface, the density ρ (N-m/m³) is assumed to be uniform throughout the process, i.e. independent of temperature, moisture and position at any instant t, the mass flux $q^{(M)}{}_i$ (Kg/m²sec) carries the chemical potential μ (N-m/Kg) in or out of the system through the boundary and the influx is assumed to be positive, e (N-m/Kg) is the specific internal energy, X_i (N/Kg) is a component of the body force and σ_{ij} (N/m²) is a mechanical stress tensor, and the work done on the system is considered to be positive.

Substituting equation (5.3.2.2), (5.3.2.3), (5.3.2.4),

(5.3.2.5) and (5.3.2.6) into equation (5.3.2.1), the first law of thermodynamics will result in the balance of momentum and energy such that

$$\int_V \rho h^{(H)} dV - \int_S q^{(H)}{}_i n_i \, dS - \int_S \mu q^{(M)}{}_i n_i dS$$
$$= \int_V \rho \dot{e} dV + 1/2 d/dt \int_V \rho p_i p_i dV - \int_V \rho X_i p_i dV$$
$$- \int_S \sigma_{ij} n_j p_i dS \qquad (5.3.2.8)$$

where each of the surface integrals is transformed by the divergence theorem to a volume integral such as

$$\int_S q^{(H)}{}_i n_i dS = \int_V q^{(H)}{}_{i,i} dV \qquad (5.3.2.9)$$

$$\int_S \mu q^{(M)}{}_i n_i dS = \int_V \mu q^{(M)}{}_{i,i} dV \qquad (5.3.2.10)$$

and

$$\int_S \sigma_{ij} p_i n_j dS = \int_V \sigma_{ij,j} p_i dV + \int_V \sigma_{ij} p_{i,j} dV \qquad (5.3.2.11)$$

Collecting terms and letting γ_{ij} be the strain tensor, the time rate-of-change of this expression may be written

$$\dot{\gamma}_{ij} = 1/2(\dot{u}_{i,j} + \dot{u}_{j,i}). \qquad (5.3.2.12)$$

Equation (5.3.2.8) then becomes

$$\int_V (\rho\dot{p}_i - \rho X_i - \sigma_{ij,j}) p_i dV + \int_V (\rho\dot{e} - \rho h^{(H)}$$

$$+ q^{(H)}_{i,i} + \mu q^{(M)}_{i,i} + \sigma_{ij} p_{i,j}) \, dV = 0 \qquad (5.3.2.13)$$

The local form of momentum and energy balance equation are expressed by

$$\rho\dot{p}_i - \rho X_i - \sigma_{ij,j} = 0 \qquad (5.3.2.14)$$

and

$$\rho\dot{e} - \rho h^{(H)} + q^{(H)}_{i,i} + \mu q^{(M)}_{i,i} - \sigma_{ij} p_{i,j} = 0 \qquad (5.3.2.15)$$

5.4- Entropy Balance and Entropy Production

According to the second law of thermodynamics [49,66], the entropy S (N-m/°K) may be introduced for any macroscopic system and is expressed by

$$dS = d_e S + d_i S \qquad (5.4.1)$$

where the entropy increase of the system dS is composed of two and only two terms $d_e S$ and $d_i S$. The term $d_e S$ is derived from heat transfer into or out of the system across the boundary, and the term $d_i S$ is the entropy produced inside the system [49,66]. The second law of thermodynamics states that $d_i S$ must be zero for reversible (i.e. equilibrium) processes and positive for irreversible processes:

$$d_i S \geq 0 \qquad (5.4.2)$$

The entropy transfer term $d_e S$, on the other hand, may be positive, zero or negative, depending upon the interaction of the system with its surroundings. For open systems, $d_e S$ also contains a term connected with the transfer of matter. The equations (5.4.1) and (5.4.2) can be combined in the form as

$$\int_V \rho \dot{s} dV = -\int_S q^s{}_i n_i dS + \int_V S \, dV \qquad (5.4.3)$$

where $\dot{s}$ (N-m/Kgsec°K) is the rate of change of specific entropy density, $q^s{}_i$ (N-m/m^{2}sec°K) is the component of entropy flux and S (N-m/m^{3}sec°K) is the entropy source strength or entropy production density.

It is appropriate to describe the density of each extensive property (such as mass and energy) of the system with continuous functions of spatial coordinates. Using Gauss' theorem, equation (5.4.3) may result in the form

$$\int_V (\rho \dot{s} + q^s{}_{i,i} - S) dV = 0 \qquad (5.4.4)$$

Since equation (5.4.1) and (5.4.2) must hold for an arbitrary volume V, the local expression for the second law of thermodynamics may be written

$$\rho\dot{s} + q^{s}{}_{i,i} = S \tag{5.4.5}$$

and

$$S \geq 0 \tag{5.4.6}$$

In much of continuum mechanics, it is often assumed (based upon statistical mechanics of irreversible processes) that the stress tensor may be decomposed into two parts [46,99],

$$\sigma_{ij} = \sigma^{(C)}{}_{ij} + \sigma^{(D)}{}_{ij} \tag{5.4.7}$$

where $\sigma^{(C)}{}_{ij}$ is a conservative stress tensor, and $\sigma^{(D)}{}_{ij}$ is a dissipation stress tensor. With this assumption the energy equation (5.3.2.15) may be written as

$$\begin{aligned} &\rho\dot{e} - \rho h^{(H)} + q^{(H)}{}_{i,i} + \mu q^{(M)}{}_{i,i} \\ &- \sigma^{(C)}{}_{ij}p_{i,j} - \sigma^{(D)}{}_{ij}p_{i,j} = 0 \end{aligned} \tag{5.4.8}$$

where the term $\sigma^{(D)}{}_{ij}p_{i,j}$ is the rate of energy dissipated by the stress. On the other hand, if the continuum undergoes a reversible process, there will be no energy dissipated by this stress.

In order to obtain more explicit expressions for the entropy flux $q^{s}{}_{i}$ and the entropy production S, it is necessary to relate the conservation laws and the rate of change of entropy. The Gibbs relation of a reversible process for the specific quantities is written as

$$\rho T\dot{s} = \rho\dot{e} - \sigma^{(C)}{}_{ij}p_{i,j} - \rho h^{(H)} \qquad (5.4.9)$$

where ρ, s, e, $\sigma^{(C)}{}_{ij}$ and $p_{i,j}$ were defined previously, and T (°K) is the absolute temperature. Equation (5.4.8) and (5.4.9) may be combined to yield

$$\rho T\dot{s} = - q^{(H)}{}_{i,i} - \mu q^{(M)}{}_{i,i} + \sigma^{(D)}{}_{ij}p_{i,j} \qquad (5.4.10)$$

Dividing equation (5.4.10) by the absolute temperature T, it yields an expression for the rate of change of entropy

$$\rho\dot{s} = - q^{(H)}{}_{i,i}/T - \mu q^{(M)}{}_{i,i}/T + \sigma^{(D)}{}_{ij}p_{i,j}/T \qquad (5.4.11)$$

Now if A_i and B are both arbitrary functions of position, then

$$(A_iB)_{,i} = BA_{i,i} + A_iB_{,i} \qquad (5.4.12)$$

Utilizing this relation, equation (5.4.11) may be transformed into

$$\rho\dot{s} + \Big[(q^{(H)}_i + \mu q^{(M)}_i)/T \Big]_{,i} = q^{(H)}_i(1/T)_{,i}$$

$$+ q^{(M)}_i(\mu/T)_{,i} + \sigma^{(D)}_{ij}p_{i,j}/T \qquad (5.4.13)$$

This equation is just identical with equation (5.4.5) provided that the entropy flux density and entropy production density are defined as follows:

$$q^{s}_i = 1/T(q^{(H)}_i + \mu q^{(M)}_i) \qquad (5.4.14)$$

and

$$S = q^{(H)}_i(1/T)_{,i} + q^{(M)}_i(\mu/T)_{,i} + \sigma^{(D)}_{ij}p_{i,j}/T \qquad (5.4.15)$$

Expanding equation (5.4.15) yields

$$S = - (q^{(H)}_i/T^2)T_{,i} + q^{(M)}_i\mu_{,i}/T$$

$$- (q^{(M)}_i\mu/T^2)T_{,i} + \sigma^{(D)}_{ij}p_{i,j}/T \qquad (5.4.16)$$

Equation (5.4.14) demonstrates that for open systems the entropy flux q^{s}_i consists of two parts: one is the "reduced" heat flux $q^{(H)}_i$, the other is connected with the diffusive flux of matter $q^{(M)}_i$. Equation (5.4.15) demonstrates that the entropy production [49,66] is composed of heat conduction, diffusion, heat source and the rate of change of energy dissipation due to dissipative stress. In this equation, there appears one term for each process (energy transfer, diffusion, heat source and dissipative work) and each term vanishes when the corresponding process ceases. In other words, in the computation of the entropy production due to the simultaneous presence of several processes it is only necessary to add the productions which would accompany the processes as if they took place seperately.

5.5- The Phenomenological Equations and Onsager Principle

It is known empirically that for a large class of irreversible phenomena and under a wide range of experimental conditions, the irreversible flows are linear functions of the thermodynamic forces, as expressed by the phenomenological laws which are introduced ad hoc in the purely phenomenological theories of irreversible processes. An example is Fourier's law for heat conduction,

$$q^{(H)}{}_i = -K_{ij}T_{,j} \tag{5.5.1}$$

which expresses the fact that the components of the heat flow are linear functions of the components of the temperature gradient where K_{ij} (N-m/msec°K) is heat conductivity. A second example is Fick's law [48] for mass diffusion,

$$q^{(M)}{}_i = -D_{ij}C_{,j} \tag{5.5.2}$$

which establishes a linear relation between the diffusive flow of matter and the concentration gradient where, D_{ij} (Kg/m-sec) is the material diffusivity. Also included in this kind of description are the terms for such cross-effects as thermal diffusion in which the diffusive flow of mass depends linearly upon both the concentration and temperature gradients. Under the restriction of the linear assumption, the phenomenological equations may be expressed by

$$q_i = L_{ik}X_k \tag{5.5.3}$$

where q_i and X_k are any of the Cartesian components of the independent fluxes and the thermodynamic forces respectively. These terms appear in the expression for entropy production, which is of the form [49]

$$S = q_iX_i \tag{5.5.4}$$

where the quantities L_{ik} are called the phenomenological coefficients [49]. Substituting equation (5.5.3) into (5.5.4) for the entropy production, a quadratic expression results in the thermodynamic forces. This relationship has the form

$$S = L_{ik}X_iX_k \tag{5.5.5}$$

which must be positive definite, or at least positive semi-definite. A sufficient condition for this is that all principal co-factors of the symmetric matrix with elements $L_{ik} + L_{ki}$ are non-negative. This implies that all diagonal elements are positive whereas the off-diagonal elements must satisfy, for instance, conditions of the form $L_{ii}L_{kk} \geq 1/4(L_{ik} + L_{ki})^2$.

The advantages of the systematic formulation of irreversible thermodynamics is that all local thermodynamic state variables of the system may be determined by the conservation laws, entropy balance equations and the phenomenological equations. On the other hand the phenomenological equations can also be derived through this formulation.

In equation (5.4.16) all components of the vectorial and tensorial fluxes must be considered as homogeneous linear functions of all components of the vectorial and tensorial forces. A direct consequence of this is that Curie's principle of symmetry does not hold here [49 ,66]. However, the reciprocity law of Onsager and Casimir is valid. In this theory, the generalized forces are divided into two different types "forces of α-type" and "forces of β-type". The "forces of α-type" are even-valued with reference to time reversal while "forces of β-type" are uneven. The formula used to find the phenomenological coefficients [49 ,66] is

$$\alpha_{ij} = s_i s_j \alpha_{ji} \qquad (i,j = 1,2,\ldots,n) \qquad (5.5.5)$$

where $\quad s_k = 1 \quad$ if X_k is a force of α-type

$\varepsilon_k = -1$ if X_k is a force of β-type

If X_i and X_j are of the same type, then equation (5.5.5) is reduced to the form

$$\alpha_{ij} = \alpha_{ji} \tag{5.5.6}$$

which are referred to as Onsager coefficients. However if X_i and X_j belong to different types of forces, then equation (5.5.6) becomes

$$\alpha_{ij} = -\alpha_{ji} \tag{5.5.7}$$

which are referred to as Casimir coefficients. Equation (5.5.6) is denoted as the Onsager reciprocity relations, while equations (5.5.5) and (5.5.7) are called the Onsager - Casimir reciprocity relations [49 ,66]. By introducing a new flux $\bar{q}^{(H)}{}_i$, defined as

$$\bar{q}^{(H)}{}_i = q^{(H)}{}_i + \mu q^{(M)}{}_i \tag{5.5.8}$$

the entropy production S in equation (5.4.16) can then be written as

$$S = -(\bar{q}^{(H)}{}_i/T^2)T_{,i} + (q^{(M)}{}_i/T)\mu_{,i}$$
$$+ \sigma^{(D)}{}_{ij}p_{i,j}/T \tag{5.5.9}$$

The dissipation function Ω ($N\text{-}m/m^3 sec$) is defined by

$$\Omega = T\,\dot{S} \qquad (5.5.10)$$

The equation (5.5.9) may then be written as

$$\Omega = -\bar{q}^{(H)}{}_i T_{,i}/T + q^{(M)}{}_i \mu_{,i} + \sigma^{(D)}{}_{ij}\; p_{i,j} \qquad (5.5.11)$$

From the previous studies [184,185], the dissipative energy contributed by the inertial coupling terms between the rigid-body motion and stresses is very small in comparison with the strain energy. Hence, these terms related to the rigid-body motion may be neglected to make $p_{i,j} \simeq \dot{\gamma}_{ij}$. The equation (5.5.11) may then be restated as

$$\Omega = -\bar{q}^{(H)}{}_i T_{,i}/T + q^{(M)}{}_i \mu_{,i} + \sigma^{(D)}{}_{ij}\; \dot{\gamma}_{ij} \qquad (5.5.12)$$

with the thermodynamic forces

$$X^{(H)}{}_i = -\, T_{,i} \qquad (5.5.13)$$

$$X^{(M)}{}_i = -\, \mu_{,i} \qquad (5.5.14)$$

$$X_{ij} = -\dot{\gamma}_{ij} \qquad (5.5.15)$$

From equation (5.5.12), the first and second terms on the right-hand side are a scalar product of two polar vectors and the last term is a scalar product of two tensors of order 2. The phenomenological equations (5.5.1) may be derived by the Onsager - Casimir reciprocity relation [49,66] and equation (5.5.12). This equation is assumed to be applied to an anisotropic continuous medium under the premise that the temperature difference θ (°R) is small compared to the absolute temperature T, and the reference temperature T_e is defined as the temperature at the unstrained state These terms are governed by the relationship

$$T = T_e + \theta \qquad (5.5.16)$$

which permits the phenomenological equations then to be expressed by

$$\sigma^{(D)}{}_{ij} = L_{11}\dot{\gamma}_{ij} - L_{12}\theta_{,i}/T - L_{13}\mu_{,i} \qquad (5.5.17)$$

$$\bar{q}^{(H)}{}_{i} = L_{21}\dot{\gamma}_{ij} + L_{22}\theta_{,i}/T + L_{23}\mu_{,i} \qquad (5.5.18)$$

$$q^{(M)}{}_{i} = L_{31}\dot{\gamma}_{ij} + L_{32}\theta_{,i}/T + L_{33}\mu_{,i} \qquad (5.5.19)$$

The stress tensor $\sigma^{(D)}{}_{ij}$ may be replaced by σ_{ij} by superimposing $\sigma^{(C)}{}_{ij}$ onto the equation (5.5.17), for instant, a general form of the constitutive equation for viscoelastic materials under the environment of isothermal and constant moisture concentration is represented by

$$\sigma_{ij} = C_{ijkl}\gamma_{kl} + G_{ijkl}\dot{\gamma}_{kl} \qquad (5.5.20)$$

where C_{ijkl} and G_{ijkl} are the fourth-order tensors of elastic moduli and damping coefficients, respectively. The gradient of chemical potential may be expressed in terms of the concentration gradient [49 ,66] when μ is assumed to be constant. Thus

$$\mu_{,i} = \mu C_{,i} \qquad (5.5.21)$$

The phenomenological coefficients may be represented as follows:

$$\begin{aligned}\sigma_{ij} = C_{ijkl}\gamma_{kl} + G_{ijkl}\dot{\gamma}_{kl} - \beta^{(H)}{}_{ijk}\theta_{,k} \\ - \beta^{(M)}{}_{ijk}\,\mu C_{,k}\end{aligned} \qquad (5.5.22)$$

$$\bar{q}^{(H)}{}_{i} = T\beta^{(H)}{}_{ijk}\dot{\gamma}_{jk} + K_{ij}\theta_{,j} + T\lambda_{ij}\mu C_{,j} \qquad (5.5.23)$$

$$q^{(M)}{}_{i} = \beta^{(M)}{}_{ijk}\dot{\gamma}_{jk} + \lambda_{ij}\theta_{,j} + \xi_{ij}C_{,j} \qquad (5.5.24)$$

At this stage, the physical interpretation of the phenomenological coefficients should be made in equation (5.5.22), (5.5.23) and (5.5.24) such as

$\beta^{(H)}{}_{ijk}$ ($N\text{-}m/m^2\text{-}^\circ K$) is the third-order tensor of anisotropic thermoelastic moduli,

$\beta^{(M)}{}_{ijk}$ (Kg/m^3)is the third-order tensor of hygroscopic moduli,

K_{ij} ($N\text{-}m/m\text{-}sec\text{-}^\circ K$) is the second-order tensor of heat conductivity

λ_{ij} ($Kg/m\text{-}sec\text{-}^\circ K$) is the second-order tensor of hygrothermal coefficient

ξ_{ij} ($Kg/m\text{-}sec$) is the second-order tensor of material diffusivity

Substituting equation (5.5.22), (5.5.23) and (5.5.24) into the equation of mass balance (5.3.1.1), equation of motion (5.3.2.14) and equation of energy balance (5.3.2.15) yield three partial differential equations governing the dynamic hygrothermal response of anisotropic media. Thus

$$\rho dC/dt = \beta^{(M)}{}_{ijk}\dot{\gamma}_{jk,i} + \lambda_{ij}\theta_{,ij} + \xi_{ij}C_{,ij} \qquad (5.5.25)$$

$$\rho\dot{e} - \rho h^{(H)} + T\beta^{(H)}{}_{ijk}\dot{\gamma}_{jk,i} + K_{ij}\theta_{,ij} + T\lambda_{ij}\mu C_{,ij}$$

$$- (C_{ijkl}\gamma_{kl} + G_{ijkl}\dot{\gamma}_{kl,j}$$

$$- \beta^{(H)}{}_{ijk}\theta_{,k} - \beta^{(M)}{}_{ijk}\mu C_{,k})\dot{\gamma}_{ij} = 0 \qquad (5.5.26)$$

$$\rho\dot{p}_i - \rho X_i - C_{ijkl}\gamma_{kl,j} - G_{ijkl}\dot{\gamma}_{kl,j} - \beta^{(H)}{}_{ijk}\theta_{,kj}$$

$$+ \beta^{(M)}{}_{ijk}\mu C_{,kj} = 0 \qquad (5.5.27)$$

The strain tensor may also be represented in terms of the deformal displacements using equation (5.3.2.12). Since the strain tensor γ_{ij} is symmetric, it implies that the third-order tensor β_{ijk} has the following property

$$\beta_{ijk} = \beta_{ikj}. \qquad (5.5.28)$$

Substituting equations (5.5.27) and (5.5.28) into equation (5.5.24), (5.5.25) and (5.5.26) yields

$$\rho dC/dt - \beta^{(M)}{}_{ijk}\dot{u}_{j,ki} - \lambda_{ij}\theta_{,ij} - \xi_{ij}C_{,ij} = 0 \qquad (5.5.29)$$

$$\rho\dot{e} - \rho h^{(H)} + T\beta^{(H)}{}_{ijk}\dot{u}_{j,ki} + K_{ij}\theta_{,ij} + T\lambda_{ij}\mu C_{,ij}$$

$$- (C_{ijkl}u_{k,l} + G_{ijkl}\dot{u}_{k,l} - \beta^{(H)}{}_{ijk}\theta_{,k}$$

$$- \beta^{(M)}{}_{ijk}\mu C_{,k})\dot{u}_{i,j} = 0 \qquad (5.5.30)$$

$$\rho\dot{p}_i - \rho X_i - C_{ijkl}u_{k,lj} - G_{ijkl}\dot{u}_{k,lj} + \beta^{(H)}{}_{ijk}\theta_{,jk}$$

$$+ \beta^{(M)}{}_{ijk}\mu C_{,jk} = 0 \tag{5.5.31}$$

These equations are subjected to the following boundary conditions

$$u_i = \bar{u}_i \qquad \text{on } S_u \tag{5.5.32}$$

$$\Theta = T_a \qquad \text{on } S_\Theta \tag{5.5.33}$$

$$C = C_a \qquad \text{on } S_c \tag{5.5.34}$$

$$g_i = \bar{g}_i \qquad \text{on } S_\sigma \tag{5.5.35}$$

$$q^{(H)} = \bar{Q}^{(H)} \qquad \text{on } S_H \tag{5.5.36}$$

$$q^{(M)} = \bar{Q}^{(M)} \qquad \text{on } S_m \tag{5.5.37}$$

and also the initial conditions

$$u(x,y,z,0) = 0 \tag{5.5.38}$$

$$\Theta(x,y,z,0) = \Theta_o \tag{5.5.39}$$

$$C(x,y,z,0) = C_o \tag{5.5.40}$$

In this chapter, the governing equations for the mass balance, momentum balance and energy balance are derived by applying the first

and second laws of thermodynamics, classical continuum mechanics and the Onsager's Principle. These governing equations are also subjected to the various boundary conditions and initial conditions. Therefore, these formulate three coupled initial-boundary value problems. A variational principle is employed as an alternative methodology to derive the governing equations and the associated boundary conditions, and it will be presented in the next chapter.

CHAPTER 6

A THEORETICAL INVESTIGATION ON THE LINEAR COUPLED HYGROTHERMOELASTODYNAMIC ANALYSIS OF MECHANISM SYSTEMS

6.1 Background

Modern composite materials possess certain characteristics that are superior to the traditional metallic designs, and the increasing use of these materials in structural applications requires that the response of such materials to both environmental exposure and mechanical loads be fully understood. This in turn requires analytical and experimental methods which predict changes in the properties of the material during exposure to an environment in which both the temperature and the moisture level vary. This chapter presents a variational principle from which the governing equations of motion, energy balance and mass balance are derived and a finite element formulation is also performed in order to obtain a numerical method to render a tractable solution to these complicate problem. In order to address this class of problems, and develop a design methodology for engineering incorporated with these problems, considering a composite material is exposed to an environment in which the temperature T_a and the moisture content m_a vary with time t in a prescribed manner. It is required to find the following parameters:

1. the temperature distribution $T(x,t)$ inside the material as a function of position and time,
2. the moisture concentration $c(x,t)$ within the material as a function of position and time,
3. the total amount (mass) of moisture inside the material $M(t)$ as a function of time,
4. changes in the performance of material, such as elastic modulus as a function of time,
5. the response of the material under combined mechanical and hygrothermal loadings.

Under certain circumstances solutions to the hygrothermal problem (notes 1-3 above) can be obtained analytically, answers to problems involving changes in performance (note 4) must be obtained by testing, and the response of the material (note 5) may be obtained by both experimental and analytical means after the above points were performed. An overview of the methods of solution pertaining to these problems are given below. Details are provided in the various articles which follow and in the references quoted.

Experimental studies performed under elevated temperatures and various relative humidities in references [93,143,150,215], indicate that for many materials (especially the graphite/epoxy composites) Fickian diffusion is a reasonable approximation and the calculations based on Fick's law were found to adequately decribe both the moisture aborption and desoption processes. Solutions to problems governed by notes 1 and 2 can be obtained analytically when the following conditions are met:

1. Heat is transferred through the material by conduction alone and can be described by Fourier's law [130].
2. The moisture diffusion phenomena can be described by a concentration-dependent form of Fick's law [130,143].
3. The temperature inside the material approaches equilibrium much faster than the moisture diffusion process, consequently, the Fourier heat conduction and Fick mass diffusion equations can be decoupled [143].
4. The thermal conductivity and the mass diffusivity depend only on temperature and are independent of moisture concentration or stress levels inside the material [217,218].

Non-Fickian diffusion has also been observed in some composite materials [216,217,218,219]. For these materials moisture absorption and desorption can not described well by a concentration-dependent form of Fick's law. Calculations performed on the basis of Fick's law fail if:

1. cracks develop in the material or delamination occurs, which essentially alters the structure of the material,
2. moisture propagates along the fiber-matrix interface,
3. there are voids in the matrix, and
4. the matrix itself exhibits non-Fickian behavior (even without cracks).

The first three of the above conditions involve some form of micro-structural discontinuity within the material. Frequently, such discontinuities can be minimized by appropriate manufacturing procedures. Whether the diffusion process through the matrix is Fickian or non-Fickian depends on the relative rates at which the polymer structure and the moisture distributions change [48,100]. When the polymer structure changes much faster than the moisture concentration, the diffusion process can be described adequately by Fick's law. If the relaxation process, which is the change of the residual stresses of a polymer structure caused by swelling phenomena inside the material, develops at a rate comparable to the diffusion processes, then the diffusion is defined as non-Fickian [143,215].

Fick's law is generally applicable to rubbery polymers but often fails to describe the diffusion process in a glassy polymer [215]. The transition from a glassy to a rubbery state occurs at the glass transition temperature. The glass transition temperature itself depends on the moisture concentration. The absorbed moisture will generally decrease the glass transition temperature, thereby affecting the diffusion behavior of the material [100].

Whether moisture transported through a composite is by Fickian or by non-Fickian diffusion process depends on the material and on the environmental conditions. Thus, the general diffusion law for a specific situation must be determined by experimental testing. If the diffusion process is Fickian, then the moisture distribution at each instant in the material can be calculated readily. Suitable analyses to adequately describe non-Fickian diffusion have not yet been developed.

Moisture and temperature may affect the performance of composite materials. To date, changes in the following performance parameters have been explored: (a) tensile strength, (b) elastic moduli, (c) fatigue behavior, (d) creep, (e) stress rupture, and (f) response to dynamic impact [144,151,153,211,215].

At elevated temperatures a degradation of the mechanical behavior occurs since the moisture diffusivity, D, is strongly dependent upon the temperature. An empirical formula $D = D_e \exp(-E_0/RT)$ governs this situation, where D_e and E_0 are pre-exponential factor and the activate energy required for one unit of mass to move inside solid, respectively [[illegible],92,146]. R is universal gas constant and T is the absolute temperature. Therefore, the coupling effect between temperature and moisture is found to be more significant when this material undergoes a sudden change in surfaçe temperature. The stresses due to coupling effect can deviate from the uncoupled results anywhere from 20 to 80% depending on the surface temperature gradient. A consequence of these heat transfer and diffusion phenomena is that the damping properties and also the natural frequencies of the structure are affected. This further complicate the task of designing composite systems which must successfully operate in practice when simultaneously exposed to a wide spectrum of both hygrothermal and dynamic loading conditions.

In most theoretical research publications on modeling the hygrothermal response of composites, the heat and moisture diffusion equations are generally decoupled in order to establish a mathematically tractable problem, but this approach is not always appropriate. As indicated in references [146] and [143] under service conditions in engineering practice, a structure is simultaneously subjected to both hygrothermal and mechanical environments, hence a formulation coupling hygrothermal and mechanical loading is generally required.

A classical approach, based upon the first and second laws of thermodynamics, non-equilibrium thermodynamics and classical continuum mechanics, is developed and documented in chapter 5. The governing equations has been generated in order to describe the physical behavior of a continuous medium undergoing mechanical, thermal and hygroscopic loading. In addition, G. Herrmann [71] formulated a variational theorem for an anisotropic three-dimensional medium and for a more general class of boundary conditions by employing Boit's thermoelastic potential and dissipation function. In establishing this theorem the kinematic variables were taken to be the solid displacement and entropy displacement. The dynamic variables were the stress, which has to be resolved into an isothermal part and a thermal part, the temperature increment above a reference temperature, and a force, which is related to the entropy displacement. In contrast to this, M. Ben-Amoz [22] constituted a mixed variational principle by employing Hu-Washizu's principle, from which all field equations are deduced from the extended functional.

Herein, a variational principle for the linear coupled hygrothermoelastodynamic analysis of mechanism systems is presented which provides the basis for developing the equations governing the hygrothermoelastic response of planar flexible mechanism systems subjected to both mechanical and hygrothermal loading. These systems are modeled as chains of continua with anisotropic elastic constitutive equations. By permitting arbitrary independent variations of the system parameters for each link, approximating equations of motion, equations of heat and mass transfer and boundary conditions may be systematically constructed. Subsequently, a finite element formulation based upon this variational principle is developed in order to provide a numerical scheme in order to solve the equations. The problem is intractable when approached from a purely analytical basis.

6.2 Variational Principle

Consider a three-dimensional anisotropic body of volume V bounded by a surface S which describes a general spatial motion while being subjected to mechanical and hygrothermal loadings. The total surface area S is divided into regions S_σ, S_u, S_H, S_θ, S_D and S_M on which surface tractions, displacements, entropy displacements, temperature, hygroscopic displacements [213] and moisture concentration, respectively, are prescribed.

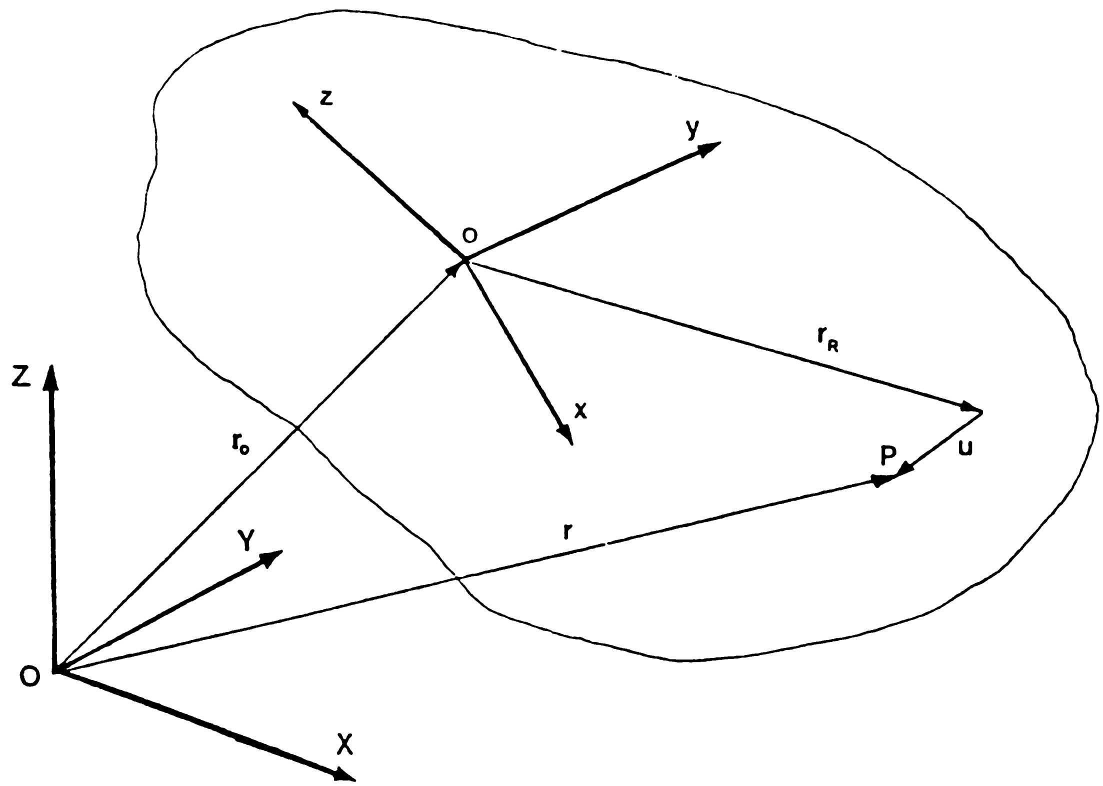

Figure 6.1 Definition of Axes System and Position Vectors

Figure 6.1 defines the inertial frame OXYZ and also the body axes oxyz, which is the Lagrangian frame fixed in the body in a reference state of temperature T_0 (°K), entropy density s_0 (N-m/m³-°K), moisture concentration M_0 (Kg/Kg), flow-potential density π_0 (N-m/m³), and zero stresses and strains. Employing a subscript notation and the summation of convention, at time t, a general point, P, in the continuum has the position vector

$$r_i = r_{oi} + r_{Ri} + u_i \tag{6.2.1}$$

where r_{oi} (m) are the components relative to oxyz of the position vector of the origin of the body axes relative to the origin of the inertial frame. Similarly, r_{Ri} represents the position vector of point P in the reference state relative to the origin of the body axes and u_i is the deformation displacement vector.

The velocity associated with the time rate of change of r_i is written as P_i (m/sec). Then with ρ (Kg/m³) as the mass density and δ_{ij} as the Kronecker delta, the kinetic energy density, T (N-m/m³), of the system is

$$T = 1/2\rho P_i \delta_{ij} P_j \tag{6.2.2}$$

In order to establish the equations governing the motion of a link of a flexible mechanism system, the principle of virtual work must be generalized using the first and second laws of thermodynamics, to yield the problem of determining the stationary conditions of the functional

$$G = \int_{t1}^{t2}\Big[\int_V \left[T-W+D+\theta s+\pi M+X_i r_i\right]dV$$
$$+ \int_{SH} (1/\tilde{p}\theta_e)\ \bar{Q}^{(H)}\theta dS_H + \int_{S\sigma} \bar{g}_i r_i dS_\sigma$$
$$+ \int_{SD} (1/\tilde{p}M_e)\ \Omega\bar{Q}^{(M)}M\ dS_D\Big]dt \qquad (6.2.3)$$

subject to a number of auxiliary conditions or constraints. In equation (6.2.3) the term θ represents the temperature increment above the reference temperature θ_e, s represents the entropy-density increment above a reference entropy-density s_e, π is the flow-potential density increment above a reference density π_e, M is the moisture concentration increment above a reference concentration M_e, X_i (N/m^3) are the body forces per unit volume, $\bar{Q}^{(H)}$ ($N\text{-}m/m^2\text{-}sec$) and $\bar{Q}^{(M)}$ ($N/m^2\text{-}sec$) are the prescribed heat and mass transfer, and $\bar{g}_i$ are the prescribed surface tractions, Ω (N-m/N) is the specific chemical potential. The term, W, is hygrothermoelastic potential density, W ($N\text{-}m/m^3$) defined by

$$W = 1/2\ C_{ijkl}\gamma_{kl}\gamma_{ij} + \theta_e/2c\ (s-\beta_{ij}\gamma_{ij} + \mu M)^2$$
$$+ M_e/2b\ (\pi-\alpha_{ij}\gamma_{ij}+\mu\theta)^2 \qquad (6.2.4)$$

C_{ijkl} (N/m^2) being the symmetric tensor of elastic moduli in the isothermal state, c ($N\text{-}m/m^3\text{-}^\circ K$) is the specific heat per unit volume ($c=\rho\bar{c}$, where $\bar{c}$ is the conventional specific heat with units of $N\text{-}m/kg\text{-}^\circ K$

in the reference state; β_{ij} ($N\text{-}m/m^3\text{-}{}^\circ K$) and α_{ij} ($N\text{-}m/m^3$) is the symmetric tensors governed by the thermal-expansion and diffusive-expansion properities of the medium, respectively; μ ($N\text{-}m/m^{3\,\circ}K$) is the hygrothermal coefficient; b ($N\text{-}m/m^3$) is the hygroscopic capacity. The function D ($N\text{-}m/m^3$) is dissipation function due to the irreversibility of heat conduction and mass diffusion in the medium and is defined as

$$D = (1/2\tilde{p}\theta_0 K_{ij}) q_i^{(H)} q_j^{(H)}$$

$$+ (1/2\tilde{p}M_0 D_{ij}) \Omega q_i^{(M)} q_j^{(M)} \qquad (6.2.5)$$

where $\tilde{p}$ is the mathematical operator $\tilde{p} = d/dt$, K_{ij} ($N\text{-}m/m\text{-}sec\text{-}{}^\circ K$) and D_{ij} (N/msec) are the thermal conductivity and mass diffusivity potential tensors, respectively, and $q_i^{(H)}$ ($N\text{-}m/m^2\text{-}sec$) $q_i^{(M)}$ ($N/m^2\text{-}sec$) are defined below.

The constraints imposed upon the parameters in equation (6.2.3) may be formulated as the strain displacement equations

$$\gamma_{ij} = 1/2 (u_{i,j} + u_{j,i}) \qquad (6.2.6)$$

where comma (,) denotes spatial differentiation; the velocity rate-of-change of position statement

$$P_i = \tilde{r}_{oi} + \tilde{u}_i + e_{ijk}\dot{\theta}_j(r_{ok}+r_{Rk}+u_k) \tag{6.2.7}$$

where ($\tilde{\ }$) represents the time rate of change with respect to the moving frame oxyz, ($^{\circ}$) defines the absolute rate of change, e_{ijk} is the alternating tensor, and components of the angular velocity vector for the moving axes are represented by $\dot{\theta}_j$;

$$q_i^{(H)} = -K_{ij}\theta_{,j} \tag{6.2.8}$$

and

$$q_i^{(M)} = -D_{ij}M_{,j}-G_{ijkl}\gamma_{kl,j} \tag{6.2.9}$$

where G_{ijkl} (N/m-sec) is the hygroelastic modulus. These are the phenomenological equations describing the heat and mass transfers, which are also known as Fourier's and modified Fick's equations, respectively [42,43]. The mechanical boundary condition on region S_u are,

$$\bar{u}_i = u_i \tag{6.2.10}$$,

the thermal boundary condition on region S_θ are

$$\bar{\theta} = \theta \tag{6.2.11}$$

and the hygroscopic boundary condition on region S_M are

$$\bar{M} = M \tag{6.2.12}$$

A free variational problem with auxiliary conditions may be constructed by the Lagrange multiplier method which incorporates the constraints within the original functional after each condition is first multiplied by an undetermined multiplier, λ, with numerical superscript and appropriate tensor indicial subscripts. The functional G, for the free variational problem becomes the functional J, where

$$\begin{aligned}
J = \int_{t_1}^{t_2} \Big[& \int_V \big[T-W+D+\theta s+\pi M+X_i r_i\big]dV + \int_{S\sigma} \bar{g}_i r_i dS_\sigma \\
& + \int_{SH} (1/\tilde{p}\theta_o)\, \bar{Q}^{(H)}\theta dS_H + \int_{SD} (1/\tilde{p}M_o)\, \Omega\bar{Q}^{(M)} M dS_D \\
& + \int_V \lambda_{ij}^{(1)}\big[\gamma_{ij}-1/2\ (u_{i,j}+u_{j,i})\big]dV \\
& + \int_V \lambda_i^{(2)}\big[q_i^{(H)}+K_{ij}\theta_{,j}\big]dV \\
& + \int_V \lambda_i^{(3)}\big[q_i^{(M)}+D_{ij}M_{,j}+G_{ijkl}\gamma_{kl,j}\big]dV \\
& + \int_V \lambda_i^{(4)}\big[P_i-(\tilde{r}_{oi}+\tilde{u}_i+e_{ijk}\vartheta_j\ (r_{ok}+r_{Rk}+u_k))\big]dV \\
& + \int_{Su} \lambda_i^{(5)}\ (u_i-\bar{u}_i)dS_u + \int_{S\theta} \lambda^{(6)}\ (\theta-\bar{\theta})dS_\theta \\
& + \int_{SM} \lambda^{(7)}(M-\bar{M})dS_M\ \Big]dt
\end{aligned} \tag{6.2.13}$$

The variational equation corresponding to the above equation may be obtained by taking variations of the system variables and setting the resulting expression equal to zero. Hence using the definitions (6.2.2), (6.2.4) and (6.2.5), this is written

$$\delta J = 0 = \int_{t1}^{t2} \Big[\int_V \rho P_i \delta P_i - C_{ijkl}\gamma_{kl}\delta\gamma_{ij}$$

$$- \Theta_o/c(s-\beta_{ij}\gamma_{ij}+\mu M)(\delta s-\beta_{ij}\delta\gamma_{ij}+\mu\delta M)$$

$$- M_o/b(\pi-\alpha_{ij}\gamma_{ij}+\mu\Theta)(\delta\pi-\alpha_{ij}\delta\gamma_{ij}+\mu\delta\Theta)$$

$$+ (1/\tilde{p}\Theta_o K_{ij})q_j^{(H)}\delta q_i^{(H)} + (1/\tilde{p}M_o D_{ij}) \Omega q_j^{(M)}\delta q_i^{(M)}$$

$$+ s\delta\Theta + \Theta\delta s + \pi\delta M + M\delta\pi + X_i\delta r_i \Big]dV + \int_{S\sigma}\bar{s}_i\, \delta r_i dS_\sigma$$

$$+ \int_{SH} (1/\tilde{p}\Theta_o)\, \bar{Q}^{(H)}\delta\Theta dS_H + \int_{SD} (1/\tilde{p}M_o)\, \Omega\bar{Q}^{(M)}\delta M dS_D$$

$$+ \int_V \delta\lambda_{ij}^{(1)}\big[\gamma_{ij}-1/2(u_{i,j}+u_{j,i})\big]dV$$

$$+ \int_V \lambda_{ij}^{(1)}\big[\delta\gamma_{ij}-1/2(\delta u_{i,j}+\delta u_{j,i})\big]dV$$

$$+ \int_V \delta\lambda_i^{(2)}(q_i^{(H)}+K_{ij}\Theta_{,j})dV$$

$$+ \int_V \lambda_i^{(2)}(\delta q_i^{(H)}+K_{ij}\delta\Theta_{,j})dV$$

$$+ \int_V \delta\lambda_i^{(3)}(q_i^{(M)}+D_{ij}M_{,j}+G_{ijkl}\gamma_{kl,j})dV$$

$$+ \int_V \lambda_i^{(3)}(\delta q_i^{(M)}+D_{ij}\delta M_{,j}+G_{ijkl}\delta\gamma_{kl,j})dV$$

$$+ \int_V \delta\lambda_i^{(4)}\big[P_i-(\tilde{r}_{oi}+\tilde{u}_i+e_{ijk}\dot{\vartheta}_j(r_{ok}+r_{Rk}+u_k))\big]dV$$

$$+ \int_V \lambda_i^{(4)}\big[\delta P_i-(\delta\tilde{r}_{oi}+\delta\tilde{u}_i+e_{ijk}\delta\dot{\vartheta}_j(r_{ok}+r_{Rk}+u_k))\big]dV$$

$$+ \int_{Su}\lambda_i^{(5)}\delta u_i dS_u + \int_{Su}\delta\lambda_i^{(5)}(\bar{u}_i-u_i)dS_u$$

$$+ \int_{S\Theta}\lambda^{(6)}\delta\Theta dS_\Theta + \int_{S\Theta}\delta\lambda^{(6)}(\Theta-\bar{\Theta})dS_\Theta$$

$$+ \int_{SM}\lambda^{(7)}\delta M dS_M + \int_{SM}\delta\lambda^{(7)}(M-\bar{M})dS_M \Big]dt \qquad (6.2.14)$$

Utilizing Gauss' theorem, the sixteenth product in equation (6.2.14) may be written as

$$-\int_V \lambda_{ij}^{(1)} 1/2(\delta u_{i,j}+\delta u_{j,i})dV$$

$$= -\int_S \lambda_{ij}^{(1)} n_j \delta u_i \, dS + \int_V \lambda_{ij,j}^{(1)} \delta u_i dV \qquad (6.2.15)$$

where n_j is the unit vector outward normal to S.

Similiarly, the eighteenth and the twentieth products in (6.2.14) may be written as

$$\int_V \lambda_i^{(2)} K_{ij} \delta\theta_{,j} dV$$

$$= \int_S K_{ij} \lambda_i^{(2)} n_j \delta\theta dS - \int_V \lambda_{i,j}^{(2)} K_{ij} \delta\theta dV \qquad (6.2.16)$$

and

$$\int_V \lambda_i^{(3)} \left[D_{ij} \delta M_{,j} + G_{ijkl} \delta\gamma_{kl,j} \right] dV$$

$$= \int_S \left[D_{ij} \lambda_i^{(3)} n_j \delta M + G_{ijkl} \lambda_i^{(3)} n_j \delta\gamma_{kl} \right] dS$$

$$- \int_V \left[\lambda_{i,j}^{(3)} D_{ij} \delta M + \lambda_{i,j}^{(3)} G_{ijkl} \delta\gamma_{kl} \right] dV \qquad (6.2.17)$$

The terms under the eleventh integral must be subjected to integration-by-parts over time. This integration procedure is subject to the constraint that variations are not permitted at the extremes of the time interval. Finally, by permitting the variations to coincide with the actual displacements that occur during the time interval dt, then

$$\delta r_i = \delta r_{oi}+\delta u_i+e_{ijk}\delta\phi_j(r_{ok}+r_{Rk}+u_k) \qquad (6.2.18)$$

Upon incorporating these re-arrangements into equation (6.2.14), the characteristic equations for this class of mixed dynamical problem in hygrothermoelasticity may be obtained by permitting independent arbitrary variations of the system parameters, and this operation also enables the undetermined multipliers to be expressed as functions of the system variables. These operations yield the following equations.

The constitutive equations

$$\lambda_{ij}^{(1)} = C_{ijkl}\gamma_{kl} - \beta_{ij}\theta - \alpha_{ij}M - G_{ijkl}\lambda_{k,l}^{(3)}$$

$$= \sigma_{ij} \qquad (6.2.19)$$

$$q_i^{(H)} = -K_{ij}\theta_{,j} \qquad (6.2.20)$$

and

$$q_i^{(M)} = -D_{ij}M_{,j}-G_{ijkl}\gamma_{kl,j} \qquad (6.2.21)$$

The equations of state are

$$\theta_o s = c\theta + \theta_o\beta_{ij}\gamma_{ij} - \theta_o\mu M \qquad (6.2.22)$$

and

$$M_o\pi = bM + M_o\alpha_{ij}\gamma_{ij} - M_o\mu\theta. \tag{6.2.23}$$

The multiplier $\lambda_i^{(4)} = \rho\mathring{P}_i$, and the equations of motion are written as

$$\sigma_{ij,j} + X_i = \rho\mathring{P}_i. \tag{6.2.24}$$

The balance of linear and angular momentum also emerge from the analysis and are written

$$\int_V X_i dV + \int_{S\sigma} \bar{g}_i dS_\sigma = \int_V \rho\mathring{P}_i dV \tag{6.2.25}$$

and

$$\int_V e_{ijk}X_i(r_{ok}+r_{Rk}+u_k)dV + \int_{S\sigma} e_{ijk}\bar{g}_i\ (r_{ok}+r_{Rk}+u_k)dS_\sigma$$
$$= \int_V e_{ijk}\rho\mathring{P}_i(r_{ok}+r_{Rk}+u_k)dV. \tag{6.2.26}$$

The multiplier $\lambda_i^{(2)}$ is defined by

$$\lambda_i^{(2)} = -(\ 1/\tilde{p}\theta_o K_{ij}\ )q_j^{(H)} \tag{6.2.27}$$

which enables the energy equation to be developed from

$$s = \mu M - K_{ij}\lambda_{i,j}^{(2)}. \tag{6.2.28}$$

Hence, upon substituting for $\lambda_i^{(2)}$ and applying the mathematical operator $\tilde{p}$, this yields

$$\Theta_o \overset{\circ}{s} = \Theta_o \mu \overset{\circ}{M} - q_{i,i}^{(H)}. \tag{6.2.29}$$

Similarly, the multiplier $\lambda_i^{(3)}$ is defined by

$$\lambda_i^{(3)} = -(\ 1/\tilde{p} M_o D_{ij}\ ) \Omega q_j^{(M)} \tag{6.2.30}$$

and hence

$$M_o \overset{\circ}{\pi} = M_o \mu \overset{\circ}{\Theta} - \Omega q_{i,i}^{(M)}. \tag{6.2.31}$$

Equations (6.2.6)-(6.2.11) also emerge as characteristic equations, as anticipated. In addition, the following Lagrange multipliers $\lambda^{(5)}$, $\lambda^{(6)}$ and $\lambda^{(7)}$ are obtained from the process of taking arbitrary variations.

$$\lambda^{(5)} = \lambda_{ij}^{(1)} n_j \tag{6.2.32}$$

$$\lambda^{(6)} = -\lambda_i^{(2)} n_j K_{ij} = (1/\tilde{p}\Theta_o) q_i^{(H)} n_i \tag{6.2.33}$$

and

$$\lambda^{(7)} = -\lambda_i^{(3)} n_j D_{ij} = (1/\tilde{p} M_o) \Omega q_i^{(M)} n_i \tag{6.2.34}$$

The previous three equations enable the following surface traction boundary conditions to be obtained

$$\bar{S}_i = \sigma_{ij}n_j \tag{6.2.35}$$

as anticipated. Finally, the heat and mass flux boundary conditions are expressed as

$$\bar{Q}^{(H)} = q_i^{(H)}n_i \tag{6.2.36}$$

and

$$\bar{Q}^{(M)} = q_i^{(M)}n_i \tag{6.2.37}$$

Using the above definitions of the Lagrange multipliers, the first variation of functional J, from which the equations governing the hygrothermoelastodynamical analysis of mechanism systems may be obtained, is written

$$\delta J = 0 = \int_{t1}^{t2} \Big[\int_V \delta\gamma_{ij}\Big[\sigma_{ij}$$

$$-C_{ijkl}\gamma_{kl}+\beta_{ij}\theta + \alpha_{ij}M-1/(\tilde{p}M_oD_{kl})G_{ijkl}\ \Omega q_{r,r}^{(M)}\ \Big]dV$$

$$+ \int_V \delta s\Big[\theta-\theta_o/c\ \ (s-\beta_{ij}\gamma_{ij}+\mu M)\Big]dV$$

$$+ \int_V \delta\pi\Big[M-M_o/b\ \ (\pi-\alpha_{ij}\gamma_{ij}+\mu\theta)\Big]dV$$

$$+ \int_V \delta u_i\Big[\sigma_{ij,j}+X_i-\rho\ddot{P}_i\Big]dV$$

$$+ \int_V \delta\theta\Big[s-\mu M+(1/\tilde{p}\theta_o)\ q_{i,i}^{(H)}\Big]dV$$

$$+ \int_V \delta M\left[\pi-\mu\theta+(1/\tilde{p}M_o)\ \Omega q_{i,i}^{(M)}\right]dV$$

$$+ \int_V \delta\sigma_{ij}\left[\gamma_{ij}-1/2(u_{i,j}+u_{j,i})\right]dV$$

$$- \int_V (\delta q_i^{(H)}/\tilde{p}\theta_o K_{ik})\left[q_k^{(H)}+K_{kj}\theta_{,j}\right]dV$$

$$- \int_V (\delta q_i^{(M)}/\tilde{p}M_o D_{is})\Omega\left[q_s^{(M)}+D_{sj}M_{,j}+G_{sjkl}\gamma_{kl,j}\right]dV$$

$$- \int_V \rho\delta P_i\left[p_i-\tilde{r}_{oi}-\tilde{u}_i-e_{ijk}\dot{\phi}_j(r_{ok}+r_{Rk}+u_k)\right]dV$$

$$+ \delta r_{oi}\left[\int_V X_i dV+\int_{S\sigma}\bar{s}_i dS_\sigma-\int_V\rho\dot{P}_i dV\right]$$

$$+\delta\phi_j\left[\int_V e_{ijk}X_i(r_{ok}+r_{Rk}+u_k)dV\right.$$

$$+ \int_{S\sigma} e_{ijk}\bar{s}_i(r_{ok}+r_{Rk}+u_k)dV$$

$$\left.- \int_V e_{ijk}\rho\dot{P}_i(r_{ok}+r_{Rk}+u_k)dV\right]$$

$$- \int_{S\sigma} \delta u_i(s_i-\bar{s}_i)dS_\sigma + \int_{Su} \delta s_i(u_i-\bar{u}_i)dS_u$$

$$+ \int_{S\theta} (\delta q_i^{(H)}n_i/\tilde{p}\theta_o)(\theta-\bar{\theta})dS_\theta$$

$$+ \int_{SH} (\delta\theta/\tilde{p}\theta_o)(\bar{Q}^{(H)}-q_i^{(H)}n_i)dS_H$$

$$+ \int_{SM} (\delta q_i^{(M)}n_i/\tilde{p}M_o)\Omega(M-\bar{M})dS_M$$

$$+ \int_{SD} (\delta M/\tilde{p}M_o)\Omega(\bar{Q}^{(M)}-q_i^{(M)}n_i)dS_D\ \Big]dt \qquad (6.2.38)$$

Independent arbitrary variations of the deformation displacement, strain, stress, absolute velocity, and the kinematic parameters defining the rigid-body motion, and the entropy density, flow-potential density, temperature and moisture concentration field, enable equation (6.2.38) to yield, as Euler equations, the field equations and boundary conditions for this class of hygrothermoelastodynamic problem. This variational principle also provides a basis for finite element formulation which will be developed in next section.

6.3 Finite Element Formulation

The objective, herein, is to develop a "displacement" finite element formulation for a single one-dimensional finite element with two exterior nodes, each having five nodal degrees of freedom. Since this analysis is to investigate the vibrational behavior of linkages fabricated with straight slender flexible beam-shaped composite laminates, the flexural deformation field be modeled by the element is governed by the classical Bernoulli-Euler hypothesis. Two nodal variables W and ϕ describe the flexural displacement and slope, respectively, U describes the longitudinal displacement, T denotes the temperature field and M is the moisture concentration.

Defining the nodal "displacement" vector for the element by

$$[U]^T = [U_1, W_1, \phi_1, T_1, M_1, U_2, W_2, \phi_2, T_2, M_2] \qquad (6.3.1)$$

and the general solid-body displacement is denoted as

$$u(x,t) = [N^s][U] \qquad (6.3.2)$$

and the temperature field and moisture concentration are expressed by

$$\theta(x,t) = [N^h][T] \tag{6.3.3}$$

and

$$m(x,t) = [N^m][M] \tag{6.3.4}$$

where $[N^s]$, $[N^h]$ and $[N^m]$ are shape functions which describe the spatial distribution of displacements, temperature and moisture concentration, respectively, throughout the element. These functions are independent of time. However, $[U]$, $[T]$ and $[M]$ are time dependent.

Incorporating equations (6.3.2)-(6.3.4) into equation (6.2.38), then the discretized variational equation may be written as

$$\delta J = 0$$

$$= \int_{t1}^{t2} \Big[\int_V [\delta\gamma_{xx}]^T \Big[[\sigma_{xx}]$$

$$-[C][B^s][U]+[\beta][N^h][T]+[\alpha][N^m][M]$$

$$-1/(\tilde{p}M_o)[D]^{-1}[G]\Omega\partial[q^{(M)}]/\partial x \Big] dV$$

$$+ \int_V [\delta s]^T \Big[[N^h][T]-\theta_o/c \ ([s]-[\beta][\gamma_{xx}]+\mu[N^m][M] \ ) \Big] dV$$

$$+ \int_V [\delta\pi]^T \Big[[N^m][M]-M_o/b \ ([\pi]-[\alpha][\gamma_{xx}]+\mu[N^h][T]) \Big] dV$$

$$+ \int_V [\delta U]^T [N^s]^T \Big[\partial[\sigma_{xx}]/\partial x+[X]-\rho[\ddot{P}] \Big] dV$$

$$+ \int_V [\delta T]^T [N^h]^T \Big[[s]-\mu[N^m][M] +(1/\tilde{p}\theta_o) \ \partial[q^{(H)}]/\partial x \Big] dV$$

$$+ \int_V [\delta M]^T [N^m]^T \Big[[\pi]-\mu[N^h][T]+(1/\tilde{p}M_o) \ \Omega\partial[q^{(M)}]/\partial x \ \Big] dV$$

$$+ \int_V [\delta\sigma_{xx}]^T \Big[[\gamma_{xx}] - [B^s][U] \Big] dV$$

$$- \int_V ([\delta q^{(H)}]^T [K]^{-1}/\tilde{p}\theta_o) \Big[[q^{(H)}] + [K][B^h][T] \Big] dV$$

$$- \int_V ([\delta q^{(M)}]^T [D]^{-1}/\tilde{p}M_o)\Omega \Big[[q^{(M)}] + [D][B^m][M]$$

$$+ [G][B^s][\gamma] \Big] dV$$

$$- \int_V \rho [\delta P]^T \Big[[P] - [N_R][P_R] - [N^s][\dot{U}] \Big] dV$$

$$- \int_{S\sigma} [\delta U]^T [N^s]^T ([g] - [\bar{g}]) dS_\sigma + \int_{Su} [\delta g]^T [N^s] \; ([U] - [\bar{U}]) dS_u$$

$$+ \int_{S\theta} ([\delta q^{(H)}]^T/\tilde{p}\theta_o) [N^h] ([T] - [\bar{T}]) dS_\theta$$

$$+ \int_{SH} ([\delta T]^T [N^h]^T/\tilde{p}\theta_o) ([\bar{Q}^{(H)}] - [Q^{(H)}]) dS_H$$

$$+ \int_{SM} ([\delta q^{(M)}]^T/\tilde{p}M_o) [N^m] \Omega ([M] - [\bar{M}]) dS_M$$

$$+ \int_{SD} ([\delta M]^T [N]^T/\tilde{p}M_o) \Omega ([\bar{Q}^{(M)}] - [Q^{(M)}]) dS_D \Big] dt \qquad (6.3.5)$$

where [C] (N/m^2) is the elastic modulus matrix; [β] ($N\text{-}m/m^{3}{}^\circ K$) and [α] ($N\text{-}m/m^3$) are thermal-expansion and hygroscopic-expansion coefficient matrices; $[N_R]$ contain the shape functions approximating the rigid-body kinematics (see chapter 2) while $[P_R]$ is the column vector containing the nodal rigid-body kinematic degrees of freedom. The nodal absolute velocity components are defined by [P]; the surface tractions, heat and mass fluxes are defined by [g], $[Q^{(H)}]$ and $[Q^{(M)}]$, respectively; [B] is the spatial derivative of shape function [N]. Because the rigid-body equations of motion are of no consequence here, they may be removed from the formulation by taking variations $[\delta r_{oi}]$ and $[\delta\phi_i]$ to be zero.

Substituting the constitutive equations of the first integral and the tenth integral into the equations of equilibrium yields the expression

$$-[\delta U]^T \Big[\Big[\int_V [N^s]^T\rho[N^s][\ddot{U}]+[B^s]^T[C][B^s][U]$$

$$-[B^s]^T[\beta][N^h][T]-[B^s]^T[\alpha][N^m][M]$$

$$+1/(\tilde{p}M_e[D]^{-1}[B^s]^T[G]\Omega\partial[q^{(M)}]/\partial x\Big]dV$$

$$+\int_V [N^s]^T\rho[N_R][\ddot{P}_R]dV - \int_V [N^s]^T[X]dV$$

$$-\int_{S\sigma}[N^s]^T[\bar{g}]dS_\sigma \Big] \qquad (6.3.6)$$

The following definitions are introduced,

$$[M_R^s] = \int_V[N^s]^T\rho[N_R]dV \qquad (6.3.7)$$

$$[M^{ss}] = \int_V[N^s]^T\rho[N^s]dV \qquad (6.3.8)$$

$$[K^{ss}] = \int_V[B^s]^T[C][B^s]dV \qquad (6.3.9)$$

$$[K^{sh}] = -\int_V[B^s]^T[\beta][N^h]dV \qquad (6.3.10)$$

$$[K^{sm}] = -\int_V[B^s]^T[\alpha][N^m]dV \qquad (6.3.11)$$

Substituting equations (6.3.7)-(6.3.11) into (6.3.6) yields

$$-[\delta U]^T \Big[[M^{ss}][\ddot{U}]+[K^{ss}][U]+[K^{sh}][T]+[K^{sm}][M]$$

$$+[M_R^s][\dot{P}_R]-\int_V [N^s]^T[X]dV-\int_{S\sigma}[N^s]^T[\bar{g}]dS_\sigma$$

$$+\int_V 1/(\tilde{p}M_e)[D]^{-1}[G][B^s]^T\Omega\partial[q^{(M)}]/\partial x dV \Big] \qquad (6.3.12)$$

The second integral expression in equation (6.3.5) may be employed to eliminate s from the energy equation in the fifth integral of (6.3.5). The energy equation may then be written as

$$\int_V [\delta T]^T \Big[\theta_e[N^h]^T[\beta][B^s][\dot{U}]+c[N^h]^T[N^h][\dot{T}]$$

$$-2\mu\theta_e[N^h]^T[N^m][\dot{M}]+[B^h]^T[K][B^h][T]\Big]dV$$

$$-\int_{SH} [\delta T]^T[N^h]^T[K][B^h][T]dS_H \qquad (6.3.13)$$

Upon introducing the following definitions

$$[C^{hs}] = \int_V [N^h]^T\theta_e[\beta][B^s]dV \qquad (6.3.14)$$

$$[C^{hh}] = \int_V [N^h]^T c[N^h]dV \qquad (6.3.15)$$

$$[C^{hm}] = -\int_V [N^h]^T 2\mu\theta_e[N^m]dV \qquad (6.3.16)$$

$$[K^{hh}] = \int_V [B^h]^T[K][B^h]dV \qquad (6.3.17)$$

$$[\bar{Q}^{(H)}] = -[K][B^h][T] \qquad (6.3.18)$$

equation (6.3.13) may then be written as

$$[\delta T]^T\Big[[C^{hs}][\hat{U}] + [C^{hh}][\hat{T}] + [C^{hm}][\hat{M}] + [K^{hh}][T]$$

$$+ \int_{SH}[N^h]^T[\bar{Q}^{(H)}]dS_H\Big] \qquad (6.3.19)$$

Similarly, the equation of mass balance may be written as

$$[\delta M]^T\Big[[C^{ms}][\hat{U}] + [C^{mh}][\hat{T}] + [C^{mm}][\hat{M}] + [K^{mm}][M]$$

$$+[K^{ms}][\gamma] + \int_{SD}[N^m]^T\Omega[\bar{Q}^{(M)}]dS_D\Big] \qquad (6.3.20)$$

where

$$[C^{ms}] = \int_V [N^m]^T M_e[\alpha][B^s]dV \qquad (6.3.21)$$

$$[C^{mh}] = -\int_V [N^m]^T 2\mu M_e[N^h]dV \qquad (6.3.22)$$

$$[C^{mm}] = \int_V [N^m]^T b[N^m]dV \qquad (6.3.23)$$

$$[K^{mm}] = \int_V [B^m]^T \Omega[D][B^m]dV \qquad (6.3.24)$$

$$[K^{ms}] = \int_V [B^m]^T \Omega[G][B^s]dV \qquad (6.3.25)$$

$$[\bar{Q}^{(M)}] = -[D][B^m][M] \qquad (6.3.26)$$

The final form of the discretized finite element formulation for the variational equation of motion (6.2.38) may now be written as

$$\delta J = 0$$

$$= \int_{t1}^{t2} \Big[\int_V [\gamma_{xx}]^T \Big[[\sigma_{xx}]-[C][B^s][U]$$

$$+[\beta][N^h][T]+[\alpha][N^m][M]-1/(\tilde{p}M_e)[D]^{-1}[G]\Omega\partial[q^{(M)}]/\partial x\Big]dV$$

$$+ \int_V [\delta s]^T\Big[[N^h][T]-\Theta_e/c \ ([s]-[\beta][B^s][U]+\mu[N^m][M])\Big] \ dV$$

$$+ \int_V [\delta\pi]^T\Big[[N^m][M]-M_e/b \ ([\pi]-[\alpha][B^s][U]+\mu[N^h][T]) \ \Big]dV$$

$$+ \ [\delta U]^T\Big[\ [M^{ss}][\ddot{U}]+[K^{ss}][U]+[K^{sh}][T]+[K^{sm}][M]$$

$$+[M_R^s][\mathring{P}_R]-\int_V [N^s]^T[X]dV-\int_{S\sigma} \ [N^s]^T([\bar{g}]-[g])dS$$

$$+\int_V 1/(\tilde{p}M_e)[D]^{-1}[G][B^s]^T\Omega\partial[q^{(M)}]/\partial x dV\Big]$$

$$+ \ [\delta T]^T\Big[\ [C^{hs}][\mathring{U}]+[C^{hh}][\mathring{T}]+[C^{hm}][\mathring{M}]+[K^{hh}][T]$$

$$+\int_{SH} \ [N^h]^T([\bar{Q}^{(H)}]-[Q^{(M)}])dS_H\Big]$$

$$+ \ [\delta M]^T\Big[\ [C^{ms}][\mathring{U}]+[C^{mh}][\mathring{T}]+[C^{mm}][\mathring{M}]+[K^{mm}][M]$$

$$+\int_{SD} \ [N^m]^T([\bar{Q}^{(M)}]-[Q^{(M)})dS_D\Big]$$

$$+ \ \int_V \ [\delta\sigma]^T\Big[[\gamma]-[B^s][U]\Big]dV$$

$$+ \ \int_V \ ([\delta q^{(H)}]^T[K]^{-1}/\tilde{p}\Theta_e)\Big[[q^{(H)}]+[K][B^h][T]\Big]dV$$

$$+ \ \int_V \ ([\delta q^{(M)}]^T[D]^{-1}/\tilde{p}M_e)\Big[[q^{(M)}]+[D][B^m][M]$$

$$+[G][B^s][\gamma] \ \Big]dV$$

$$- \int_V \rho[\delta P]^T\Big[[P]-[N_R][P_R]-[N][\mathring{U}]\Big]dV$$

$$+ \int_{Su} [\delta g]^T[N^s]([U]-[\bar{U}])dS_u$$

$$+ \int_{S\theta} ([\delta q^{(H)}]^T/\tilde{p}\theta_o)[N^h]([T]-[\bar{T}])dS_\theta$$

$$+ \int_{SM} ([\delta q^{(M)}]^T/\tilde{p}M_o)[N^m]([M]-[\bar{M}])dS_M \qquad (6.3.27)$$

Equation (6.3.27) contains the field equations and prescribed displacement, temperature and moisture concentration boundary conditions for one finite element. These governing equations may be obtained by taking arbitrary independent variations of the variables in this variational equation of motion. The resulting matrix formulation must be pre- and post-multiplied by standard transformation matrices in order that this general statement be used to develop a finite element model of a specific linkage. After an appropriate modeling of a physical problem by employing these governing equations and boundary conditions, solutions for these equations will be sought by using a proper numerical scheme.

6.4 Parameter Definition

For calculating temperature, moisture distribution and the deflection of the composite laminate, a full knowledge of the following parameters is required:

1. geometry: dimensions of the specimens,

2. boundary conditions: ambient temperature and the level

of the relative humidity,

3. initial conditions: temperature distribution and moisture concentration inside the material,

4. material properties: density ρ, elastic moduli C_{ijkl}, thermal-expansion coefficients β_{ij}, diffusion-expansion coefficients α_{ij}, heat capacity c, thermal conductivity K_{ij}, hygrothermal coefficient μ, hygroscopic capacity b, moisture diffusivity D, maximum moisture content M_m, and a relationship between the maximum moisture content and the ambient conditions.

The density, thermal-expansion coefficient, diffusion-expansion and specific heat are generally known. However, the determination of the other coefficients are more difficult and will now be discussed.

6.4.1 Elastic Moduli C_{ijkl}

Data are available showing the effects of moisture and temperature on the buckling, tensile, and compressive moduli of various composite laminate [153,218]. The available data on these moduli were compiled by Shen and Springer [218] in a manner similar to the tension test data. On the basis of available information, the following major observations can be made.

6.4.1.1 Temperature Effects

For 0-degree and $\pi/4$ laminates, the temperature (in the range of 200 to 450K) has a negligible effect on the elastic moduli regardless of the moisture content of the material. For 90-degree laminates, an increase in temperature causes a decrease in the elastic moduli in the direction perpendicular to fiber. For example an increase in temperature from 300 to 450 K, the elastic modulus of AS-5/3501 [221] may decrease by as much as 50 to 90 percent. The decrease in the modulus depends upon both the temperature and moisture content.

6.4.1.2 Moisture Effects

For 0-degree and $\pi/4$ laminates, there appears to be very little change in the elastic moduli over the entire spectrum of moisture content from dry to fully saturated. This conclusion appears to be valid regardless of temperature in the range 200 to 450 K. For 90-degree laminates, the elastic moduli decrease considerably with increase in the moisture content. The decrease in the value of the modulus of Modmor II/Narmco 5206 [222] may be as high as 50 to 90 percent in the temperature range of 200 to 400°K.

6.4.2 Thermal Conductivity K_{ij}

The thermal conductivity of a material is a measure of the speed at which heat is conducted through a material. This material property may also depend on the moisture concentration and on the stress level as well as on temperature [93,152]. However, the variations of K_{ij} with both moisture concentration and with stress are not known in detail for most composite material [146,217]. Mathematical models are based upon the assumption that K_{ij} is a function of temperature only [152]. The thermal conductivity, K_{ij}, can also be approximated from the known fiber and matrix conductivities [152]. For many composite materials, the thermal conductivity K_{ij} is 10^4 to 10^6 times larger than mass diffusivity D_{ij} [93,143]. Thus, the temperature equilibrates much faster than the moisture concentration.

6.4.3 Mass Diffusivity D_{ij}

The mass diffusivity characterizes the speed at which moisture is transported through the material. The value of D depends on the material, on the fluid surrounding the material, on the moisture concentration inside the material, on the stress level inside the material, and on the temperature. In calculating the moisture content inside the material D is assumed to depend only on temperature. In many practical problems this is an adequate approximation. The diffusivity of a composite material may be determined directly from tests [93,143], or may be approximated from the known fiber and matrix properties [143].

6.4.4 Hygroscopic Capacity b

The hygroscopic capacity, b, is a measure of absorbed energy carried by the moisture moving through the material and is analogous to the heat capacity. It can be expressed mathematically by [118]

$$b = 1/M_o(\partial\pi/\partial m)_{\gamma,\theta} \qquad (6.4.4.1)$$

The hygroscopic capacity, b, can be represented explicitly by ($b=\Omega\bar{b}$) [42,43] where Ω (N-m/N) is the specific chemical potential, and $\bar{b}$ is generally a material property which may be interpreted as mass of moisture being absorbed per unit volume of the material. The material property $\bar{b}$ is generally known by experimental testing and the definition of specific chemical potential will be described in the following subsection.

6.4.5 Specific Chemical Potential Ω

Several assumptions are made in order to find the specific chemical potential in this study:

1. The transferred moisture is considered as saturated vapor and this is further assumed to be an ideal gas.
2. Since the moisture diffusion velocity is assumed to be slow and no elevation in the diffusion process, i.e. no potential energy resulted from gravitational force, the kinetic and potential energies associated with this phenomena are considered to be negligible.

The derivation of the specific chemical potential Ω is described briefly as following: The specific chemical potential of a pure substance is equal to its specific Gibbs function g at the same state [223], therefore, the specific Gibbs function $g_{T,P}$ of a substance at temperature T and pressure P is, by definition,

$$g_{T,P} = h_{T,P} - Ts_{T,P} \tag{6.4.5.1}$$

The enthalpy of an ideal gas at temperature T and pressure P can be written as

$$h_{T,P} = h_T^{\circ} \tag{6.4.5.2}$$

where h_T° represents both the enthalpy of formation and the enthalpy difference between 298°K and the specific temperature T. The standard state of an ideal gas is defined at 1 atmosphere and 25°C, and that is symbolized by the superscript °.

The absolute entropy, s, at temperature T and pressure P are assumed to be related by

$$s_{T,P} = s_T^{\circ} - R \ln P \tag{6.4.5.3}$$

The specific chemical potential of an ideal gas may be obtained by combining equations (6.4.5.1), (6.4.5.2) and (6.4.5.3), and is expressed by

$$\Omega = g_{T,P} = g_T^{\circ} + RT \ln P \qquad (6.4.5.4)$$

where the unit of the quantity P is in atmospheres, R is the universal gas constant and g° is defined by

$$g^{\circ} = h_T^{\circ} - Ts_T^{\circ} \qquad (6.4.5.5)$$

6.4.6 Maximum Moisture Content M_m

The maximum moisture content M_m (%) is the moisture level within the material. This can be attained asymptotically under certain conditions, after a prolonged period of exposure to a moist ambient environment at constant temperature and at constant relative humidity. For materials exposed to humid air the maximum moisture content appears to be insensitive to temperature and depends on the relative humidity ϕ in the following manner: $M_m = a\phi^f$ [93,143]. The terms a and f are constants which depend on material and are determined experimentally. Experimental evidence suggests that the value of f is near unity [93].

The above relationship greatly facilitates the calculations, however, it is only an approximation, in fact, M_m generally varies with temperature. Twenty percent variations in M_m with temperature are common for most graphite/epoxy composite laminate in the temperature range of 300–400°K [93]. An advanced theory should be (has not yet been) developed in order to accurately predict the maximum moisture content after the chemical and mechanical properties of composite materials being clearly understood experimentally [145].

In many situations changes in the value of M_m have been observed after the maximum, asymptotic value of M_m has been reached [93]. Both increases and decreases in M_m have been observed [93,143]. The increase in M_m is hypothesized as being due to cracks developing in the material and also, possibly, to non-Fickian diffusion. A decrease in M_m may be caused by loss of material due to leaching or cracking [215]. The above relationship $M_m = a\emptyset^f$ is invalid when the composite structure is near failure as manifested by the formation of microcracking or delamination.

6.5 Illustrative Example

Having established a theory describing a high-speed flexible linkage mechanism constructed from polymeric fibrous composite laminates operating in an environment characterized by variations in both temperature and humidity, a sample problem will be presented in order to illustrate the applicability of this theory.

All of the experimental publications reviewd in section 6.1 of this chapter were focused upon the static analysis of hygrothermal effects on graphite/epoxy composite materials and/or neat epoxy resin, only one paper was devoted to a dynamic analysis [211]. The analysis of a composite material under static loading greatly simplifies the investigation since under the static loads the strain rate is zero. Consequently, the coupling effects between the moisture distribution and strain rate in equation (6.2.27) and also between the temperature distribution and the strain rate in the same equation are zero. Furthermore, the external loading imposed upon the composite material are assumed to be limited in order to prevent the formation of micro-cracks which are resulted from the excessive stress levels. And the micro-cracks in the composite material may result in non-Fickian diffusion due to the changes of saturation level.

In 1978, Whitney and Browning [217] experimentally studied the diffusion of AS/3501-5 graphite/epoxy and 3501-5 (Hercules Inc.) neat resin coating. Unidirectional and bidirectional, $[0/90]_s$, specimens were also included in this investigation.

Seven neat epoxy resin specimens used in these experiments were thin plates of dimension 508mm square with a thickness of 3.18mm. All of the composite materials data reported were obtained by testing sixteen 4-ply specimens which machined from large autoclave-cured panels fabricated from the Hercules AS/3501-5 graphite/epoxy prepreg system. These composite specimens were 508mm square and 0.64mm thick. In order to provide an initially dry condition, all absorption specimens were preconditioned in a vacuum oven at 93°C and under full vacuum until a near equilibrium weight was obtained. Dry specimens were placed in an environmental chamber under constant temperature and humidity conditions. Specimens were removed from the chambers at various time intervals for weight measurement (see the scatter symbols on Figures 6.2, 6.3 and 6.4 from page 195 to 197). Absorption experiments on neat resin specimens were run at 75 percent relative humidity with a temperature of 82°C, and at 95 percent relative humidity with a temperature of 71°C. Unidirectional composite data were also obtained at 95 percent relative humidity with two different temperature conditions of 49°C and 71°C, while the test conditions for bidirectional composite laminates were at a relative humidity of 95 percent with a temperature of 49°C, and at 95 percent relative humidity and with a temperature of 71°C.

In accordance to the experimental work performed by Whitney and Browning [217] as mentioned above, the problem definitions for the analytical analyses are to determine the moisture content of three kinds of materials, i.e. neat epoxy resin coatings, unidirectional composites and bidirectional composite laminates. The geometry of the specimens and the boundary conditions of each case are described as following:

I. An initially dry neat resin plate with dimension of 508mm x 508mm x 3.18mm is placed in an environmental chamber under two constant temperature and humidity conditions: the first is at 75 percent relative humidity with a temperature of 82°C, the other is at 95 percent relative humidity with a temperature of 71°C.

II. An initially dry unidirectional composites with dimension of 508mm x 508mm x 0.64mm is placed in an environmental chamber which has a constant relative humidity of 95 percent and two different temperature

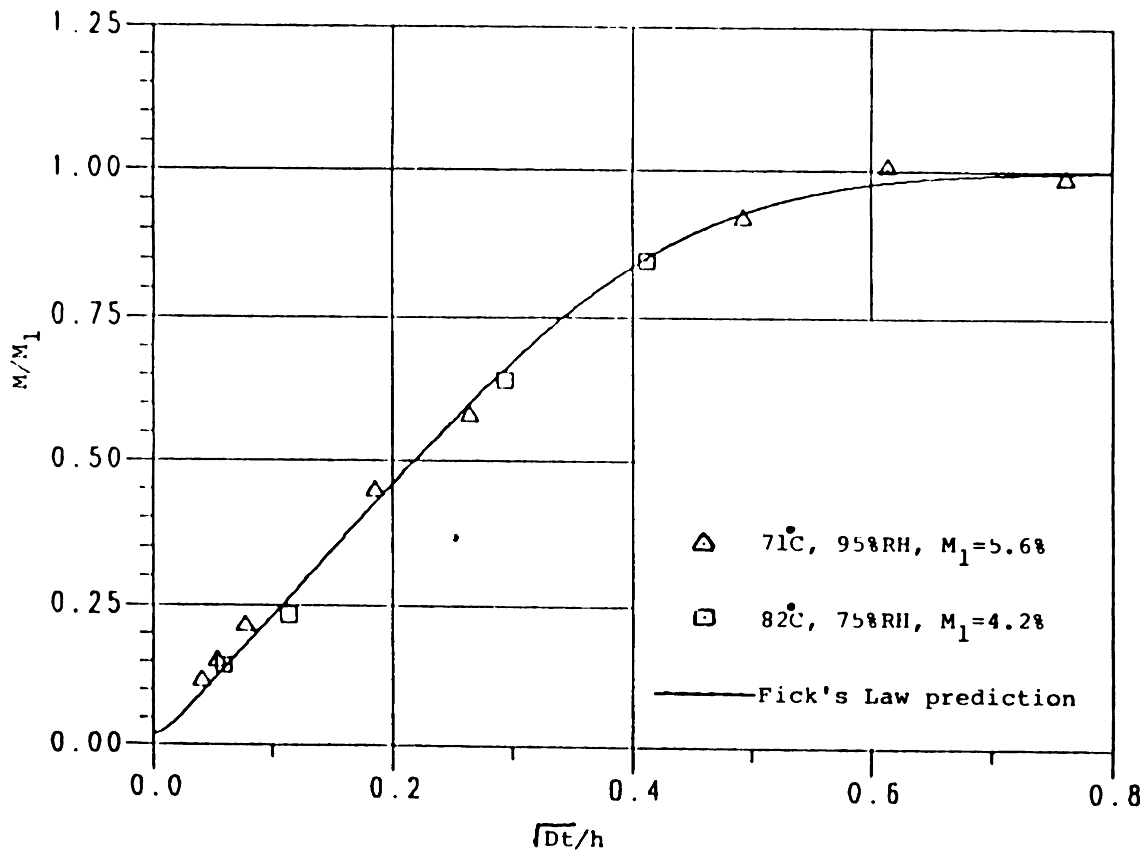

Figure 6.2 **Plot of Experimental Data versus Fick's Law, for Neat Epoxy Resin**

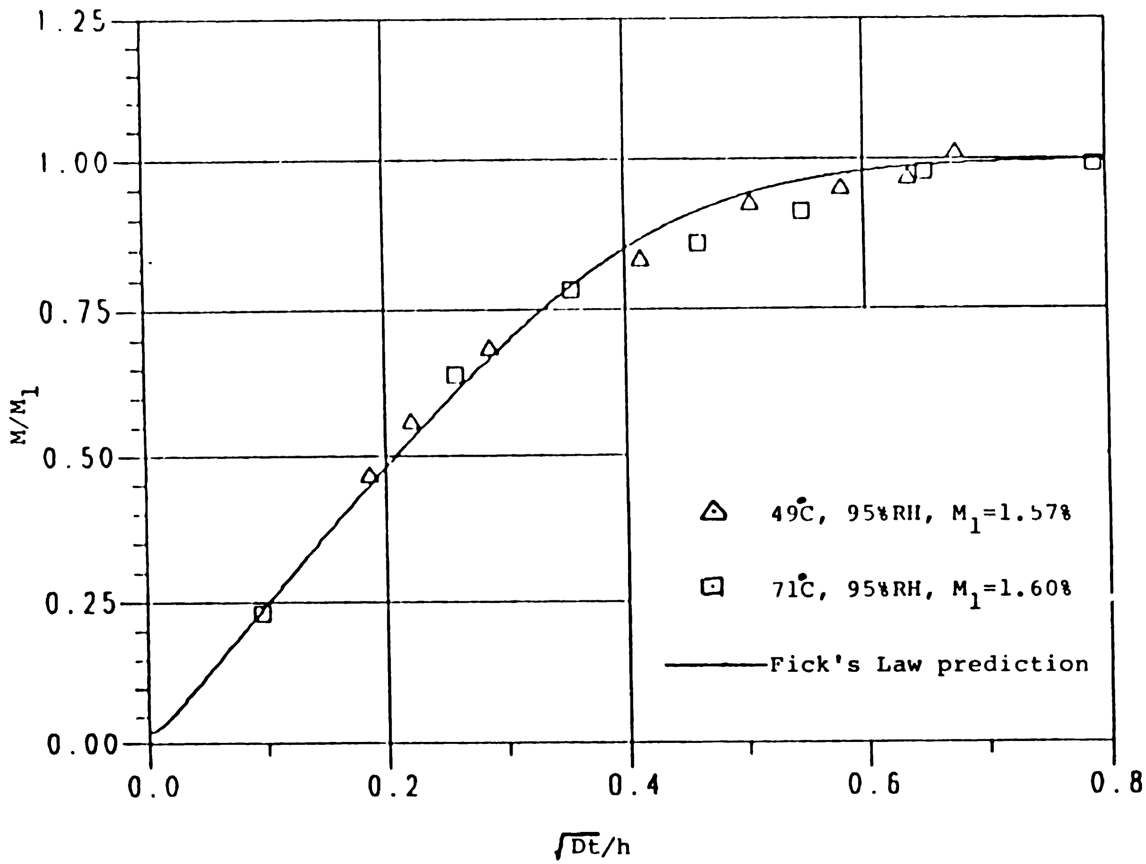

Figure 6.3 Master Plot of Experimental Data versus Fick's Law, for Unidirectional Graphite/Epoxy Composite

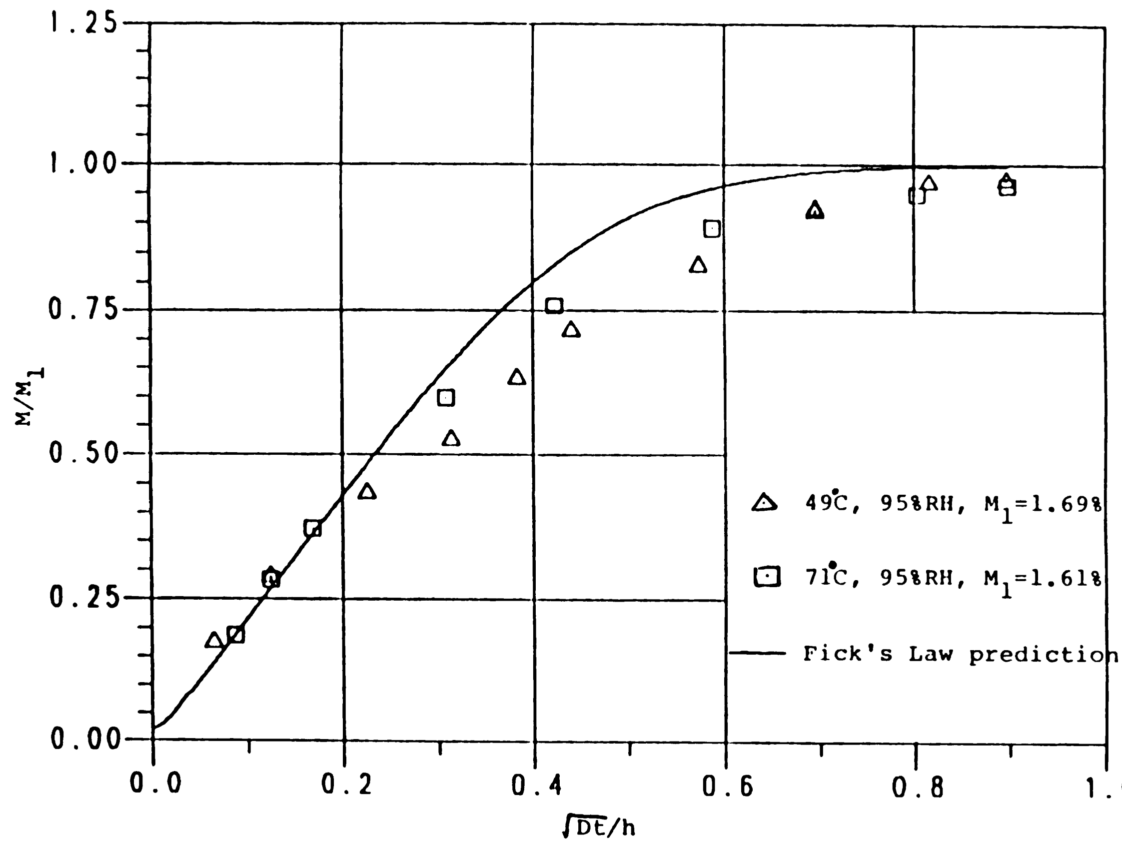

Figure 6.4 **Master Plot of Experimental Data versus Fick's Law, for Bidirectional Graphite/Epoxy Laminate**

conditions of 49°C and 71°C.

III. An initially dry bidirectional composite laminates $[0/90]_s$ with the dimension of 508mm x 508mm x 0.64mm is placed in an environmental chamber with two test conditions; one is at a relative humidity of 95 percent with temperature of 49°C, the other is at the same relative humidity with a temperature of 71°C.

6.6 Results and Discussion

Since several assumptions have been made in the "illustrative example" section (section 6.5) in order to simplify these examples to be mathematically tractable for this priliminary study, the coupling terms between the temperature distribution and the strain rate, and between the moisture concentration and the strain rate in equation (6.3.27) are assumed to be zero. Therefore, by removing the terms associated with the strain rate, the three governing equations (i.e. equations of mass balance, momentum balance and energy balance) may be written as follows:

(1) the equation of mass balance

$$[C^{mh}][\dot{T}] + [C^{mm}][\dot{M}] + [K^{mm}][M]$$

$$= -[K^{ms}][\gamma] - \int_{SD}[N^{m}]^{T}\Omega[\overline{Q}^{(M)}]dS_{D} \qquad (6.6.1)$$

(2) the equation of momentum balance

$$[K^{sh}][T] + [K^{sm}][M] + [K^{ss}][U] = \int_{V}[N^{s}]^{T}[X]dV$$

$$+ \int_{S\sigma} [N^s]^T [\bar{g}] dS_\sigma$$

$$- \int_V 1/(\tilde{p} M_o) [D]^{-1} [G] [B^s]^T \Omega \partial [q^{(M)}]/\partial x dV \qquad (6.6.2)$$

(3) the equation of energy balance

$$[C^{hh}][\dot{T}] + [C^{hm}][\dot{M}] + [K^{hh}][T] = -\int_{SH} [N^h]^T [\bar{Q}^{(H)}] \, dS_H \quad (6.6.3)$$

The above three equations are further simplified by assuming that there is no natural boundary conditions in each equation and the body force may be neglected from equation (6.6.2), therefore, specimens are only subjected to prescribed essential boundary conditions. In addition, the last term on the right-hand side of equation (6.6.2) may also be neglected because that the deformation resulted from the mass-flux gradient is insignificant [42,43]. By assuming the deformation induced by the temperature and moisture is decoupled, therefore, the equation of momentum balance (6.6.2) may be written as

$$[K^{ss}][U] = -[K^{sh}][T] - [K^{sm}][M]. \qquad (6.6.4)$$

The equations of mass balance (6.6.1) and the energy balance (6.6.3) coupled by the cross-effect between temperature and moisture may be expressed by

$$[C^{mh}][\dot{T}] + [C^{mm}][\dot{M}] + [K^{mm}][M] = -[K^{ms}][\gamma] \qquad (6.6.5)$$

and

$$[C^{hh}][\dot{T}] + [C^{hm}][\dot{M}] + [K^{hh}][T] = 0 \qquad (6.6.6)$$

A solution for these equations will be sought using the Crank-Nicolson method [134] of direct integration which use the following statements to update the temperature and moisture distribution in the specimens

$$[T]_{t+\Delta t} = [T]_t + \left[\theta[\dot{T}]_{t+\Delta t} + (1-\theta)[\dot{T}]_t\right]\Delta t \qquad (6.6.7)$$

and

$$[M]_{t+\Delta t} = [M]_t + \left[\theta[\dot{M}]_{t+\Delta t} + (1-\theta)[\dot{M}]_t\right]\Delta t \qquad (6.6.8)$$

where the Crank-Nicolson value $\theta=0.5$ for stability of solution. Knowing the initial conditions, equations (6.6.7) and (6.6.8) may be rearranged, and subjected into equations (6.6.5) and (6.6.6) prior to solving for temperature and moisture distribution in time $t+\Delta t$.

After several manipulations, the final form of equations (6.6.5) and (6.6.6) may be expressed by

$$[C^{mh}][T]_{t+\Delta t} + [A][M]_{t+\Delta t} = [C^{mh}][T]_t$$

$$+ [B][M]_t - [P]\Delta t \qquad (6.6.9)$$

where

$$[A] = [C^{mm}]+\Delta t\theta[K^{mm}] \tag{6.6.10}$$

$$[B] = [C^{mm}]-\Delta t(1-\theta)[K^{mm}] \tag{6.6.11}$$

$$[P] = \theta[K^{ms}][\gamma]_{t+\Delta t}+(1-\theta)[K^{ms}][\gamma]_t \tag{6.6.12}$$

and

$$[\tilde{A}][T]_{t+\Delta t} + [C^{hm}][M]_{t+\Delta t} = [\tilde{B}][T]_t + [C^{hm}][M]_t \tag{6.6.13}$$

where

$$[\tilde{A}] = [C^{hh}]+\Delta t\theta[K^{hh}] \tag{6.6.14}$$

$$[\tilde{B}] = [C^{hh}]-\Delta t(1-\theta)[K^{hh}] \tag{6.6.15}$$

With all direct integration methods, solution instability must be considered carefully, this problem occurs in earlier time-steps are transmitted with amplification into subsequent steps and it was avoided here by choosing θ=0.5. Under these conditions the system is unconditional stable. Finally, a numerical value must be assigned to the step-size Δt. Since the thermal conductivity is much larger than the mass diffusion coefficient, the determination of the integration step-size Δt must base on the thermal conductivity in order to obtain a stable solution. A stability analysis [134] demostrates that the numerical scheme (6.6.9) and (6.6.13) are stable without oscillations if the minimum eigenvalue λ of the equation

$$\det([\bar{B}]-\lambda[\bar{A}]) = 0 \qquad (6.6.16)$$

is greater than 0 and less than 1.

Figure 6.2 shows a comparison between the experimental results and the analytical predictions of the Hercules 3501-5 neat resin exposed to environments defined by a relative humidity of 95 percent with a temperature of 71°C and a relative humidity of 75 percent with a temperature of 82°C. Since the neat resin may be assumed to be an isotropic material, the components of mass diffusivity tensor D_{ij} in any direction are considered to be identical. Good correlations between the experimental data in reference [217] and the computational results by classical Fick's law analyses are obtained. The hygrothermal effects, i.e. temperature changes caused by the rate of change of moisture concentration and moisture concentration changes resulted from the rate of change of temperature distribution, is not significant because the initial temperature distribution of the specimens is at 93°C which is close to the test temperature of the environmental chamber.

The unidirectional graphite/epoxy composites, AS/3501-5, were also exposed to two test conditions: one at relative humidity of 95 percent and temperature of 49°C, the other at relative humidity of 95 percent and temperature of 71°C. However the test environments for bidirectional graphite/epoxy composites, $[0/90]_s$, were 95 percent relative humidity with a temperature of 49°C and 95 percent relative humidity with a temperature of 71°C. The comparisons between experimental results and analytical results obtained from classical

Fick's law analyses for unidirectional and bidirectional composite laminates are presented in Figure 6.3 and Figure 6.4, respectively.

Upon comparing the results presented in Figure 6.3 with Figure 6.4, it is evident that there is superior theoretical/experimental correlation for the unidirectional specimens to the bidirectional specimens. It is evident, therefore, that the mathematical model is more appropriate for analyzing unidirectional material. Figure 6.4 indicates a rather significant descrepency between the theoretical predictions by a model incorporating the classical Fick's law and the experimental results of the bidirectional composite laminates. The test data approach equilibrium at a slower rate than that predicted by Fick's law.

Whitney and Browning postulated [217] that large in-plane tensile residual stresses were created which were a consequence of the environmental change increasing the initial through-the-thickness diffusion coefficient; the swelling relieves the residual stresses and in addition, the diffusivity decreases. The diffusion coefficient then approaches the diffusivity of a unidirectional composite as the residual stresses are completely relieved. If swelling continues, the residual stress becomes compressive in nature and a further decrease in the diffusivity may be anticipated, asymptotically approaching a lower limit. These statements are all hypotheses and a direct proof of a stress-dependent diffusion process requires a measurement of the diffusion coefficient under various constant-stress conditions. Alternative approach includes modifying Fick's mass diffusion law by incorporating a stress-dependent term in the diffusion equation. This is presented in equation (6.1.9), and is rewritten here for convenience as

$$q_i^{(M)} = -D_{ij}M_{,j} - G_{ijkl}\gamma_{kl,j} \qquad (6.6.17)$$

The units of G_{ijkl}, in equation (6.6.17) are same as the diffusion coefficient D_{ij}, therefore, it may be interpreted as the coupling effects between mass flux and elastic deformation gradient.

The value of G must be determined experimentally, however, analytical analyses can provide a lower-bound and an upper-bound on its numerical values. Thus upon examining Figure 6.5 on page 205, the lower bound of coefficient G is 9.013E-10 because if the value is lower than this, the curve of moisture content obtained from modified Fick's law will have no difference from the curve of the classical Fick's law, while the upper-bound being set as 1.27E-8 since if the value exceeds this, the moisture content of this material will be negative which is not acceptable from a physical standpoint

Figure 6.6 on page 206 shows a better agreement between the experimental data and the analytical result (solid line) predicted using a model with the modified Fick's law than the analytical result obtained using classical Fick's law. However, these analytical results need to pursue the accurate G value experimentally.

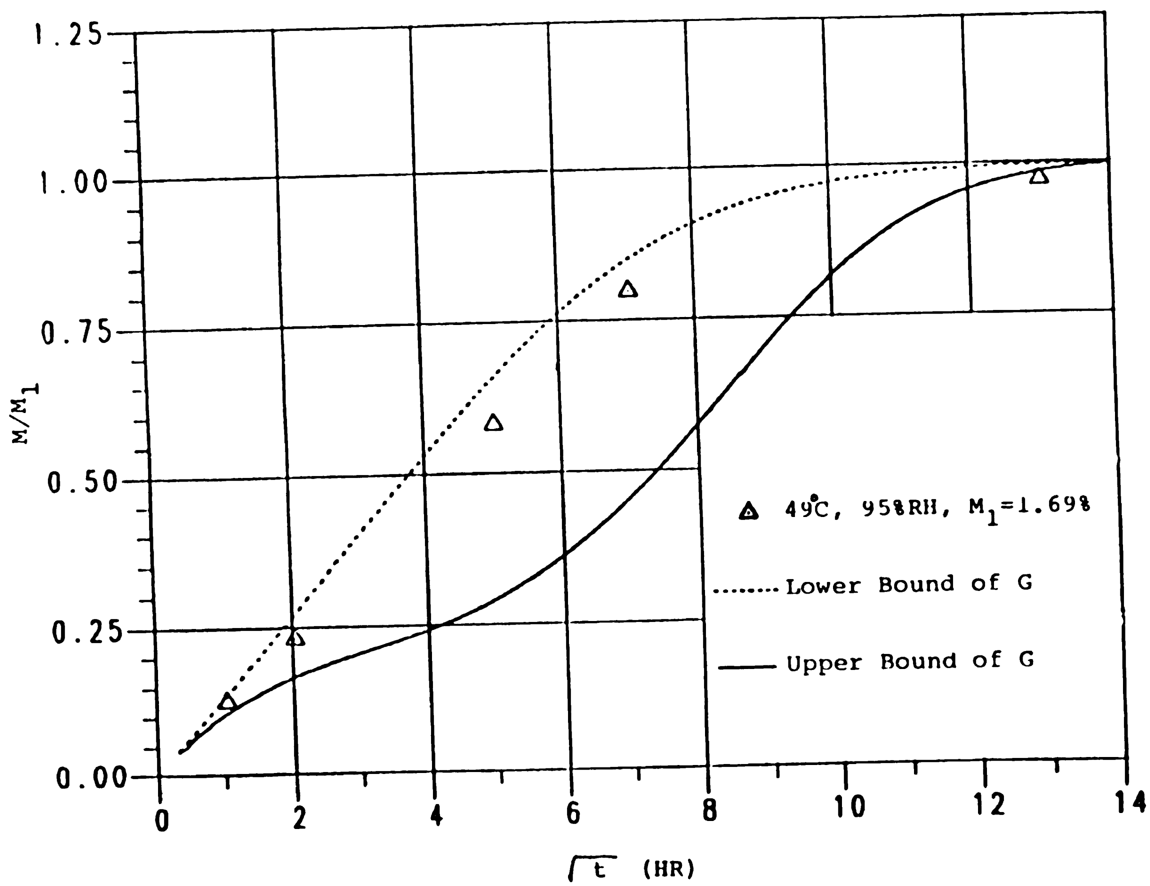

Figure 6.5 Comparison of Data, the Upper Bound and the Lower Bound for G (Hygroelastic Modulus) Based on the Modified Fick's Law, for Bidirectional Graphite/Epoxy Composite

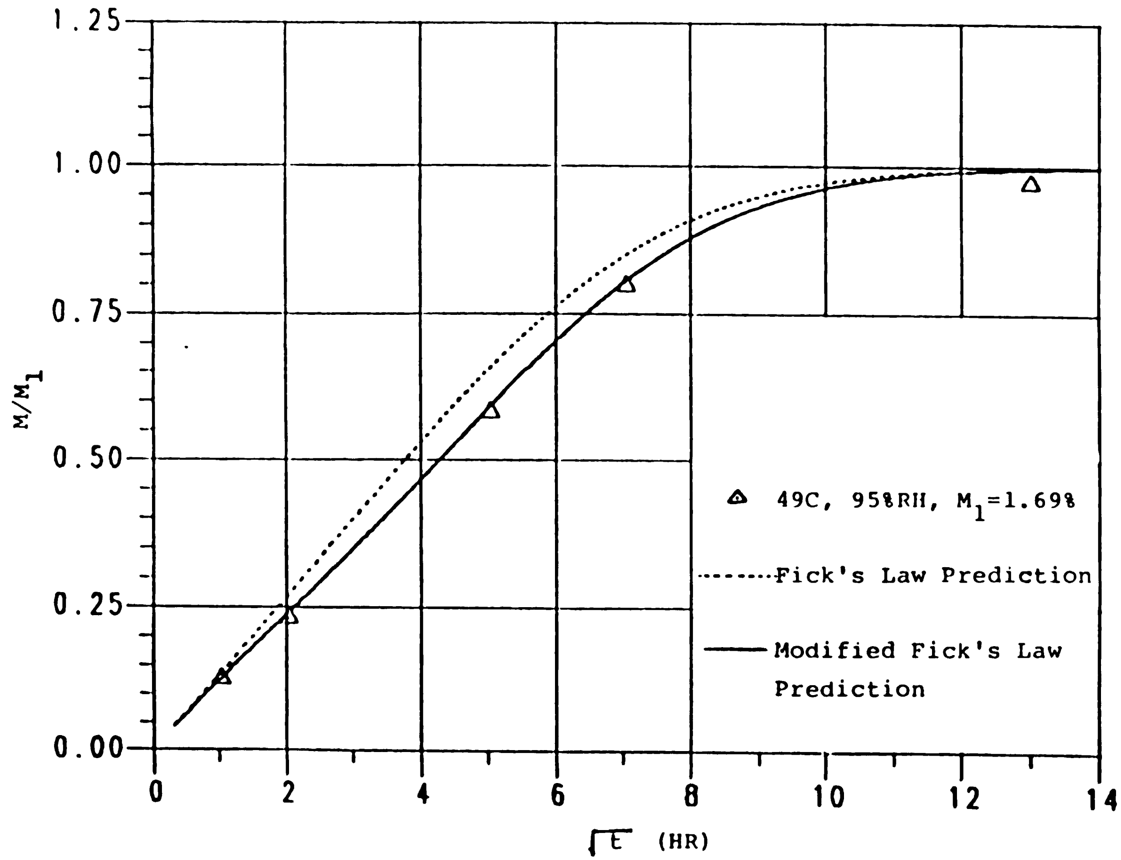

Figure 6.6 **Comparison of Data, Fick's Law and Modified Fick's Law, for Bidirectional Graphite/Epoxy Composite**

Both equation (5.5.19) and equation (6.6.17) describe the relationship between mass flux and the driving forces. The mass flux in equation (5.5.19) is driven by strain rate rather than driven by the strain gradient as in equation (6.6.17). Equation (5.5.19) is derived from the point of view of irreversible thermodynamics, therefore, the strain rate plays a role as a thermodynamic force and features in an irreversible process. However, equation (6.6.17) indicates that the mass flux is driven by the strain gradient. This hypothesis is motivated specifically by the experimental evidence of bidirectional composite materials [217].

In order to relate equation (6.6.17) to Whitney and Browning's postulation on their experimental investigation, the coefficient G may be divided into two variables such as $G=\lambda E$ where E is the elastic modulus and λ may be considered to be the moisture diffusion velocity within the continuum and is material-dependent. Therefore, the second term on the right-hand side of (6.6.17) may be interpreted as that the mass flux is generated by the strain gradient along the through-the-thickness direction. This assumption is referred to the gas or liquid diffusion under pressure difference [145]. Again the phenomenological coefficients have to be determined experimentally.

CHAPTER 7

DISCUSSION, CONCLUSIONS

Theoretical and experimental studies have been undertaken in order to investigate the dynamic response of the high-speed flexible linkages constructed from both commercial metals and graphite-epoxy composite laminates. Variational principles form the kernel of the theoretical studies and are employed to derive the equations of motion which govern the dynamic behavior of the mechanism systems. In addition, the variational principles provide the bases for finite element formulations. This computational approach has been recognized as a very effective numerical tool for solving these complex mathematical problems.

In chapter 2, correlations between computer simulations and experimental results are reasonably good in the sense of phase and amplitude content. These have offered some degree of confidence in the mathematical models, variational approaches, finite element formulations, the solution techniques and also the assumptions made herein. A comparative study on the selection of Timoshenko and Euler-Bernoulli beam elements for modeling flexible linkages, and also the number of elements needed to effectively model the systems, was performed by Gamache and Thompson [57]. In addition, a study of the element interpolation function and the number of elements required was investigated by several researchers [46,57,102] in order to obtain an accurate and efficient solution technique.

By observing the degree of agreement between experimental and theoretical results in Figures (4.6)-(4.10), it is apparent that the mathematical models developed in this research, for analyzing the dynamic response of linkages fabricated from commercial metals, is also capable of predicting the response of linkages made from composite materials. In general, good phase agreement between the theoretical and experimental results for four-bar linkage mechanisms was obtained. This was anticipated since the consistent mass matrix formulation utilized in this research does yield a stiffness idealized system [182] comparing to the actual system. Furthermore, the damping coefficient of the four-bar linkage mechanism was experimentally determined according to the procedures documented in reference [154] and this mechanism was also carefully adjusted in order to avoid bearing clearances and out-of-plane motion. However, the phase descrepencies occured in Figures 4.5 and 4.6 for slider-crank mechanism may be attributed to the viscous behavior and the dynamic friction of the slider assembly.

There are amplitude discrepencies in Figures 4.9 and 4.10 between the experimental and computational results. It is postulated that these discrepencies may be attributed to the imperfect modeling of the constitutive equation of the material. This is somewhat nonlinear and in addition the behavior of this polymeric material is dependent upon the environmental conditions. Other possibilities responsible for the amplitude discrepencies include the fluctuation of crank speed, which is assumed to be constant in the computer simulation.

The industrial applications of the previously derived theories may be mainly dependent upon the fields of application. For example, safety and reliability are the most important factors in the aerospace industry, therefore, mechanical components of the aircraft may be designed with larger safety factors in order to prevent any possible failure. However, in most industrial applications, the cost of a product plays a crucial role in order to make it more competitive in the marketplace. Therefore, qualitative figures for justifying the degree of accuracy are not available and this parameter from the design specification essentially depends upon the strategies for marketing the product. The design engineers should no doubt comply with the guidances of the strategies.

Sanders and Tesar [137] suggested that for stiff-designed industrial mechanism systems the deformations are largely due to the quasi-static application of cyclically varing inertial forces acting on the links. Therefore, the correlation of the quasi-static response is certainly important because it has a dominant influence in order to maintain a specific level of precision for its functional operation. The amplitude of vibrational response with higher frequency superimposed upon the quasi-static response are normally small compared with the amplitude of the quasi-static response. Therefore, from the above statement a 10 percent amplitude discrepency in the sense of relative agreement of dynamic response between computer simulation and experimental results should be acceptable in general industrial applications.

Theoretical investigations have been developed in chapters 5 and 6 in order to predict the temperature and the moisture concentration distribution inside the link materials, and the dynamic response of the linkage mechanism subjected to both mechanical and hygrothermal loadings.

In chapter 5, irreversible thermodynamics provides a general framework for deriving the governing equations. There are two advantages for this approach. First, this approach has found a great variety of applications in modeling the "real world" phenomena [49,66]. For example, in addition to the physical phenomena described in chapter 5, this approach may also be able to model chemical reactions occured within the system, and the aspect when an electromagnetic field acts upon a material system. Secondly, the solutions of the differential equations, such as equations (5.5.29), (5.5.30) and (5.5.31), may be easily sought by using the method of weighted residuals [55,56]. However, the physical insight, possessed only in the variational integrals, is not able to obtained explicitly by this method. The disadvantage of this approach is that the domain of validity of this theory is essentially the one for which local equilibrium is attained and the phenomenological equations are linearly defined. Therefore, the total entropy production, which leads to the generation of phenomenological equations, may be formed by summing the entropy production of each irreversible process.

There are two advantages documented herein for the mixed variational approach. The first is that it may be applicable to the condition of geometrical nonlinearity and this situation occurs frequently in machinery elastodynamics. Secondly, more insight may be deduced from utilizing this approach via a finite element formulation. The mixed variational approach has incorporated auxiliary conditions such as the strain-displacement equation, phenomenological equations and essential boundary conditions into the Hamilton's principle. So the functional depends upon temperature, moisture concentration, displacement, specific entropy density, flow potential density , strain and stress. As the basis of an elementary approximation, each field can be independently selected to achieve the discrete model, namely, the approximation function for the stresses may be different from that of the strains.

The disadvantage of this mixed variational principle is the rather complex mathematics, and it may create some degree of difficulty for the industrial utilization. In addition, from mathematical point of view this variational principle is somewhat imperfect because of the non self-adjointness existing in the heat conduction and mass diffusion equations [56,62]. Therefore, future work may be based on the notation of Stieltjes convolution integral adopted in the variational principle so as to ensure the existence of the self-adjointness property.

The selection of the appropriate approach to be adopted is the key for practising design engineers. The evaluatory criteria are governed by the type of the problem involved and the degree of accuracy required for the particular design purpose. A careful evaluation of the above considerations toward the problem should guide us in search of an appropriate approach.

The scientific method requires the interplay of theory and experiment in all research endeavors and this fundamental notion is particularly important in the study of composite materials because the behavior of the constituents is so complex. As an extension of the current work, a systematically experimental program for validating the theory with experimental evidence has been established. It provides a sound basis for testing hypotheses and can also be instrumental in guiding and directing further experimental work.

In the first phase of the experimental program, test coupons should be exposed to a variety of hygroscopic loadings while under the conditions of constant temperature and zero mechanical loading and vice verse in order to determine the basic properties of the composites, such as the coefficients of thermal expansion, the diffusivities, thermal conductivities, the coefficients of moisture expansion, and the coefficients of hygrothermal cross-effects. The techniques to be adopted for performing these tests are well documented in the literature. See, for example, reference [224].

The second phase of the experimental program should initially involve subjecting composite plate and beam specimens to static mechanical loads in an air environment with static values of temperature and humidity. A variety of response curves should be generated under conditions of variable humidity at constant temperature and vice versa, while maintaining a constant static mechanical loading. These specimens should be housed in an environmental chamber and several fixtures should be employed to impose the mechanical loading using either dead-weights or screw and locknut arrangements incorporating load-cells at the fixture-specimen interface. The flexural and uniaxial structural deformations should be monitored by strain gages mounted on the test specimens, and a variety of response characteristics should be generated using a combination of discrete temperature and humidity combinations.

The experimental results should then be compared with the predictions of finite element based computer simulations which incorporate the mathematical models from the theoretical development. If the correlation between the theoretical and experimental results is unsatisfactory, then the models would be modified, but if it is favorable, the test specimens could then be exposed to dynamic hygrothermal loading in conjunction with the same values of the discrete static mechanical loading employed previously. Again the mathematical models would be evaluated. The dynamic hygrothermal excitation could be imposed on the specimens by the environmental chamber using a microprocessor-based programmer/controller. These devices are marketed by the manufacturer of these chambers, and they compute and generate precision time related set point signals for the profile of the desired hygrothermal environment.

The third phase of the program would have the same algorithm as the second phase with the exception of dynamical mechanical loading being imposed on the composite specimens. This would be accomplished by locating the specimens in dynamic test-fixtures that incorporate a vibration exciter which can subject the specimen to a broad range of dynamic loading characteristics. This vibration exciter would be positioned inside the environmental chamber provided that the conditions developed by the environment chamber are within the exciter specification. When this is not possible, the exciter would then be bolted to the outside of the chamber and a push-rod arrangement employed to excite the specimens through the access port. The excitation of the specimens would be monitored by accelerometers. The response would again be monitored by strain gages. These dynamic tests would include the excitation of double-cantilever arrangements to study the dependence of material damping on temperature and moisture.

These results will provide an important data set for the final phase of this research which concerns the study of linkage mechanisms fabricated with composite laminates. By incorporating strain-gaged beam-shaped specimens into both four-bar linkages and also slider-crank mechanisms, these specimens will be exposed to a wide variety of loads at different speeds to effectively test the predictive capabilities of the mathematical models developed in the theoretical investigation.

Finally, the contributions achieved in this work to the state of the art may be summarized as follows:

1. An experimental study performed in chapter 3 clearly proves the effectiveness of the new design methodology proposed by Thompson et al

[158,160,173,178]. This advocates that composite materials should be employed to reduce the elastodynamic phenomena, such as link deflections and dynamic stresses.

2. Theoretical investigations have been developed by utilizing the concept of irreversible thermodynamics, and a mixed variational principle. These provide the capacity for analyzing the physical phenomena that govern the response of the linkage mechanisms which are subjected to both mechanical and hygrothermal loadings.

3. An experimental program presented as the future work provides a systematic process for exploring the material properties, the static response of the material and, furthermore, the dynamic response of the linkage mechanisms under varing temperature and humidity environmental conditions. This experimental work essentially supports the theoretical development as being a useful check for comparing the mathematical model with the experimental evidence.

This future work is an essential ingredient for developing a viable design methodology based on the design and fabrication of machine systems with composite materials. Such an approach could precipitate the evolution of the next generation of machinery products, thereby making a substantial contribution to the evolution of the factory-of-the-future.

BIBLIOGRAPHY

BIBLIOGRAPHY

1. Adali, S., "Multiobjective Design of an Antisymmetric Angle-Ply Laminated by Nonlinear Programming," Transaction of ASME, Journal of Mechanisms, Transmissions, and Automation in Design, Vol. 105, 1983, pp. 214-218.

2. Adams, R. D. and Bacon, D. G. C., "Effect of Fibre Orientation and Laminate Geometry on the Dynamic Properties of CFRP," Journal of Composite Materials, Vol. 3, 1973, pp. 402-428.

3. Adams, R. D. and Bacon, D. G. C., "Measurement of the Flexural Damping Capacity and Dynamic Young's Modulus of metals and Reinforced Plastics," Journal of physics D: applied Physics, Vol. 6, 1973, pp. 27-41.

4. Advanced Composite Materials--Environmental Effects, ASTM STP 658, ASTM, 1978.

5. Agarwal, D. and Broutman, L. J., Analysis and Performance of Fiber Composites, John Wiley and Sons, New York, 1980.

6. Adkins, J. E., "Non-linear Diffusion, III. Diffusion through Isotropic Highly Elastic Solids," Philosophical Transactions of the Royal Society, A, 256, 1964, pp. 301-316.

7. Alexander, R. M. and Lawrence, K. L., "Dynamic Strains in a Four-Bar Mechanism," Proceedings of the Third Applied Mechanisms Conference, Stillwater, OK, Nov. 1973, Paper No. 26.

8. Alexander, R. M. and Lawrence, K. L., "An Experimental Investigation of the Dynamic Response of an Elastic Mechanism," ASME Journal of Engineering for Industry, Vol. 96, No. 1, 1974, pp. 268-274.

9. Alexander, R. M. and Lawrence, K. L., "Experimentally Determined Strains in an Elastic Mechanism," ASME Journal of Engineering for Industry, Vol. 97, No. 3, 1975, pp. 791-794.

10. Allred, R. E., "The Effect of Temperature and Moisture Content on the Flexural Response of Kevlar/Epoxy Laminates," Journal of Composite Materials, Vol. 15, 1981, pp. 100-116.

11. Ashton, J. E. and Whitney, J. M., Theory of Laminated Plates, Technomic Publishing Co., Westport, Conn., 1970.

12. Badlani, M. and Midha, A., "Effects of Internal Material Damping on the Dynamics of a Slider-Crank Mechanism," ASME, Journal of Mechanisms, Transmissions, and Automation in Design, Vol. 105, No. 3, 1983, pp. 452-459.

13. Bagci, C., "Elastic Stability and Buckling Loads of 3-D Systems Using Spatial Finite Line Elements," Computers and Structures, Vol. 12, No. 2, 1979, pp. 731-743.

14. Bagci, C., "Methods of Elastodynamics of Mechanical, Structural and Industrial Robotic Systems Using Finite Line Elements," ASME Paper No. 83-WA/DSC-7.

15. Bahgat, B. M. and Willmert, K. D., "Finite Element Vibrational Analysis of Planar Mechanisms," Mechanism and Machine Theory, Vol. 11, 1976, pp. 47-71.

16. Bargmann, H., "Recent Development in the Field of Thermally Induced Waves and Vibrations," Nuclear Engineering Design, Vol. 27, 1974, pp. 372-385.

17. Barr, A. D. S., "Dynamic Instabilities in Moving Beams and Beams Systems," Proceedings of the Second International Congress on the Theory of Machines and Mechanisms, Zakopane, Poland, Vol. 1, 1969, P.365.

18. Barr, A. D. S., "Some Aspects of the Analysis of the Vibration and Stability of Mechanisms," Proceedings of the Euromech 22 Conference of I.U.T.A.M. Dynamics of Mechanisms, Newcastle-upon-Tyne, Sept. 1970.

19. Barr, A. D. S. and McWhannel, D. C., "Parametric Instability in Structures Under Support Motion," Journal of Sound and Vibration, Vol. 14, No. 4, 1971, pp. 491-509.

20. Bengisu, M. T., Zuccaro, D. and Thompson, B. S., "An Experimental Investigation of the Effects of Clearance in Plain Journal Bearings on Bending Strains in Flexible Four-Bar Linkages," ASME Paper No. 82-DET-16.

21. Bathe, K. J. and Wilson, E. L., Numerical Methods in Finite Element Analysis, Englewood Cliffs, New Jersey: Prentice-Hall, Inc., 1976.

22. Ben-Amoz, M., "On a Variational Theorem in Coupled Thermoelasticity," ASME Journal of Applied Mechanics, Vol. 32, No. 4, 1965, pp. 943-945.

23. Bert, C. W., "Material Damping: An Introductory Review of Mathematical Models, Measurements and Experimental Techniques," Journal of Sound and Vibration, Vol. 29(2), 1973, pp. 129-153.

24. Biggs, M. C., "Constrained Minimization Using Recursive Equality Constrained Quadratic Programming," Numerical Method for Nonlinear Optimization, Academic Press, London, 1972.

25. Biggs, M. C., "Constrained Minimisation Using Recursive Quadratic Programming: Some Alternative Subproblem Formulations," Towards Global Optimization, Proceedings of a Work Shop at the University of Cagliari, Italy, Oct. 1974, edited by L.C.W. Dixon and G.P. Szegö, North-Holland Publishing Co., Amsterdam, Netherland.

26. Biot, M. A., "Thermoelasticity and Irreversible Thermodynamics," Journal of Applied Physics, Vol. 27, No. 3, 1956, pp. 240-253.

27. Biot, M. A., Variational Principles in Heat Transfer, The Clarendon Press, Oxford, London, 1972.

28. Biot, M. A., "Complementary Forms of the Variational Principles for Heat Conduction and Convection," Journal of the Franklin Institude, Vol. 283, No. 5, 1967, pp. 372-378.

29. Blejwas, T. E., "The Simulation of Elastic Mechanisms Using Kinematic Constraints and Lagrange Multipliers," Mechanism and Machine Theory, Vol. 10, No. 4, 1981, pp. 441-445.

30. Blikstad, M., Sjöblom, P. O. W. and Johannesson, T. R., "Long-term Moisture Absorption in Graphite-Epoxy Angle-Ply Laminates," Journal of Composite Materials, Vol. 18, 1984, pp. 32-46.

31. Boley, B. A., "Thermally Induced Vibrations of Beams," Journal of the Aeronautical Sciences, Vol. 23, 1956, pp. 179-181.

32. Boley, B. A. and Barber, A. D., "Dynamic Response of Beams and Plates to Rapid Heating," Journal of Applied Mechanics, Vol. 24, 1957, pp. 413-416.

33. Boley, B. A. and Weiner, J., Theory of Thermal Stresses, Wiley, New York, 1960.

34. Bolotin, V. V., The Dynamic Stability of Elastic System, Holden-Day, San Francisco, 1964.

35. Brigham, E. O., The Fast Fourier Transform, Prentice-Hall, Inc., Englewood Cliffs, New Jersey, 1974.

36. Browning, C. G., Husman, G. E. and Whitney, J. M., "Moisture Effects in Epoxy Resin Matrix Composites," Composite Materials: Testing and Design, ASTM STP 617, ASTM, 1977, pp. 481-496.

37. Carpenter, W. C., "Viscoelastic Stress Analysis," International Journal for Numerical Methods in Engineering, Vol. 4, 1972, pp. 357-366.

38. Carslaw, H. S. and Jaeger, J. C., Conduction of Heat in Solids, 2nd edition, Clarendon Press, 1960.

39. Christensen, R. M., Theory of Viscoelasticity: An Introduction, Second edition, Academic Press, N.Y. 1982.

40. Christensen, R. M., Mechanics of Composite Materials, John Wiley and Sons, New York, 1979.

41. Christensen, R. M. and Naghdi, P. M., "Linear non-isothermal viscoelastic solids," Acta Mechanica Vol. 1, 1967, pp. 1-12.

42. Chung, T. J. and Prater, J. L., "A Constitutive Theory for Anisotropic Hygrothermoelasticity with Finite Element Applications," Journal of Thermal Stresses, Vol. 3, 1980, pp. 435-452

43. Chung, T. J. and Bradshaw, R. J., "Irreversible Hygrothermomechanical Behavior and Numerical Analysis in Anisotropic Materials," Journal of Composite Materials, Vol. 15, 1981, pp. 502-520.

44. Cleghorn, W. L., Fenton, R. G. and Tabarrok, B., "Optimum Design of High-Speed Flexible Mechanisms," Mechanism and Machine Theory, Vol. 16, No. 4, 1981, pp. 399-406.

45. Cleghorn, W. L., Fenton, R. G. and Tabarrok, B., "Finite Element Analysis of High-Speed Flexible Mechanisms," Mechanism and Machine Theory, Vol. 16, No. 4, 1981, pp. 407-424.

46. Cleghorn, W. L. and Konzelman, C. L., "Comparative Analysis of Finite Element Types Used in Flexible Mechanism Models," Proceedings of the 8th OSU Applied Mechanisms Conference, St. Louis, MO, Sept. 1983, pp. 30-1 to 30-7.

47. Conner, J. J. and Brebbia, C. A., Finite Element Techniques for Fluid Flow, Newnes-Butterworths, London, Boston, 1976.

48. Crank, J., The Mathematics of Diffusion, Clarendon Press, Oxford, 1979.

49. De Groot, S. R. and Mazur, P., Non-Equilibrium Thermodynamics, Dover Publications, Inc., New York, 1984.

50. Donnelly, R. J., Herman, R. and Prigogine, I., Non-Equilibrium Thermodynamics Variational Techniques and Stability, Preceedings of A Symposium Held at the University of Chicago, May 17-19, 1965, The University of Chicago Press.

51. Dubowsky, S. and Young, S. C., "An Experimental and Analytical Study of Connection Forces in High-Speed Mechanisms," ASME Journal of Engineering for Industry, Vol. 97, 1975, pp. 1166-1174.

52. Erdman, A. G. and Sandor, G. N., "Kineto-Elasto-Dynamics--A

Review of State of Artand Trends," Mechanism and Machine Theory, Vol. 7, 1972, pp. 19-33.

53. Erdman, A. G., Sandor, G. N. and Oakberg, R. G., "A General Method for Kineto-Elastodynamic Analysis of Mechanisms," ASME Journal of Engineering for Industry, Vol. 94B, 1972, pp. 1193-1205.

54. Flügge, W., Viscoelasticity, Second Edition, Springer-Verlag, Berlin, 1975.

55. Finlayson, B. A., The Method of Weighted Residuals and Variational Principles, Academic Press, New York, 1970.

56. Finlayson, B. A. and Scriven, L. E., "On the Search for Variational Principles," International Journal of Heat and Mass Transfer, Vol. 10, 1967, pp. 799-821.

57. Gamache, D. and Thompson, B. S., "The Finite Element Design of Linkages --A Comparison of Timoshenko and Euler-Bernoulli Elements," ASME Paper No. 81-DET-109, 1981.

58. Gandhi, M. V. and Thompson, B. S., "The Finite Element Analysis of Flexible Components of Mechanical Systems Using a Mixed Variational Principle," ASME Paper No. 80-DET-64, 1980.

59. Germain, P., Nguyen, Q. S. and Suquet, P., "Continuum Thermodynamics," ASME, Journal of Applied Mechanics, Vol. 50, 1983, pp. 1010-1020.

60. Golebiewski, E. P. and Sadler, J. P., "Analytical and Experimental Investigation of Elastic Slider Crank Mechanisms," ASME Journal of Engineering for Industry, Vol. 98, Nov. 1976, pp. 1266-1271.

61. Green, A. E. and Lindsay, K. E., "Thermoelasticity," Journal of Elasticity, Vol. 2, 1972, pp. 1-7.

62. Gurtin, M. E., "Variational Principles for Linear Initial-Value Problems," Quarterly of Applied Mathematics, Vol. 22, 1964, pp. 252-256.

63. Gurtin, M. E. and Sternberg, E., "On the Linear Theory of Viscoelasticity," Archives for Rational Mechanics and Analysis, Vol. 11, 1962, pp. 291-356.

64. Gurtin, M. E., "Variational Principles in The Linear Theory of Viscoelasticity," Archives for Rational Mechanics and Analysis, Vol. 13, 1963, pp. 179-191.

65. Gurtin, M. E., "On the Linear Theory of Diffusion through an Elastic Solid ," Proceedings of Environmental Degradation of Engineering Materials, VPI Press, Blacksburg, 1977, pp. 107-119.

66. Haase, R., Thermodynamics of Irreversible Processes, Addison-Wesley Publishing Company Inc., Reading, Massachusetts, 1969.

67. Hashin, Z., "Analysis of Composite Materials- A Survey," ASME, Journal of Applied Mechanics, Vol. 50, 1984, pp. 481-505.

68. Haines, R. S., "On Predicting Vibrations in Realistically Proportioned Linkage Mechanisms," ASME Journal of Mechanical Design, Vol. 103, No. 3, 1981, pp. 706-711.

69. Hartranft, R. J. and Sih, G. C., "The Influence of the Soret and Dufour effects on the Diffusion of Heat and Moisture in Solids," International Journal of Engineering Science, Vol. 18, 1980, pp. 1375-1383.

70. Heller, R. A., Brinson, H. F., and Thakker, A. B., "Environmental Effects on Fiber-Reinforced Composites," Polymer Engineering and Science, Vol. 15, Nov. 1975, pp. 781-788.

71. Herrmann, G., "On Variational Principles in Thermoelasticity and Heat Conduction," Quarterly of Applied Mathematics, Vol. 21, No. 2, 1963, pp.151-155.

72. Hertz, J., "High Temperature Strength Degradation of Advanced Composites," Space Shuttle Materials, Society of Aerospace Materials and Process Engineers, Vol. 3, Oct. 1970, pp. 9-16.

73. Hiel, C., Private Communication, Virginia Polytechnic Institute and State University.

74. Hirano, Y., "Optimum Design of Laminated Plates Under Shear," Journal of Composite Materials, Vol. 13, 1979, pp. 329-334.

75. Hoggert, J. T., Vibration and Damping Behavior of Advanced Composite Materials, Rep. DZ-126187-1, Boeing Co., Seattle.

76. Holzlöhner, U., "A Finite Element Analysis for Time-Dependent Problems," International Journal for Numerical Methods in Engineering, Vol. 8, 1974, pp. 55-69.

77. Horgan, C. O., "Saint-Venant End Effects in Composites," Journal of Composite Materials, Vol. 16, 1982, pp. 411-422.

78. Ignaczak, J., "Linear Dynamic Thermoelasticity-A Survey," Shock and Vibration Digest, Vol. 13, No. 9, 1981, pp. 3-8.

79. Imam, I., Sandor, G. N., and Kramer, S. N., "Deflection and Stress Analysis in High Speed Planar Mechanisms with Elastic Links," ASME Journal of Engineering for Industry, Vol. 95B, 1973, pp. 541-548.

80. Imam, I. and Sandor, G. N., "A General Method of Kineto-Elasto-Dynamic Design of High-Speed Mechanisms," Mechanism and Machine Theory, Vol. 8, No. 4, 1973, pp. 497-516.

81. Imam, I. and Sandor, G. N., "High Speed Mechanism Design--A General Analytical Approach," ASME Journal of Engineering for Industry, Vol. 97, 1975, pp. 609-628.

82. Jandrasits, W. G. and Lowen, G. G., "The Elasto-Dynamic Behavior of a Counter-weighted Rocker Link with an Overhanging Endmass in a Four-bar Linkage, Part I - Theory, Part II - Application and Experiment,"ASME Journal of Mechanical Design, Vol. 101, 1979, pp. 77-98.

83. Jones, R. M., Mechanics of Composite Materials, Scripta Book Co., Washington, D.C., 1975.

84. Khan, M. R., Thornton, W. A. and Willmert, K. D., "Optimality Criterion Techniques Applied to Mechanism Design," ASME Journal of Mechanical Design, Vol. 100, 1978, pp. 319-327.

85. Kim, R. Y. and Whitney, J. M., " Effects of Temperature and Moisture on Pin Bearing Strength of Composite Materials," Journal of Composite Materials, Vol. 10, 1976, pp. 149-155.

86. Kishimoto, A. K., Izumihara, Y. and Sakata, M., "Dynamic Analysis of Cracked Linear Viscoelastic Solids by Finite Element Method Using Singular Element," International Journal of Fracture, Vol. 16, No. 2, 1980, pp. 97- 109.

87. Kline, K. A. and DeSilva, C. N., "Variational Principles for Linear Coupled Thermoelasticity with Microstructure," International Journal of Solids and Structures, Vol. 7, 1971, pp. 129-142.

88. Kohli, D., Hunter, D. and Sandor, G. N., "Elastodynamic Analysis of a Completely Elastic System," ASME, Journal of Engineering for Industry, Vol. 99, No. 3, 1977, pp. 604-609.

89. Leitman, M. J., "Variational Principles in the Linear Dynamic Theory of Viscoelasticity," Quarterly of Applied Mathematics, Vol. XXIV, No. 1, 1966, pp. 37-46.

90. Lekszycki, T. and Olhoff, N., "Optimal Design of Viscoelastic Structures under Forced Steady-State Vibration," Journal of Structure Mechanics, Vol. 9, No. 4, 1981, pp. 363-387.

91. Liao, D. X., Sung, C. K. and Thompson, B. S., "The Optimal Design of Symmetric Laminated Beams Considering Damping," Journal of Composite Materials, in press, 1985.

92. Liao, D. X., Sung, C. K. and Thompson, B. S., "The Design of Flexible Robotic Manipulators with Optimal Arm Geometries and Fabricated from Composite Laminates with Optimal Material Properties," International Journal of Robotics Research, submitted July, 1985.

93. Loos, A. C. and Springer, G. S., " Moisture Absorption of Graphite-Epoxy Composites Immersed in Liquids and in Humid Air" Journal

of Composite Materials, Vol. 13, 1979, pp. 131-147.

94. Lord, H. W. and Shulman, Y., "A Generalized Dynamic Theory of Thermoelasticity," Journal of Mechanics and Physics Solids, Vol. 15, 1967, pp. 299-309.

95. Lowen, G. G. and Jandrasits, W. G., "Survey of Investigation into the Dynamic Behavior of Mechanisms Containing Links with Distributed Mass and Elasticity," Mechanism and Machine Theory, Vol. 7, 1972, pp. 3-17.

96. Lynch, F. Des., "A Finite Element Method of Viscoelastic Stress Analysis with Application to Rolling Contact Problems," International Journal for Numerical Methods in Engineering, Vol. 1, 1969, pp. 379-394.

97. Malmstadt, H. V., Enke, C. G. and Crouch, S. R., Electronics and Instrumentation for Scientists, Chapter 8, Benjamin-Cummings Publishing Co. Inc., Reading, MA, USA, 1981.

98. Malone, D. W. and Connor, J. J., "Finite Elements and Dynamic Viscoelasticity," ASCE, Journal of the Engineering Mechanics Division, Vol. 97, No. EM4, August 1971, pp. 1145-1158.

99. Malvern, L. E., Introduction to the Mechanics of A Continuous Medium, Englewood Cliffs, New Jersey: Prentice-Hall Inc., 1969.

100. Mckague, E. L., Reynolds, J. D. and Halkias, J. E., "Moisture Diffusion in Fiber-Reinforced Plastics," ASME Journal of Engineering Materials and Technology, Vol. 98, Jan. 1976, pp. 92-95.

101. Massalas, C. V. and Kalpakidis, V. K., "Coupled Thermoelastic Vibrations of A Simply Supported Beam," Journal of Sound and Vibration, Vol. 83, No. 3, 1983, pp. 425-429.

102. Midha, A., Badlani, M. L. and Erdman, A. G., "A Note on the Effects of Multi-Element Idealization of Planar-Elastic-Linkage Members," Proceedings of the 5th O.S.U. Applied Mechanisms Conference, Oklahoma City, Oklahoma, Nov. 6-9, 1977, pp. 27-1 to 27-11.

103. Midha, A., Erdman, A. G. and Frohrib, D. A., "An Approximate Method for the Dynamic Analysis of Elastic Linkages," ASME Journal of Engineering for Industry, Vol. 99B, 1977, pp. 449-455.

104. Midha, A., Erdman, A. G. and Frohrib, D. A., "Finite Element Approach to Mathematical Modeling of High Speed Elastic Linkages," Mechanism and Machine Theory, Vol. 13, 1978, pp. 603-618.

105. Midha, A., Erdman, A. G. and Frohrib, D. A., "A Closed-Form Numerical Algorithm for the Periodic Response of High-Speed Elastic Linkages," ASME Journal of Mechanical Design, Vol. 101, No. 1, 1979, pp. 154-162.

106. Midha, A., Erdman, A. G. and Frohrib, D. A., "A Computationally Efficient Numerical Algorithm for the Transient Response of High-Speed Elastic Linkages ," ASME Journal of Mechanical Design, Vol. 101, No. 1, 1979, pp. 138-148.

107. Nath, P. K. and Ghosh, A., "Kineto-Elastodynamic Analysis of Mechanisms by Finite Element Method," Mechanism and Machine Theory, Vol. 15, 1980, pp. 179-197.

108. Nath, P. K. and Ghosh, A., "Steady-State Response of Mechanisms with Elastic Links by Finite Element Methods," Mechanism and Machine Theory, Vol. 15, 1980, pp. 199-211.

109. Nayfeh, A. and Nemat-Nasser, S., "Thermoelastic Waves in Solids with Thermal Relaxation," Acta Mechanics, Vol. 12, 1971, pp. 53-69.

110. Newmark, N. M., "A Method of Computations for Structural Dynamics," Journal of Engineering Mechanics Division, ASCE Proceedings, Vol. 85, No. EM3, 1959, pp. 67-94.

111. Ni, R. G. and Adams, R. D., "The Damping and Dynamic Moduli of Symmetric Laminated Composite Beams--Theoretical and Experimental Results," Journal of Composite Materials, Vol. 18, pp.104-121.

112. Nickell, R. E. and Sackman, J. L., "Variational Principles for Linear Coupled Thermoelasticity," Quarterly of Applied Mathematics, Vol. XXVI, No. 1, 1968, pp. 11-26.

113. Nickola, W. E., "Strain Gage Measurements on Plastic Models," presented at the Fall Meeting of the Society for Experimental Stress Analysis, Idaho Falls, Idaho, 1975.

114. Niordson, F. I., "On the Optimal Design of a Vibrating Beam," Quarterly Applied Mathematics, Vol. 23, No. 1, 1965, pp. 47-53.

115. Noise Control in Strain Gage Measurements, Tech-Note TN-501, Micromeasurements Group, Raleign, NC.

116. Novozhilov, V. V., Foundations of the Nonlinear Theory of Elasticity, Graylock Press, Rochester, N.Y., 1953.

117. Nowacki, W., Dynamic Problems of Thermoelasticity, Noordhoff International Publishing, Leyden, The Netherlands, 1975.

118. Nowacki, W., "Certain Problems of Thermodiffusion in Solids," Arch. Mech., Vol. 23, No. 6, 1971, pp. 731-755.

119. Oden, J. T. and Armstrong, W. H., "Analysis of Nonlinear, Dynamic Coupled Thermoviscoelasticity Problems by the Finite Element Method," Computer and Structure, Vol. 1, 1971, pp. 603-621.

120. Oden, J. T. and Kross, D. A., "Analysis of General Coupled

Thermoelastic Problem by the Finite Element Method," Proceedings, Second Conf. Matrix Methods in Structural Mechanics, edited by L. Berke et al., AFFDL-TR-68-150, Wright-Patterson AFB, Ohio, 1968.

121. Oden, J. T. and Poe, J., "On the Numerical Solution of a Class of Problems in Dynamic Coupled Thermoelasticity," Proceedings, 5th SECTAM, Developments in Theoretical and Applied Mechanics, edited by D. Frederick, Pergamon Press, Oxford, 1970.

122. Oden, J. T. and Aguirre-Ramirez, G., "Formulation of General Discrete Models of Thermomechanical Behavior of Materials with Memory," International Journal of Solids and Structures, Vol. 5, 1969, pp. 1077-1093.

123. Oden, J. T., Finite Elements of Nonlinear Continua, McGraw-Hill Book Company, 1972.

124. Oden, J. T. and Reddy, J. N., Variational Methods in Theoretical Mechanics, Second Edition, Springer-Verlag, New York, 1983.

125. Oliver, J. H., Wysocki, D. A. and Thompson, B. S., "The Synthesis of Flexible Linkages by Balancing the Tracer Point Quasi-Static Deflections using Microprocessor and Advanced Materials Technologies," Mechanism and Machine Theory, Vol. 20, No. 2, 1985, pp. 103-145.

126. Pagano, N. J. and Halpin, J. C., "Influence of End Constraint in the Testing of Anisotropic Bodies," Journal of Composite Materials, Vol. 2, 1968, pp. 18-31.

127. Paipetis, S. S., "Mathematical Modelling of Composites," in Developments in Composite Materials--2 Stress Analysis, G. S. Holister (ed.), Applied Science Publishers Inc., N.J., 1981.

128. Papoulis, A., The Fourier Integral and Its Applications, McGraw-Hill Co., New York, 1962.

129. Parkus, H., Thermoelasticity, Blaisdell Publishing Co., Waltham, Mass., 1968.

130. Pipes, R. B., Vinson, J. R. and Chou, T. W., "On the Hygrothermal Response of Laminated Composite Systems," Journal of Composite Materials, Vol. 10, 1976, pp. 129-148.

131. Prevost, J. H. and Tao, D., "Finite Element Analysis of Dynamic Coupled Thermoelasticity Problems with Relaxation Times," ASME, Journal of Applied Mechanics, Vol. 50, 1983, pp. 817-822.

132. Ray, J. D. and Bert, C. W., "Nonlinear Vibrations of Beams with Pinned Ends," ASME Journal of Engineering for Industry, Vol. 9, 1969, pp. 977-1004.

133. Reddy, J. N., "Modified Gurtin's Variational Principles in

the Linear Dynamic Theory of Viscoelasticity," International Journal of Solids and Structures, Vol. 12, 1976, pp. 227-235.

134. Reddy, J. N., An Introduction to The Finite Element Method, McGraw-Hill Inc., 1984.

135. Robinson, E. A. and Silvia, M. T., Digital Signal Processing and Time Series Analysis, Chapter 5, Holden-Day Inc., San Francisco, CA, USA, 1978.

136. Sarma, B. S. and Varadan, T. K., "Lagrange-Type Formulation for Finite Element Analysis of Non-linear Beam Vibrations," Journal of Sound and Vibration, Vol. 86, 1983, pp. 61-70.

137. Sanders, J. R. and Tesar, D., "The Analytical and Experimental Evaluation of Vibratory Oscillations in Realistically Proportioned Mechanisms," ASME Journal of Mechanical Design, Vol. 100, 1978, pp. 762-768.

138. Schmit, L. A., Jr. and Farashi, B., "Optimum Laminate Design for Strength and Stiffness," International Journal for Numerical Methods in Engineering, Vol. 7, 1973, pp. 519-536.

139. Schultz, A. B. and Tsai, S.W., "Dynamic Moduli and Damping Ratios in Fiber-Reinforced Composites," Journal of Composite Materials, Vol. 2, 1968, pp. 368-379.

140. Schultz, A. B. and Tsai, S. W., "Measurements of Complex Dynamic Moduli for Laminated Fibre-Reinforced Composites," Journal of Composite Materials, Vol. 3, 1969, pp.434-443.

141. Shapery, R. A., "On the Time Dependence of Viscoelastic Variational Solutions," Quarterly of Applied Mathematics, Vol. XXII, No. 3, 1964, pp. 207-215.

142. Sharif-Bakhtiar, M. and Thompson, B. S., "Reducing Acoustical Radiation from High-Speed Mechanisms by Judicious Material Selection: An Experimental Study," ASME Paper 84-DET-49, 1984.

143. Shen, C. H. and Springer, G. S., "Moisture Absorption and Desorption of Composite Materials," Journal of Composite Materials, Vol. 10, 1976, pp. 2-20.

144. Shen, C. H. and Springer, G. S., "Effects of Moisture and Temperature on the Tensile Strength of Composite Materials," Journal of Composite Materials, Vol. 11, 1977, pp. 2-16.

145. Shi, J. J., Weinman, A. S. and Rajagopal, K. R., "Applications of the Theory of Interacting Continua to the Diffusion of a Fluid Through a Nonlinear Elastic Medium," International Journal of Engineering Science, Vol. 9, 1981, pp. 871-889.

146. Sih, G. C., Shih, M. T. and Chou, G. C., "Transient

Hygrothermal Stresses in Composites: Coupling of Moisture and Heat with Temperature Varying Diffisivity," International Journal of Engineering Science, Vol. 18, 1983, pp. 19-42.

147. Sivertsen, O. I. and Walφen, Å. φ., "Non-linear Finite Element Formulations for Dynamic Analysis of Mechanisms with Elastic Components," ASME Paper 82-DET-102, 1982.

148. Song, J. O. and Haug, E. J., "Dynamic Analysis of Planar Flexible Mechanisms," Computer Methods in Applied Mechanics and Engineering, Vol. 24, 1980, pp. 358-381.

149. Springer, G. S., "Moisture Content of Composites Under Transient Conditions," Journal of Composite Materials, Vol. 11, 1977, pp. 107-122.

150. Springer, G. S., "Effects of Temperature and Moisture on Sheet Modelling Compounds," Journal of Reinforced Plastics and Composites, Vol. 2, 1983, pp. 70-89.

151. Springer, G. S., "Model for Predicting the Mechanical Properties of Composites at Elevated Temperatures," Journal of Reinforced Plastics and Composites, Vol. 3, 1984, pp. 85-95.

152. Springer, G. S. and Tsai, S. W., "Thermal Conductivities of Unidirectional Materials," Journal of Composite Materials, Vol. 1, 1967, pp. 166-173.

153. Springer, G. S., Environmental Effects of Composite Materials, Vol. I and Vol. II, Technomic Publishing Company, Inc., 1984.

154. Stamps, F. R. and Bagci, D., "Dynamic of Planar, Elastic, High-Speed Mechanisms Considering Three-Dimensional Offset Geometry: Analytical and Experimental Investigations," ASME Paper No. 82-DET-34, 1982.

155. Sunada, W. and Dubowsky, S., "The Applications of Finite Element Methods to the Dynamic Analysis of Flexible Spatial and Co-planar Linkage Systems," Journal of Mechanical Design, ASME, Vol. 103, No. 3, July 1981, pp. 643-651.

156. Sunada, W. H. and Dubowsky, S., "On the Dynamic Analysis and Behavior of Industrial Robotic Manipulators with Elastic Members," ASME Journal of Mechanisms, Transmissions, and Automation in Design, Vol. 105, No. 1, March 1983, pp. 42-51.

157. Sung, C. K. and Thompson, B. S., "A Note on the Effect of foundation Motion upon the Response of Flexible Linkages," ASME Paper No. 82-DET-26, 1982.

158. Sung, C. K. and Thompson, B. S., "Material-Selection: An Important Parameter in the Design of High-Speed Linkages," Mechanism and

Machine Theory, Vol. 19, No. 4/5, 1984, pp. 389-396.

159. Sung, C. K., Thompson, B. S., Xing, T. M. and Wang, C. H., "An Experimental Study on the Nonlinear Elastodynamic Response of Linkage Mechanisms," Mechanism and Machine Theory, in press, May, 1984.

160. Sung, C. K., Thompson, B. S., Crowley, P. and Cuccio, J., "An Experimental Study to Demonstrate the Superior Response Characteristics Mechanisms Constructed with Composite Laminates," Mechanism and Machine Theory, in press, May, 1985.

161. Sung, C. K., Thompson, B. S. and McGrath, J. J., "A Variational Principle for the Linear Coupled Thermoelastodynamic Analysis of Mechanism systems," ASME Journal of Mechanisms, Transmissions, and Automation in Design, Vol. 106, No. 3, Sept. 1984, pp. 291-296.

162. Sutherland, G.H., "Analytical and Experimental Investigation of High-Speed Elastic-Membered Linkage," ASME Journal of Engineering for Industry, Vol. 98, 1976, pp. 788-794.

163. Tajima, Y. A., "The Diffusion of Moisture in Graphite Fiber-Reinforced Epoxy Laminates," SAMPE Quarterly, 1980, pp. 1-9.

164. Tambour, Y., "On Local Temperature Overshoots Due to Transport Coupling of Heat and Moisture in Composite Materials," Journal of Composite Materials, Vol. 18, Sept. 1984, pp. 478-494.

165. Tambour, Y., " A Three-Dimensional Field Transformation for Anisotropic Coupled Heat and Moisture Transfer in Composite Materials," to be submitted to the Journal of Composite Materials, 1984.

166. Tao, D. and Prevost, J. H., "Relaxation Effects on Generalized Thermoelastic Waves," Journal of Thermal Stresses, Vol. 7, 1984, pp. 79-89.

167. Tauchert, T. R. and Adibhatla, S., "Design of Laminated Plates for Maximum Stiffness," Journal of Composite Materials, Vol. 18, 1984, pp. 58-69.

168. Tauchert, T. R. and Adibhatla, S., "Optimum Elastic Design of a Reinforced Beam," Journal of Composite Materials, Vol. 16, 1982, pp.433-445.

169. Taylor, R. L., Pister, K. S. and Goudreau, G. L., "Thermomechanical analysis of Viscoelastic Solids," International Journal for Numerical Methods in Engineering, Vol. 2, 1970, pp. 45-59.

170. Thompson, B. S., "A Survey of analytical Path-Synthesis Techniques for Plane Mechanisms," Mechanism and Machine Theory, Vol. 10, 1975, pp. 197- 205.

171. Thompson, B. S. and Ashworth, R. P., "Resonance in Planar

Linkage Mechanisms on Vibrating Foundations," Journal of Sound and Vibration, Vol. 4, No. 3, 1976, pp. 403-414.

172. Thompson, B. S. and Barr, A. D. S., "A Variational Principle for the Elastodynamic Motion of Planar Linkages," ASME Journal of Engineering for Industry, Vol. 98, Nov. 1976, pp. 1306-1312.

173. Thompson, B. S. and Gandhi, M. V., "The Finite Element analysis of Mechanism Components made from Fiber-Reinforced Composite Materials," ASME Paper No. 80-DET-63, 1980.

174. Thompson, B. S., "A Variational Formulation for the Finite Element Analysis of High-Speed Machinery," ASME Paper No. 80-WA/DSC-38, 1980.

175. Thompson, B. S., "Variational Formulations for the Finite Element Analysis of the Noise Radiation from High-Speed Machinery," ASME Journal of Engineering for Industry, Vol. 103, No. 4, Nov. 1981, pp. 385-391.

176. Thompson, B. S., Zuccaro, D., Gamache, D. and Gandhi, M. V., "An Experimental and Analytical Study of a Four Bar Mechanism with Links Fabricated from a Fiber-Reinforced Composite Material," Mechanism and Machine Theory, Vol. 18, No. 2, 1983, pp. 165-171.

177. Thompson, B. S., Zuccaro, D., Gamache, D. and Gandhi, M. V., "An Experimental and Analytical Study of the dynamic Response of Linkage Fabricated from a Unidirectional Fiber-Reinforced Composite Laminate," ASME Journal of Mechanisms, Transmissions, and Automation in Design, Vol. 105, No. 3, Sept. 1983, pp. 528-536.

178. Thompson, B. S. and Sung, C. K., "A Variational Formulation for the Dynamic Viscoelastic finite Element analysis of Robotic Manipulators Constructed from Composite Materials," ASME Journal of Mechanisms, Transmissions, and Automation in Design, Vol. 106, No. 2, 1984, pp. 183- 190.

179. Thompson, B. S. and Sung, C. K., "The Design of Robots and Intelligent Manipulators Using Composite Materials," Mechanism and Machine Theory (in press).

180. Thompson, B. S. and Sung, C. K., "A Variational Formulation for the Nonlinear Finite Element Analysis of Flexible Linkages: Theory, Implementation and Experimental Results," ASME Journal of Mechanisms, Transmissions and Automation in Design, Vol. 106, No. 4, 1984, pp. 482-488.

181. Thompson, B. S. and Sung, C. K., "A Variational Theorem for the Viscoelastodynamic Analysis of High-Speed Linkage Machinery Fabricated from Composite Materials," ASME Paper No. 83-DET-6, 1983.

182. Tong, P., Pian, T. H. H. and Bucciarelli, L. L., "Mode Shapes and Frequencies by Finite Element Method using Consistent and

Lumped Masses," Computer and Structure, Vol. 1, 1971, pp. 623-638.

183. Tsai, S. W. and Hahn, H. T., Introduction to Composite Materials, Technomic Publishing Company, Westport, Connecticut, 1980.

184. Turcic, D. A. and Midha, A., "Generalized Equations of Motion for the Dynamic Analysis of Elastic Mechanism Systems," ASME Journal of Dynamic Systems, Measurements and Control, Vol. 106, 1984, pp. 243-248.

185. Turcic, D. A. and Midha, A., "Dynamic Analysis of Elastic Mechanism Systems, Part I: Application, and Part II: Experimental Result," ASME Journal of Dynamic Systems, Measurements and Control, Vol. 106, 1984, pp. 249-260.

186. Wallace, D. B. and Seireg, A., "A Finite Element Based Procedure for Simulating the Transient Response and Failure of a Two-Dimensional Continuum with Nonlinear Material Characteristics," ASME, Journal of Engineering for Industry, Vol. 92, Feb., 1973, pp. 345-352.

187. Washizu, K., Variational Methods in Elasticity and Plasticity, Oxford, New York, Pergamon Press, 1968.

188. Washizu, K., "Application of the Variational Method to Transcient Heat Conduction Problems," Aeroelastic and Structures Res. Lab., Technique Report, AD59951, 1955, pp. 17-25.

189. Weinstein, F., Putter, S. and Stavsky, Y., "Thermoelastic Stress Analysis of Anisotropic Composite Sandwich Plates by Finite Element Method," Computers and Structures, Vol. 17, No. 1, 1983, pp. 31-36.

190. Weitsman, Y., "Diffusion with Time-Varying Diffusivity with Application to Moisture-Sorption in Composites," Journal of Composite Materials, Vol. 10, 1976, pp. 193-204.

191. Weitsman, Y., "Stresses in Adhesive Joints to Moisture and Temperature," Journal of Composite Materials, Vol. 11, 1977, pp. 378-394.

192. White, J. L., "Finite Elements in Linear Viscoelasticity," Proceedings, 2nd Conf. on Matrix Methods in Structural Mechanics, edited by L. Berke et. al., AFFDL-TR-68-150, Wright-Patterson AFB, Ohio, 1968, pp. 489-516.

193. Whitney, J. M., Daniel, I. M. and Pipes, R. B., Experimental Mechanics of Fiber-Reinforced Composite Materials, Society for Experimental Stress Analysis Monograph, (4).

194. Whitney, J, M., "Three-Dimensional Moisture Diffusion in Laminated Composites," AIAA Journal, Vol. 15, Sept. 1977, pp. 1256-1358.

195. Wilson, E. L. and Nickell, R. E., "Application of the Finite Element Method to Heat Conduction Analysis," Nuclear Engineering and Design, Vol. 4, 1966, pp. 276-286.

196. Winfrey, R. C., "Elastic Link Mechanisms Dynamics," ASME Journal of Engineering for Industry, Vol. 93, 1971, pp. 268-272.

197. Winfrey, R. C., "Dynamic Analysis of Elastic Link Mechanisms by Reduction of Coordinates," ASME Journal of Engineering for Industry, Vol. 94B, No. 2, May 1972.

198. Woinowsky-Krieger, S., "The Effect of an Axial Force on the Vibration of Hinged Bars," ASME Journal of Applied Mechanics, Vol. 17, 1950, pp.35-36.

199. Wu, C. H. and Tauchert, T. R., "Thermoelastic Analysis of Laminated Plates 1: Symmetric Specially Orthotropic Laminates," Journal of Thermal Stress, Vol. 3, 1980, pp. 247-259.

200. Wu, C. H. and Tauchert, T. R., "Thermoelastic Analysis of Laminated Plates 2: Antisymmetrical Cross-ply and Angle-ply Laminates," Journal of Thermal Stress, Vol. 3, 1980, pp. 365-378.

201. Yamada, Y., Takabatake, H. and Sato, T., "Effect of Time-Dependent Material Properties on Dynamic Response," International Journal for Numerical Methods in Engineering, Vol. 8, 1974, pp. 403-414.

202. Zhang, Ce. and Grandin, H. T., "Kinematical Refinement Technique in Optimum Design of Flexible Mechanisms with External Loads Using Static Condensation," ASME Paper No. 81-DET-104.

203. Zhang, Ce. and Grandin, H. T., "Optimum Design of Flexible Mechanisms," ASME Journal of Mechanisms, Transmissions, and Automation in Design, Vol. 105, June 1983, pp. 267-272.

204. Zienkiewicz, O. C., Watson, M. and King, I. P., "A Numerical Method of Visco-Elastic Stress Analysis," International Journal of Mechanical Science, Vol. 10, 1968, pp. 807-827.

205. Zienkiewicz, O. C., "The Finite Element Method: From Intuition to Generality," Applied Mechanics Review, Vol. 23, No. 3, March 1970, pp. 249-256.

206. Zienkiewicz, O. C., The Finite Element Method, Maidenhead, England: McGraw-Hill Book Company, 1977.

207. Donea, J.,"Thermal Conductivities Based on Variational Principles," Journal of Composite Materials, Vol. 6, 1972, pp. 262-270.

208. Flaggs, D. L. and Crossman, F. W., "Viscoelastic Response of a Bonded Joint due to Transient Hygrothermal Exposure," Modern

Developments in Composite Materials and Structures, J. R. Vinson, ed. ASME (1979).

209. Flaggs, D. L. and Crossman, F. W., "Analysis of Viscoelastic Response of Composite Laminates During Hygrothermal Exposure," Journal of Composite Materials, Vol. 15, 1981, pp. 21-40.

210. Flaggs, D. L. and Vinson, J. R., "Hygrothermal Effects on the Buckling of Laminated Composite Plates," Fibre Science and Technology, Vol. 11, 1978, pp. 353-360.

211. Maymon, G., Briley, R. P. and Rehfield, L. W., "Influence of Moisture Absorption and Elevated Temperature on the Dynamic Behavior of Resin Matrix Composites: Preliminary Result," Advance Composite Materials-Environmental Effects ASTM STP 658, 1978, pp. 221-233.

212. Aoki, S., Kishimoto, K., Izumihara, Y. and Sakata, M., "The Finite Element Analysis of Cracked Linear Viscoelastic Solid by Finite Element Method using Singular Element," International Journal of Fracture, Vol. 16, No. 2, April, 1980, pp. 97-109.

213. Gurtin, M. E., "On the Linear Theory of Diffusion through an Elastic Solid," Proceedings of Environmental Degradation of Engineering Materials, VPI Press, Blacksburg, 1977, pp. 131-139.

214. Nowacki, W., "Certain Problems of Thermodiffusion in Solids," Archive Mechanics, Vol. 23, No. 6, 1971, pp. 731-755.

215. Springer, G. S., "Environmental Effects on Epoxy Matrix Composites," Composite Materials: Testing and Design (Fifth Conference). ASTM STP 674, S. W. Tsai, Ed., American Society for Testing and Materials, 1979, pp. 291-312.

216. Blikstad M., Sjöblom P. O.W. and Johannesson T. R., "Long-Term Moisture Absorption in Graphite/Epoxy Angle-Ply Laminates," Journal of Composite materials, Vol. 18, 1984, pp. 32-46.

217. Whitney, J. M. and Browning, C. E., "Some Anomalies Associated with Moisture Diffusion in Epoxy Matrix Composite Materials," Advanced Composite Materials-Environmental Effects, ASTM STP 658, J. R. Vinson, Ed., American Society of Testing and Materials, 1978, pp. 43-60.

218. Shen, C. H. and Springer, G. S., "Environmental Effects on the Elastic Moduli of Composite materials," Journal of Composite Materials, Vol. 11, 1977, pp. 250-264.

219. Gurtin, M. E. and Yatomi, C., "On a Model for Two Phase Diffusion in Composite Materials," Journal of Composite Materials, Vol. 13, 1979, pp. 126-130.

220. Thompson, B. S., "An Elastodynamic Analysis of Planar Linkage Mechanisms," Doctoral Thesis, University of Dundee, 1976.

221. Verette, R. M., "Temperature/Humidity Effects on the Strength of Graphite/Epoxy Laminates," AIAA Paper No. 75-1011, AIAA 1975 Aircraft Systems and Technology Meeting, Los Angels, California, August 4-7, 1975.

222. Hofer, Jr. K.E., Larsen, D. and Humphreys, V. E., "Development of Engineering Data on the Mechanical and Physical Properties of Advanced Composite materials," Techanical Report AFML-TR-74-266, Feb., 1975, Air Force Material Labortory, Wright-Patterson Air Force Base, Dayton, Ohio.

223. Wark, K., Thermodynamics, New York, McGraw-Hill Book Company, Third Edition, 1977.

224. Whitney, J. M., Daniel, I. M. and Pipes, R. B., Experimental Mechanics of Fiber-Reinforced Composite Materials, Society for Experimental Stress Analysis Monograph No. 4, 1982.